Porous metal implants for enhanced bone ingrowth and stability

Thesis submitted to the University of Sheffield for the degree of Doctor of Philosophy

William van Grunsven

Department of Materials Science and Engineering

September 2014

Abstract

The stability and longevity of metal bone implants has been an important issue in orthopaedics for many decades. Over the years many different approaches have been explored to improve the properties of implants, for example by reducing the stiffness, by coating the implant with osteoconductive materials and by introducing porosity which permits bone ingrowth into the implant.

For the fabrication of porous metals many techniques have been described that aim to produce structures that are strong, reliable, have the desired pore size and architecture and are cheap and easy to produce. In this thesis two fabrication techniques are investigated: a space holder-based method and electron beam melting.

Firstly, an overview is given of the structures produced using the space holder method. It shows variations in the fabrication process, such as powder shape, metal to space holder ratio and mixing method and the way in which these variations influence the properties of the structures.

Next, the results of the work on electron beam melting will be discussed. A diamond unit cell was used as a template to produce regular lattices with different strut thicknesses, porosities and relative densities. Based on initial results a graded lattice was designed in which the properties of the unit cells varied based on the location inside the lattice.

Finally, the most promising lattices were tested using a range of biological tests aiming to predict their potential for bone ingrowth. These tests include cell culture under static and dynamic conditions and bone ingrowth studies. From there results, it can be concluded that electron beam melting is a highly promising technique for the production of porous metal for orthopaedic applications and that the use of graded porous structures is a highly effective method to control both the mechanical and biological properties of bone implants.

Acknowledgements

During my work on this project I have received a lot of help from many different people. Hereby, I would like to take the opportunity to express my gratitude for all the help, support, advice and guidance that I received over the past years.

First of all, I would like to thank my supervisors, Gwen and Russell, for everything they have done for me. I am very grateful to them for giving me the opportunity to work on this project and for all their support, guidance and encouragement over the course of this project.
The funding for this project was provided by the charity Orthopaedic Research UK (formerly the Furlong Research Charitable Foundation). Additional funding for travelling expenses was provided by the Learned Society of the Department of Materials Science and Engineering, the Sheffield Metallurgical and Engineering Association and the European Society for Biomechanics. I am very grateful for their generous support.

I would also like to thank the people from the Mercury Centre for allowing me the use the EBM equipment and for a lot of help and support. These include Professor Iain Todd and many of the members of his group including Everth, Fatos and Mike. Their help has been invaluable in the work described in chapter 4. I would also like to acknowledge the help of Dr Leslie Coulton for his help regarding the MicroCT analysis and Professor Damien Lacroix and Dr Andy Olivares for the shear stress modelling.
For the biological part of the project I got a lot of support from all the people in the Kroto Research Institute. Many thanks to Robin, Mai, Mohsen and all the other people in the tissue engineering group for their help in the lab, but also for all the nice chats in the office, lunches, trips and parties. Furthermore, I would like to thank Professor Maksym Pogorielov, Professor Gennadii Tkach and Vladimir Deineka of the Medical Institute of Sumy State University for their help in the bone ingrowth study and Dr Pamela Habibivic and Niloofar Tahmasebi of the University of Twente for the equipment and training for histology.

And finally, I want to say thank you to the people around me who have always been extremely supportive over the years, my friends, my family, my parents and of course, Eva. Thank you for your continued support, for putting up with me over the past years, but most of all for believing in me.

Table of contents

Introduction

Every year almost 200,000 people in the UK require joint replacement surgery, also known as arthroplasty. There are many different conditions where a joint replacement might be necessary at some stage, but the most common cause for surgery (around 90% of cases) is osteoarthritis; other causes include avascular necrosis, fractured neck of femur, inflammatory arthropathy or chronic trauma.

The problem of restoring mobility in affected joints and relieving the pain associated with degeneration of cartilage has been a challenge to orthopaedic surgeons for centuries, but since the introduction of the first reliable total joint replacements in the 1950s significant progress has been made in improving the prognosis of patients following total joint arthroplasty. Improvements to the design of orthopaedic implants have led to an enormous increase in the stability and longevity of implants and therefore to a reduction in the percentage of patients requiring revision surgery.

One of the innovations in implant design that has seen an increase in popularity over the past decades has been the use of non-cemented porous metal implants where the implant is placed in direct contact with the surrounding bone and where implant stabilisation relies on bone ingrowth into the pores of the implant. This non-cemented approach has many advantages over the use of bone cement but it has also raised many questions regarding the optimal parameters for the design of porous metal implants; for example, pore size, relative density, stiffness, thickness of the porous layer and surface modifications can all have a profound effect on bone ingrowth and implant stability.

With the introduction of additive manufacturing (3D printing) techniques that are suitable for metals and alloys it has become possible to manufacture porous metals with greater precision and reproducibility than ever before. As a result, research into additive manufacturing techniques such as selective laser sintering and electron beam melting has become highly relevant to the field of implant design.

In this thesis, electron beam melting was used alongside a more conventional technique using a space holder to produce porous metal structures relevant to orthopaedics. The principal aims of the experimental work were:

- To investigate how porous metal structures produced by electron beam melting compare to structures produced by a non-additive manufacturing based fabrication method in terms of mechanical properties and structure.
- To indentify one or more of the most promising structures based on the results of the structural and mechanical characterisation and to evaluate these structures biologically in a series of in vitro and in vivo studies aiming to predict their suitability for application in orthopaedic implants.

The results of the fabrication and characterisation of porous metal structures using the space holder technique are described in chapter 3. The aims of the experimental work for this chapter were to produce a large range of highly porous metal foams with relative densities between 15% and 40%. Different characterisation techniques were then used to assess shrinkage, stiffness and structural properties such as pore size, pore architecture and interconnectivity between the pores; these data could be used to optimise several different parameters for the fabrication of metal foams using the space holder technique.

The objectives of the work described in chapter 4 were to optimise parameters for the production of porous metal structures by electron beam melting. Following these optimisations it was attempted to produce a graded structure consisting of different layers with different relative densities which was thought to be more versatile and where properties could be optimised for both stiffness and bone ingrowth.

Based on the analysis of the results of these two fabrication methods the most promising structures were selected for biological assessment. This biological assessment consisted of a series of tests carried out to investigate the potential for structures produced by electron beam melting, in particular for those with a graded porosity, to be used in orthopaedic implants. The in vitro experiments, described in chapter 5, aimed to investigate properties such as cell attachment of relevant cell lines (those representing early or mature osteoblasts) and the production of extracellular matrix in and around the structures. Where possible, the newly produced structures were compared with other relevant porous metal structures or with commercially available products. Furthermore, a simple fluid flow system was designed where the structures could be placed in a bioreactor and where cell behaviour could be investigated under both static and dynamic conditions.

Finally, an in vivo bone ingrowth study was carried out to compare a graded lattice to a commercially available porous metal and to a solid titanium control. These samples were implanted into a femoral defect in a rat with the aim of comparing implant stability and bone-implant contact as well as bone volume inside the implant and depth of ingrowth of the porous materials.

In summary, osteoarthritis and related conditions are a clinical problem affecting a large number of patients and electron beam melting is a technique that has revolutionised the manufacture of high-value metal components. The project described in this thesis aimed to make a contribution to bringing these two together in the search for better orthopaedic implants.

1. Background

1.1 Skeletal function and repair

In humans and other vertebrate animals the skeleton forms the body's main supportive system. It consists of bone which provides strength and protection and cartilage which provides support and facilitates joint movement. In an adult human the body normally contains 206 bones which are formed during embryonic development; most of these are formed from a cartilage intermediate that serves as a template for bone tissue formation (Marieb 2004; Van Blitterswijk 2008).

1.1.1 Cartilage

Cartilage is a type of connective tissue that that fulfils many different roles the body. Its most widely recognised role is on the joint edges of long bones where it provides lubrication and shock absorption. However, cartilage is also found in intervertebral discs, ribs, etc. The main cell type found in mature cartilage is the chondrocyte; these cells make up around 2% of the total volume. These cells are usually fully embedded in dense extracellular matrix (ECM). Cartilage ECM consists of many different components, but the main components of the ECM are collagen (mainly type II), and proteoglycans. Collagen forms a strong network which helps to provide resistance against damage due to shear stress and proteoglycans act as shock absorbers. Depending on the type of cartilage it typically contains 65 – 80% water (Marieb 2004; Van Blitterswijk 2008; Mahmoudifar et al. 2012).

All cartilage in the human body can be classified into three main categories with different chemical composition and distinct anatomical features, hyaline, elastic and fibrous cartilage. Hyaline cartilage (sometimes also known as articular cartilage) has a unique combination of liquid and protein fibres which gives it a high ability for shock absorption, a property that is essential for adequate joint function (Hunziker 2001; Marieb 2004; Van Blitterswijk 2008).

An important aspect of mature cartilage is that it is neither innervated nor vascularised; this means that supply of nutrients and oxygen to the chondrocytes that reside in the extracellular matrix depends solely on diffusion through the matrix. As these embedded chondrocytes have a very low metabolic rate there is generally sufficient diffusion for these cells to survive. However, the absence of blood vessels means that regeneration of cartilage due to damage caused by injury or wear is virtually impossible. Therefore, to date, no adequate treatment

exists for most conditions that are associated with impaired cartilage function (Van Blitterswijk 2008; Huey et al. 2012).

1.1.2 Bone

While cartilage is responsible for shock absorption in the skeleton and allows movement of the joints, bones have an important function in providing stability and protection to either individual organs or to the body as a whole (Marieb 2004). All types of bone possess a high tensile and compression strength. On a structural level, bone tissue can be classified into two main groups based on microstructure and mechanical properties (figure 1.1).

Cortical (or compact) bone, which consists of dense highly mineralised tissue is normally found on the outside of bones and has the highest tensile and loading strength. It has a mineral content of 80-90% and its main purpose is to provide stability to the body and to protect the underlying tissue (Wilkinson 2001; Marieb 2004; Shapiro 2008).

The inner part of the bone, however, has a totally different shape and function. The so-called cancellous (or spongy) bone is the more biologically active part; its structure is highly porous and it has a mineral content of around 15-25%. The remaining volume is made up of a highly vascularised network that contains the red bone marrow and the bone marrow stroma.

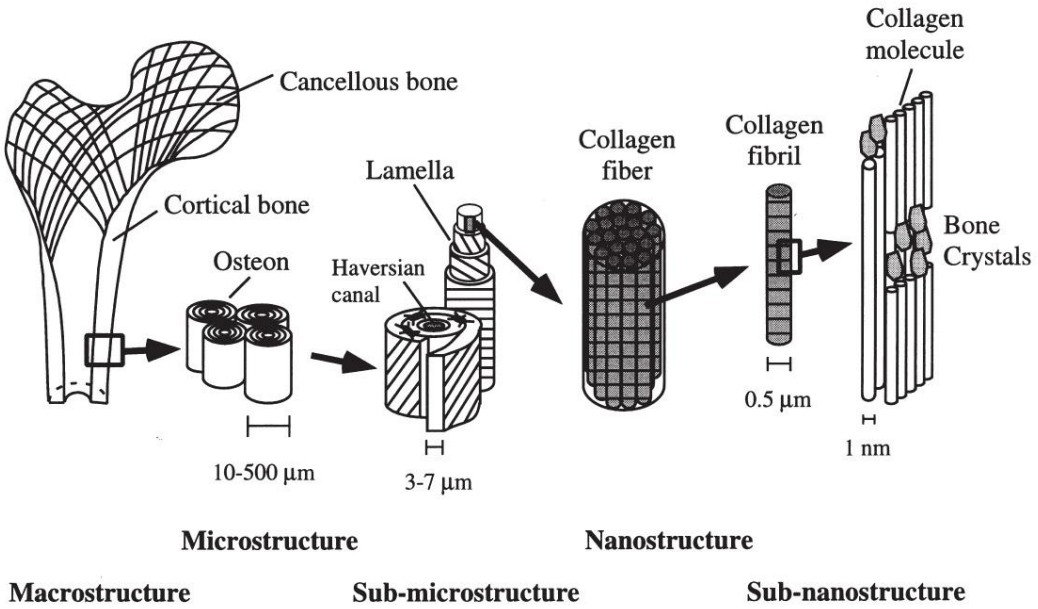

Figure 1.1: Hierarchical structure of bone, as shown by Rho et al. (Rho et al. 1998).

Bone formation starts during the foetal stage of development by two different processes. Flat bones such as the clavicles and the cranial bones will form directly from fibrous tissue; this process is known as intramembranous ossification. Clustered mesenchymal progenitor cells that are embedded in a matrix of fibrous tissue undergo osteogenic differentiation and become osteoblasts; this cluster is referred to as an ossification centre.
Subsequently, the differentiated cells start to secrete organic bone matrix, or osteoid, that precedes tissue mineralisation and deposition of calcium phosphates. In the later stages osteoblasts will become surrounded by mineralised matrix and differentiate into osteocytes (Marieb 2004).

A second process by which bone formation can take place is endochondral ossification (figure 1.2). Hereby, bone is not formed directly from fibrous tissue, but in a two-step process with a hyaline cartilage intermediate that serves as a template for the final shape of the bone. After the cartilaginous template has formed, endochondral ossification begins when the periosteum surrounding the template starts to revascularise (Marieb 2004; Shapiro 2008; Van Blitterswijk 2008).

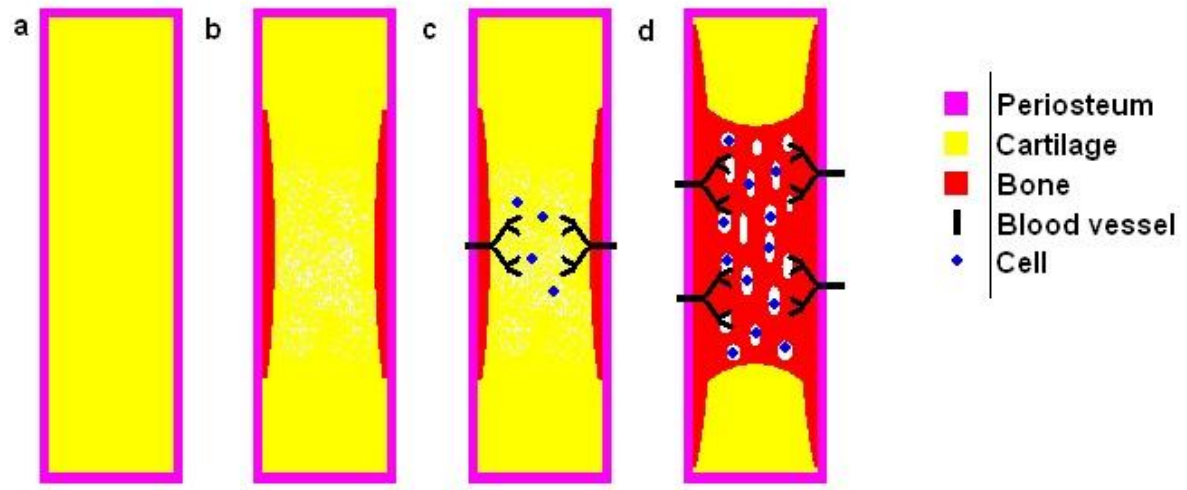

Figure 1.2: Schematic representation of endochondral bone formation from a cartilage template. (a) Periosteum surrounds the cartilage matrix which initiates the formation of bone tissue. (b) Bone collar is formed and the 'entrapped' cartilage becomes hypoxic. (c) The cartilage matrix is partially digested and revascularises, enabling osteoprogenitor cells to migrate towards the centre. (d) The progenitor cells differentiate and the cartilage matrix is gradually replaced by cancellous bone (Van Grunsven 2010).

The resultant increase in nutrient availability causes the stem cells in the periosteum to differentiate into the osteogenic lineage and to start forming a mineralised 'collar' of cortical bone around the template. This collar will cut off nutrient diffusion to the centre of the template, resulting in chondrocyte hypertrophy and the secretion of Vascular Endothelial Growth Factor (VEGF), and Matrix Metalloproteinase-13 (MMP-13) (Kronenberg 2003; Mackie et al. 2008; Van Blitterswijk 2008).

In the latter stage the hypertrophic chondrocytes die and the inner cartilage matrix deteriorates. VEGF and MMP-13 in the remaining matrix act as the central factors in restoring the potential for cell proliferation, and therefore, ossification; cartilaginous matrix is partly degraded and blood vessel formation is induced. These processes are essential for the supply of nutrients and the migration of osteoprogenitor cells which will eventually lead to the formation of cancellous bone with cavities suitable for the red marrow cells to reside in (Kronenberg 2003; Mackie et al. 2008; Van Blitterswijk 2008).
This process takes place during late gestation or shortly after birth. Complete ossification of the epiphyses or growth plate can continue until early adulthood with only the joints retaining the cartilage phenotype (Kronenberg 2003; Van Blitterswijk 2008).

1.1.3 Bone remodelling and homeostasis

Bone is often incorrectly perceived to be a relatively static tissue which after its initial formation remains unchanged for a long period of time. This is, however, not the case as both cancellous bone and cortical bone undergo continuous remodelling by a highly regulated process of bone formation and resorption.
The cells that are mainly responsible for bone formation are osteoblasts; these are small cuboidal cells that are mostly found lining the bone surface. They formed by differentiation of multipotent progenitor cells that reside in the bone marrow stroma. Hereafter, these cells will be referred to as Bone marrow-derived Multipotent Stromal Cells (BMSCs), but the term Mesenchymal Stem/Stromal Cell (MSC) is also commonly used. The steps in which the process of differentiation takes place is not entirely clear, but differentiation to a mature osteoblast seems to be preceded by differentiation into an intermediary stage called osteoprogenitor or pre-osteoblast stage. Differentiation into osteoprogenitor cells is triggered by growth factors such as Bone Morphogenetic Proteins (BMPs) and Fibroblast Growth Factor (FGF); the stage itself is characterised by loss of multipotency while retaining the

ability to divide and by the expression of the transcription factor RUNX2, which is absent is mature osteoblasts (Komori 2002).

Once a cell has become an osteoblast its main function is to synthesise the proteins that are important for bone formation and mineralisation. The most important proteins are Type I Collagen (Col1), Osteocalcin (OC), Osteonectin (ON), Osteopontin (OP, also known as Bone Sialoprotein 1, BSP1) and Alkaline Phosphatase (ALP). All these proteins have a role in either the production of the osteoid, the organic predecessor to bone tissue, or the mineralisation of osteoid by deposition of hydroxyapatite. A direct result of osteoid mineralisation around groups of osteoblasts is that the cells become trapped and will have little access to nutrients. In this stage the majority of the entrapped cells will die and in the remainder of the cells the metabolic activity will decrease dramatically and they will become osteocytes. Although osteocytes no longer produce large amounts of bone forming proteins they remain active in regulating bone homeostasis and can remain active for many years after terminal differentiation (Aubin et al. 2000; Chambers 2000).

In healthy adult humans, the rate of bone formation should be equal to the rate of bone resorption. The main cell type responsible for bone resorption is the osteoclast. Whereas bone forming cells originate in the bone marrow stroma osteoclasts are formed through the monocyte/macrophage lineage of the haematopoietic stem cells in the red bone marrow (Van Blitterswijk 2008). When attached to bone they have a very distinctive ruffled (Wilkinson 2001; Currey 2002) border on the side where the bone resorption takes place. As bone can be seen as a composite consisting of an organic (mostly collagen) and an inorganic (mineral) phase, osteoclasts have two distinct processes to break down bone tissue. Firstly, the pH of the fluid between the osteoclast and the bone is reduced to around 4 so that most of the mineral is gradually dissolved. Secondly, collagen is removed by the release of several enzymes such as tartrate resistant acid phosphatase, MMPs and cathepsin K. Although bone resorption is mainly regulated by systemic factors such as parathyroid hormone and vitamin D3 entrapped osteocytes also seem to play an essential role in the activation of osteoclasts. This was confirmed by the discovery that bone resorption by osteoclasts does not take place unless osteocytes are present and by the fact that mature osteoclasts do not have receptors for several important regulators of bone resorption (Wilkinson 2001).

1.1.4 Bone repair

Bone damage is a common injury which is usually the result of a high energy impact or excessive stress. Damage to bone tissue normally elicits a complex response of increased cell proliferation and differentiation, matrix deposition and growth factor release that results in bone formation and immobilisation of the fracture site.

The normal process of bone healing starts with an inflammatory phase. A haematoma will form at the site of the fracture as a result of damage to the surrounding vasculature. Over time the haematoma will become increasingly fibrous and serve as a matrix in which cells from adjacent tissues can proliferate and differentiate (Marieb 2004; Shapiro 2008).

In the next phase, usually called the repair phase, the initially formed fibrous tissue is gradually removed and replaced. This phase is highly dependent on the stability of the site of the fracture and the forces acting on the newly formed tissue. The two main routes through which bone regeneration can take place are direct (non cartilage-mediated) bone formation and endochondral (cartilage-mediated) bone formation.

If the developing tissue is well stabilised and the site is shielded from excessive force, repair may take place by direct bone formation. In this case bone tissue forms directly inside the fibrous tissue. Direct bone formation will result in the formation of mostly lamellar bone with an orientation parallel to the bone axis (Shapiro 2008).

Figure 1.3: Radiographs showing a displaced mid-diaphyseal humeral fracture. Top: three weeks post-injury, callus has formed and endochondral repair is ongoing, bottom: one year post injury, stable fixation with excellent remodelling and removal of all excessive callus (Shapiro 2008).

However, in the case of fractures which experience movement as a result of external forces, bone repair will usually take place through the endochondral route (Figure 1.3). In this situation the centre of the fibrous tissue will have impaired vascularisation leading to hypoxic conditions and the formation of a cartilage-like matrix. The cartilaginous tissue will not only give the fracture more stability compared to the fibrous matrix, the cells inside the matrix will also develop over time into a hypertrophic phenotype and release growth factors (such as VEGF and MMP-13) that are essential for revascularisation of the tissue. This combination of stability and restored blood supply has now created favourable conditions for bone formation inside the deteriorating cartilage matrix. Finally, the new bone tissue will gradually be remodelled; this remodelling phase results in a transition of the initially formed woven bone to lamellar bone. It also involves the removal of excessive callus and results in an increase in the strength of the tissue up to a level near its original strength (Mackie et al. 2008; Shapiro 2008; Van Blitterswijk 2008).

1.1.5 Mechanics

Healthy bone is, like many tissues in the human body, highly adaptive and it has the capacity to sense a variety of signals and to adapt its structure as a result. One of the most important stimuli that bones react to is mechanical force; this can be in the form of compression, tension, bending or torsion. In highly simplified terms, bones will react to mechanical forces by increasing their mineral density, causing an increase in stiffness and strength, whereas the absence of significant mechanical loading will result in a decrease in bone density (Currey 2002). Figure 1.4 shows a typical stress-strain curve for the uniaxial compression of human cancellous bone.

Research into the mechanical properties of bone is far from straightforward and an extremely high variability exists in the results found in literature with in some cases a more than ten-fold difference between mechanical properties measured using different experimental designs. Table 1.1 shows an overview (compiled by Rho et al.) of the stiffness of cancellous bone measured by different researchers and different experimental conditions (Rho et al. 1998). However, some of these methods (such as nanoindentation) appear to measure the properties of the solid mineral rather than cancellous bone as a porous composite; this might explain the higher values obtained for the stiffness.

Table 1.1: Overview of the different test methods used to determine the elastic modulus of cancellous bone (Rho et al. 1998).

Source	Test method	Estimate of elastic modulus (GPa)
Wolff (1892)	Hypothesis	17–20 (assumption)
Runkle and Pugh (1975)	Buckling	8.69±3.17 (dry)
Townsend et al. (1975)	Inelastic buckling	11.38 (wet)
Williams and Lewis (1982)	Back-calculating from FE models	1.30
Ashman and Rho (1988)	Ultrasound test method	12.7±2.0 (wet)
Ryan and Williams (1989)	Tensile testing	0.76±0.39
Hodgskinson et al. (1989)	Microhardness	15 (estimation)
Kuhn et al. (1989)	Three-point bending	3.81 (wet)
Mente and Lewis (1989)	Cantilever bending with FE analysis	7.8±5.4 (dry)
Choi et al. (1990)	Four-point bending	5.35±1.36 (wet)
Rho et al. (1993)	Tensile testing	10.4±3.5 (dry)
	Ultrasound test method	14.8±1.4 (wet)
Rho et al. (1997)	Nanoindentation	19.6±3.5 (dry):longitudinal direction 15.0±3.0 (dry): transverse direction

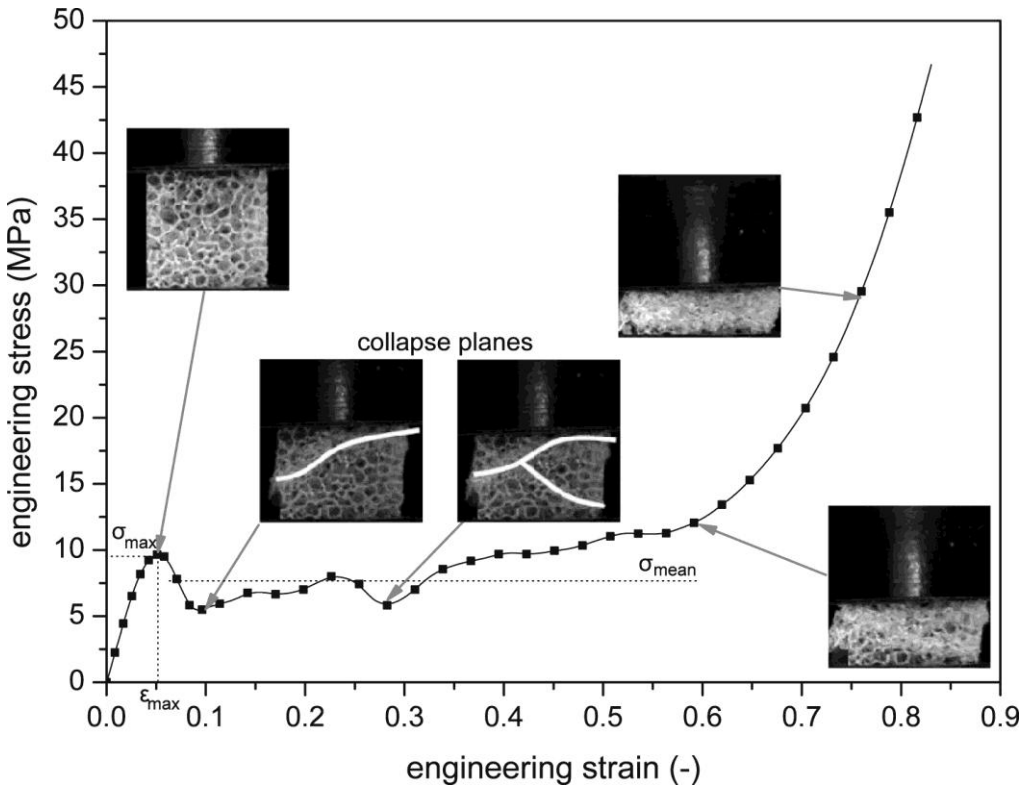

Figure 1.4: Stress-strain curve of the uniaxial compression of cancellous bone as measured by Halgrin et al. (Halgrin et al. 2012). The initial slope (0 – 0.05) represents the elastic region, which, in an ideal situation, is entirely reversible. The strain region between 0.05 and 0.6 shows the collapse of different planes in the sample; in the case of a uniform foam the fluctuations in the stress should be small in this region. The region above 0.6 shows the transition towards compression of a dense material after the porosity has entirely disappeared as a result of compression.

At a cellular level, the process of bone strengthening and weakening as a result of mechanical forces is to a large extent controlled by the cell types discussed in 1.1.3. Although bone appears to be highly rigid, on the micrometre scale external forces can still cause small deformations which, because of its porous structure, causes fluids to be squeezed through the canalicular network. Osteocytes, embedded in their own bone matrix, will normally sit at the junctions of this canalicular network and will therefore experience these deformations as fluid shear stress on their cell membrane (Currey 2002; Delaine-Smith 2013).

There are various theories about the mechanism by which osteocytes sense these stresses, but it is clear that the shear stresses result in the initiation of signalling pathways that affect osteoblast and osteoclast activity and therefore the ratio between bone formation and resorption. Factors that have been identified in signalling in response to loading are nitrous oxide (NO), prostaglandin E2 (PGE2) and cyclic adenosine monophosphate (cAMP) (Johnson et al. 1996; Delaine-Smith et al. 2012).

1.2 Implants

Adequate functioning of bone and cartilage is essential for many basic bodily functions, such as locomotion. However, many conditions exist where these normal functions deteriorate (e.g. increasing age) and medical intervention is desirable.

One of the most common causes of joint dysfunction, especially in older patients, is Degenerative Joint Disease (DJD), also known as Osteoarthritis (OA) (see box) (Sellam et al. 2010). According to Arthritis care UK, DJD is estimated to affect around 10 million people in the UK (16%) (Arthritis Care UK). In the literature, the terms DJD and OA refer to a broad range of symptoms and causes and there is little consensus regarding one universal definition. In highly simplified terms, they could be defined as any condition related to the deterioration of articular cartilage at the surfaces of joints (Koopman et al. 2005; Moskowitz et al. 2007).

Terminology

In the medical literature several terms are used to refer to degenerative joint disease. Most commonly the word ‘osteoarthritis’ is used which, because of the suffix –itis, emphasises the inflammatory nature of the disease, although it is not necessarily its main cause. ‘Degenerative joint disease’, is pathologically more accurate, as it refers to the degenerative aspect. Other terms such as ‘osteoarthrosis’ (-osis indicates more general abnormalities) or ‘degenerative arthritis’ (referring to both causes) are not commonly used (Koopman et al. 2005; Sellam et al. 2010).

Although one direct cause for DJD is normally difficult to ascertain, numerous factors have been identified to date that increase the risk or speed up the process of DJD. Generally accepted factors include age, gender, obesity, muscle weakness, genetic factors, infections and injuries to the joint (Arthritis Care UK; Arthritis Foundation; NHS ; Beck et al. 2005; Koopman et al. 2005; Moskowitz et al. 2007).

As the problem of repairing damaged or resorbed articular cartilage has not been solved to date, there is currently no treatment for DJD that is able to restore the original state of a joint (figure 1.5). However, many treatments are widely practised that aim either to slow down or stop the progression of DJD, or to alleviate symptoms of DJD, such as pain and reduced mobility.

Although some of the aforementioned risk factors are determined at birth and cannot be altered, other factors, such as obesity and muscle weakness, are partially determined by lifestyle and can therefore be manipulated in order to reduce symptoms of DJD. One study that investigated the effects of diet and exercise on pain associated with DJD found a small reduction in pain as a result of modulation of individual parameters, but only a significant decrease when the two were combined (Messier et al. 2004; Moskowitz et al. 2007).

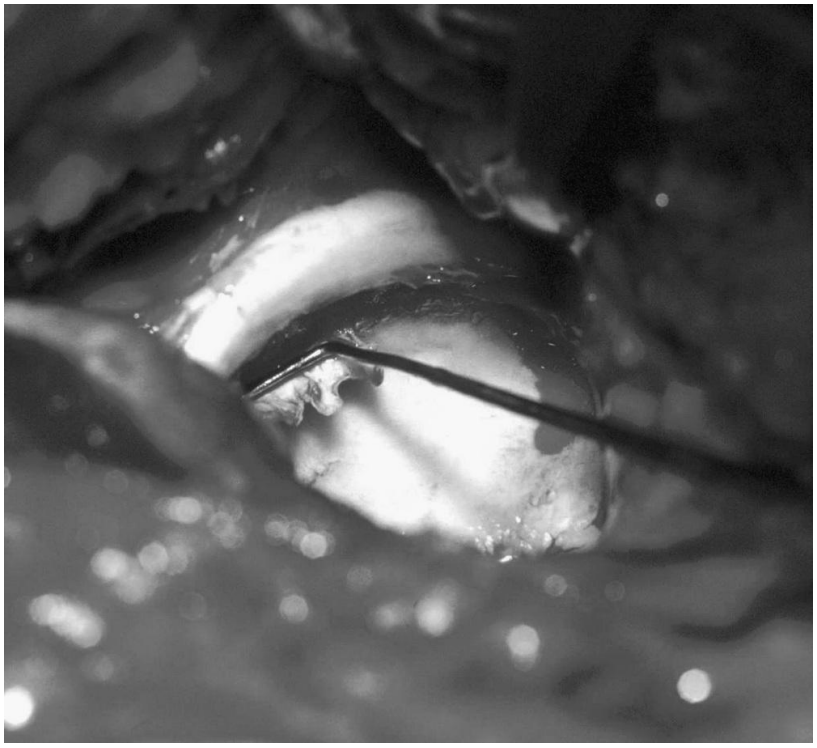

Figure 1.5: Intra-operative photograph of the acetabulum. A part of the articular cartilage is separated from the underlying bone and can be lifted with a probe (Beck et al. 2005).

Interpreting data concerning DJD and obesity is complex (Lübbeke et al. 2009; Niu et al. 2009). However, a 2009 meta-analysis that investigated the incidence of co-morbidity of obesity and twenty medical conditions found that both overweight and obesity cause an increased risk of osteoarthritis (Guh et al. 2009).

Various medicinal and pharmacological treatments exist for different stages of DJD, mostly with an analgesic, anti-inflammatory, or antipyretic function. Regular analgesics can be either systemic, such as ibuprofen or acetaminophen, or topical such as rubs, creams or ointments. Furthermore, a number of non-steroidal anti-inflammatory drugs (NSAID) are widely used because of their anti-inflammatory and analgesic properties. However, most NSAIDs have adverse effects on other body systems, for example, the kidneys, the gastrointestinal tract, or the heart, and their efficacy can be highly patient specific. Lastly, although generally avoided in the long term, opioids are sometimes used in patients with unrelenting pain that cannot be relieved by other types of medication (Messier et al. 2004; Moskowitz et al. 2007; O'Neil et al. 2012).

1.2.1 Arthroplasty

If, however, these conservative treatments appear to be ineffective or insufficient, arthroplasty can be undertaken. Arthroplasty is most commonly associated with osteoarthritis, but can also be used for severe cases of other diseases, e.g. osteoporosis (because of the increased risk of fractures at the neck of the femur), rheumatoid arthritis, avascular necrosis, and other conditions affecting bones or cartilage that cannot be treated in a non-invasive manner. Arthroplasty, in its broadest sense, is any operation aiming to improve the condition of a joint, e.g. to alleviate pain or to restore movement or function of the joint (Canale 1998). Common examples of arthroplasty include lavage, debridement, osteotomy, and (total) joint replacement (Lützner et al. 2009).

The first instances of arthroplasty were reported as early as the first half of the nineteenth century when surgeons attempted to restore joint movement in patients suffering from ankylosis simply by resecting the affected joints. Although mobility of the joints usually decreased over the years following the osteotomy, this procedure proved to be a significant improvement of the quality of life in terms of pain and mobility of the joint (Eftekhar 1978).

The latter half of the nineteenth century saw the rise of interpositional arthroplasty, in which a range of both biological and inorganic materials were applied on the articulating surfaces in order to prevent the recurrence of bone growth. These ‘interpositioning’ materials included

muscular tissue, fibrous tissue, decalcified bone, celluloid, rubbers, and metals (e.g. gold, silver, zinc, and magnesium). As with the patients with resected joints, ankylosis returned in many cases and lasting mobility was not obtained (Eftekhar 1978).

In the first half of the twentieth century, interpositional arthroplasty was further developed using more advanced materials (with the cobalt-chromium mould developed in 1936 by Smith-Petersen being a notable clinical success (Smith-Petersen 1948)), but also saw the development of replacement arthroplasty, where prosthetics were used to replace bone . The earliest reports of the use of prosthetics to replace the femoral head date back to the 1920s, but the first widespread application came with the development of a polymethylmethacrylate (PMMA) implant by the Judet brothers in 1948 (figure 1.6). In the years following, a large number of novel implants were developed using both metals and polymers that were used to replace one side of the joint and to articulate with the healthy or less affected side of the joint. However, in most cases of osteoarthritis will at some stage affect both sides of the joint and therefore failure rates remained high (Eftekhar 1978; Canale 1998; Learmonth et al. 2007).

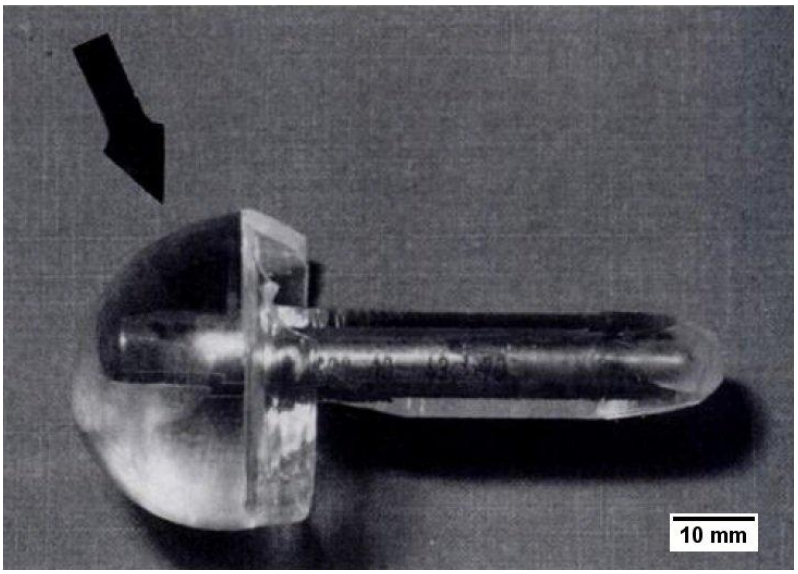

Figure 1.6: Image of a reinforced Judet implant retrieved from a patient in 1993, forty years after implantation, by Hettfleisch et al. (Hettfleisch et al. 1994).

Total joint arthroplasty

A logical solution to the difficulties associated with so-called hemiarthroplasty, was to implant fitted prostheses to replace both sides of the joint. Experiments with the technique of Total Joint Arthroplasty (TJA) using a metal-on-metal interface took place in the 1940s and

50s, but resulted in high interfacial friction and a severe inflammatory response to wear debris (Eftekhar 1978).

Sir John Charnley, one of the pioneers in this field, is credited with developing a theory on low-friction arthroplasty that would revolutionise thinking on implant composition and design. He speculated that the 'squeaking' of many existing implants might be due to a difference in friction coefficient between the metal-on-metal interface and articular cartilage. A hip arthroplasty with low-friction materials, such as polytetrafluoroethane (PTFE) (Charnley 1961; Long et al. 1998), initially showed promising results, but eventually failed due to necrosis of the femur and increased friction as a result of a sticky substance which was deposited at the joint interface (Eftekhar 1978; Canale 1998; Learmonth et al. 2007).

Following these findings, research went on to search for a further reduction of interfacial friction by reducing the diameter of the joint and using a metal-on-polymer interface; initially PTFE was used, but this material was later replaced by high-density polyethylene or ultrahigh molecular weight polyethylene. Although initially met with scepticism, application of the Charnley-arthroplasty gained almost universal acceptance around 1970. This work, together with his work on cementing of implants (Charnley 1960; Charnley 1965) and improvement of aseptic conditions during operations (Garvin et al. 1995), made Sir John one of the great orthopaedic surgeons of the twentieth century (Eftekhar 1978).

Types of implants

Currently, many joints can be treated for DJD or other conditions by means of arthroplasty (figure 1.7). The joints on which (total) joint arthroplasties are currently performed are listed below (Canale 1998).

- Knee: The first modern hinged implants were developed in the 1950s (Shiers 1954; Canale 1998). Nowadays, total knee arthroplasty is the most widely performed arthroplasty in the UK with around 91,000 operations reported to the UK's National Joint Registry (NJR) in 2012 (figure 1.8) (National Joint Registry 2013). These operations can be either constrained or unconstrained, with constraint being defined as the effect of the elements of knee implant design that provides the stability required to counteract forces about the knee after arthroplasty in the presence of a deficient soft-tissue envelope (Hwang et al. 2010).

- Hip: Total hip arthroplasty was popularised in the 1960s by Charnley. It is also a widely performed operation with good long-term results.
- Ankle: Both constrained and unconstrained arthroplasties were developed in the 1970s, but neither treatment showed successful clinical outcomes. To date, there is still debate on the use of either arthroplasty or arthrodesis as the optimal treatment for arthritis of the ankle (Haddad et al. 2007; Singer et al. 2013).
- Shoulder: Defects to the upper limb that require arthroplasty are much less common than those in weight bearing joints and are therefore not as well documented in literature. Although different designs exist, the most clinically successful total shoulder arthroplasties are performed using the unconstrained type similar to the one that was first developed by Neer et al. in 1973 (Neer et al. 1982).
- Elbow: Early designs of fully constrained metal-on-metal elbow joints were developed as early as the 1940s, but most modern implants of either the semi-constrained or unconstrained design were developed from 1975 onwards (Canale 1998).

Although all these operations all being carried out, hip and knee replacements form the vast majority of arthroplasties with the other three joints combined accounting for only around 1.5% of the total number of arthroplasties in 2012 (figure 1.8).

Figure 1.7: Images of widely used commercial implants for TJA. a: ankle (Depuy mobility, CoCr), b: elbow (Coonrad Morrey, Zimmer, Ti6Al4V), c: hip (Exeter, Stryker, Stainless steel), d: knee (Sigma, DePuy, CoCr), e: shoulder (Biomet Copeland, Ti6Al4V).

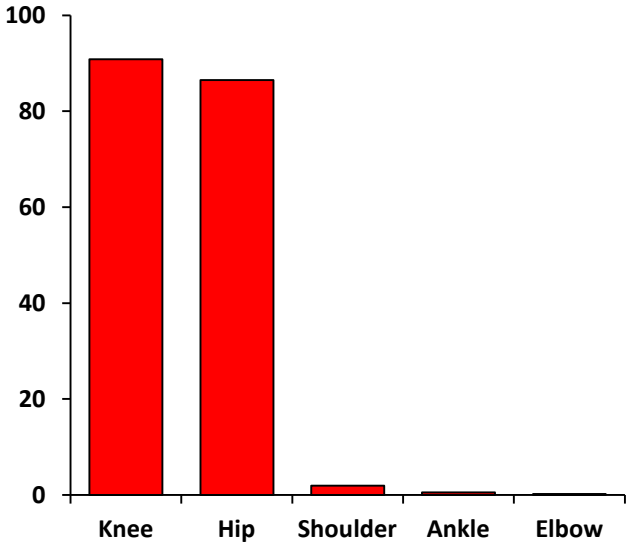

Figure 1.8: Number of TJAs (×1000) carried out in England, Wales and Northern Ireland in 2012 that were reported to the NJR (National Joint Registry 2013).

Apart from arthroplasty there are several other procedures where metal implants are commonly used for the treatment of bone-related conditions, the most common ones being plates and screws used to stabilise long bone defects, dental implants and implants for spinal fusion.

1.2.2 Bone-implant interfaces

Throughout the history of endosseous implants, adequate attachment of the implant to the surrounding tissue has always been a pivotal factor in its long-term success rate. During arthroplasty the articulating parts of the bones are removed, followed by reaming of the bone marrow to create space for the implants (figure 1.9). Fixation of the implants depends on the bond that is formed between the non-articulating surfaces of the implants and the surrounding cancellous bone.

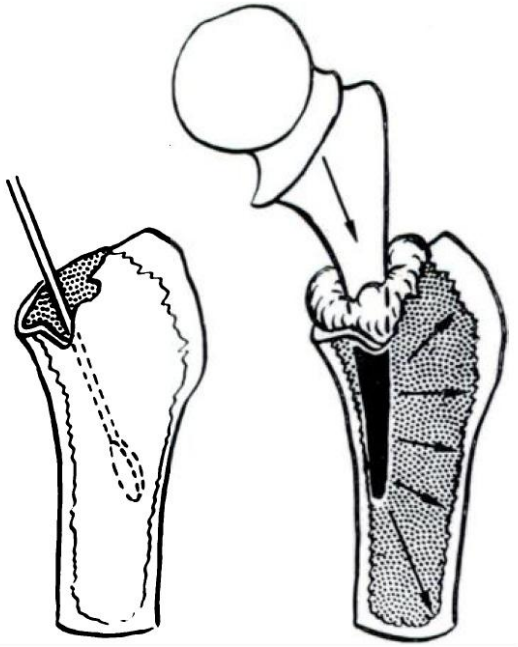

Figure 1.9: Charnley's diagram of a cemented femoral hip implant (Charnley 1960).

The terms osseointegration and bone ingrowth are often used interchangeably to describe the quality of a biomaterial-implant interface. Hereafter, *osseointegration* will be used to describe the attachment of bone tissue to the surface of a material; *bone ingrowth* will refer to the formation of bone tissue inside the pores or voids of an implant.

The two strategies used to ensure sufficient osseointegration are cemented and non-cemented implants. Both strategies have been used for several decades and have shown many improvements over the years.

Cemented implants were used as early as the mid-twentieth century, but only as an auxiliary measure to the press-fit fixation; low amounts of cement were used on implants that precisely fit into the hole in the femur. Later strategies showed considerable improvement in loosening rate when larger holes were drilled and higher volumes of cement were used to fill the space between the bone and the implant (Charnley 1965; Eftekhar 1978).

Currently, more than 30 types of cement are approved for use in the UK by the Medicines and Healthcare products Regulatory Agency (MHRA) (Lewis 2008). The cements used for fitting implants are based on polymethylmethacrylate (PMMA), also known as acrylic cement. Most formulations include: prepolymerised PMMA powder, a liquid mixture of methylmethacrylate monomer and stabiliser, radiopacifiers (such as $BaSO_4$ or ZrO_2), and initiator (e.g. benzoyl peroxide).

Although cemented TJA was the first method to show good reproducible results and is still widely practised throughout the world, there are many drawbacks associated with the use of PMMA cement. Lewis summarised the common causes for mechanical failure of cemented implants (Lewis 2008; Panesar et al. 2009). In the following years, Goldring et al. investigated explanted fibrous tissue surrounding loosened cemented implants and found that the tissue contained factors associated with osteolysis, suggesting that micromotion can trigger a vicious circle of bone resorption and further loosening of the implant (Goldring et al. 1983).

Because of many drawbacks associated with the use of PMMA-based cement (as summarised by e.g. Gruen et al. and Lewis (Gruen et al. 1979; Lewis 2008)) and because of significant loosening rates, especially in young, active patients, many orthopaedic surgeons prefer the use of non-cemented implants. In a non-cemented implant osseointegration takes place directly at the surface of the implant and therefore, these implants require highly specific surface properties (Learmonth et al. 2007; Lewis 2008).

The question of whether to use cemented or non-cemented implants for TJA is an area of ongoing debate; different studies have shown varying results and a 2013 meta-analysis showed "similar, if not better" results for cemented TJA with no significant differences in mortality and post operative complication rate and inconclusive long term results. According to the 2012 report of the NJR the vast majority of knee replacements in England and Wales are cemented (86% cemented, 3% non-cemented) while for the hip replacements the non-cemented implants are slightly more common (33% cemented, 43% non-cemented); for the remainder of the procedures 'hybrid' implants are used where one of the components is cemented and the other is non-cemented (Parker et al. 2010; Abdulkarim et al. 2013; National Joint Registry 2013).

Different rationales exist for achieving optimal osseointegration in non-cemented implants, but many, if not all, aim to mimic to some extent the surrounding bone, either structurally or chemically. Two widely used methods are to create implants that have a textured or porous superficial layer, or to coat the implant with minerals such as hydroxyapatite or other calcium phosphates (figure 1.10).

Figure 1.10: Non-cemented vs. cemented implants; two brands that are widely used for TJA. Top: hydroxyapatite-coated non-cemented implant, bottom: implant for cemented arthroplasty.

Coated implants

The use of calcium phosphates in orthopaedic surgery has been widespread for many years but was generally deemed unsuitable for TJA because of low resistance to fatigue (Canale 1998). The situation changed in 1988 when Geesink et al. described the technique of plasma coating in which metal bone implants could be covered with a layer of 50 µm hydroxyapatite (Geesink et al. 1988). Subsequently, they showed that these coated implants show an enormous increase in osseointegration (up to a 100-fold increase in interfacial strength in push-out tests, compared with non-coated implants. A layer thickness of 50 µm was chosen because a layer with a lower thickness may resorb completely during osseointegration and layers with a higher thickness have a higher chance of failure due to fatigue) (Geesink et al. 1988).

In the late 1980s, the first coated hip implants were used in the clinic (Furlong et al. 1991; D'Antonio et al. 1992; D'Antonio et al. 1992; Geesink et al. 1995). Furlong et al. were able to explant coated implants at different timepoints shortly after implantation and showed excellent early bone formation at the interface (Furlong et al. 1991). They also stated that hydroxyapatite coatings stimulated primary bone formation, whereas with metal surfaces fixation is achieved by bone ingrowth into fibrous tissue (Furlong et al. 1991).

In the following years, short-term and long-term follow-up studies have been widely reported. A 10-year follow-up, published in 2001, showed excellent long-term results for

hydroxyapatite coated femoral stems compared to most alternatives (D'Antonio et al. 2001), but less favourable results were obtained with coated implants to replace the cup of the joint (Manley et al. 1998).

The use of hydroxyapatite implants for total knee arthroplasty has also been evaluated. In 1999, Nilsson et al. published a comparative study of postoperative migration of cemented and coated tibial implants to predict the chance of aseptic loosening (Nilsson et al. 1999). It was found that tibial implants coated with hydroxyapatite show significantly higher migration rates in the short-term (<1 year), but then stabilised, while the cemented implants subsided more slowly over longer periods of time. As a result, no significant difference in implant migration was found after five years (Nilsson et al. 1999).

Long-term results were evaluated by Epinette et al. who investigated knee implants with both partially coated and fully coated stems after 10 to 15 year by clinical and radiological assessment (Epinette et al. 2007). The results showed that both implants had high survival rates and that radiolucencies at the coated interface were rare, indicating that bone had formed directly at the implant-tissue interface without a (radiolucent) layer of fibrous tissue (Epinette et al. 2007).

1.3 Porous metals

Porous metals, also known as metal foams, are an extremely versatile class of materials which have been studied for their physical, mechanical, thermal, electrical and acoustic properties (Ashby et al. 2000). They combine the favourable properties of metals, such as high stiffness and strength, durability and thermal and electrical conductivity, with 'foam-properties' such as low density, permeability to fluids and high surface area (Goodall et al. 2014).

1.3.1 Classification

As for many types of materials, classifying porous metal can be difficult and different authors have described different classification methods for porous metal, examples include fabrication method, structure, mechanical properties and applications. Goodall et al. made a classification based on structure and defined the following five categories (Goodall et al. 2014):

Isolated porosity. These are metal foams with a low volume fraction of porosity, and most commonly consists of randomly distributed pores which, due to their low volume fraction, are likely to be mostly isolated. These foams have a very small number of applications and are in many cases considered to be a defect caused during processing.

True metal foams. This type could be seen as a foam that most resembles people's everyday perception of a foam, i.e. (near) spherical pores which are closely packed together separated by thin walls of metal. These foams are characterised by a high volume fraction and surface area of porosity while maintaining a closed-cell architecture. Due to the inherent instability of the metal walls in the liquid phase producing such a foam with a uniform density and a uniform pore volume is highly problematic, although a few commercially available foams of this type exist.

Precursor based metal foams. Metals are usually much more difficult to process than many other materials; therefore, using a precursor foam can be an attractive option when producing uniform open-cell metal foams. One common method to create the metal foam from its precursor include a two-step method whereby infiltration is used to create a 'negative' or mould which is subsequently infiltrated by liquid metal giving it the shape of the original foam. Alternatively, metal can be directly deposited onto the surface of the precursor foam.

Particle packing. This is another commonly used method for making metal foams that is relatively simple from a manufacturing point of view. The method of packing particles together to create a metal foam can be employed in two ways. Firstly, metal particles can be directly packed together and sintered together to create a stable metal foam. Secondly, a negative of a typical packed-particle foam can be created by packing of a removable phase. Both methods are extremely versatile and there are many processing routes to create packed-particle type structures.

Lattices. An ideal lattice can be defined as a porous material consisting entirely of a defined (i.e. non-stochastic) unit cell. Production of these types of foams is usually less straightforward than stochastic foams, but their high reproducibility can be an attractive property for many applications. Common fabrication techniques for metal lattices include casting, weaving, bonding of metal sheets and additive layer manufacturing.

1.3.2 Mechanics

Metals and alloys have a combination of mechanical properties that make them attractive for a wide range of applications; they usually combine high strength and a relatively high stiffness with the ability to deform significantly before failure. In many cases, the main reason to use a metal foam instead of solid metals or alloys will not be because of these mechanical properties, but because of reasons such as weight reduction, cost reduction or high surface area.

There are many methods of determining the mechanical properties of a foam, but a common and simple test is the compression test to determine a stress-strain curve, which, in turn, can be used to calculate properties such as the Young's modulus and the yield strength. Gibson and Ashby (Gibson et al. 1997) gave the following schematic representations of stress-strain curves of foams (figure 1.11).

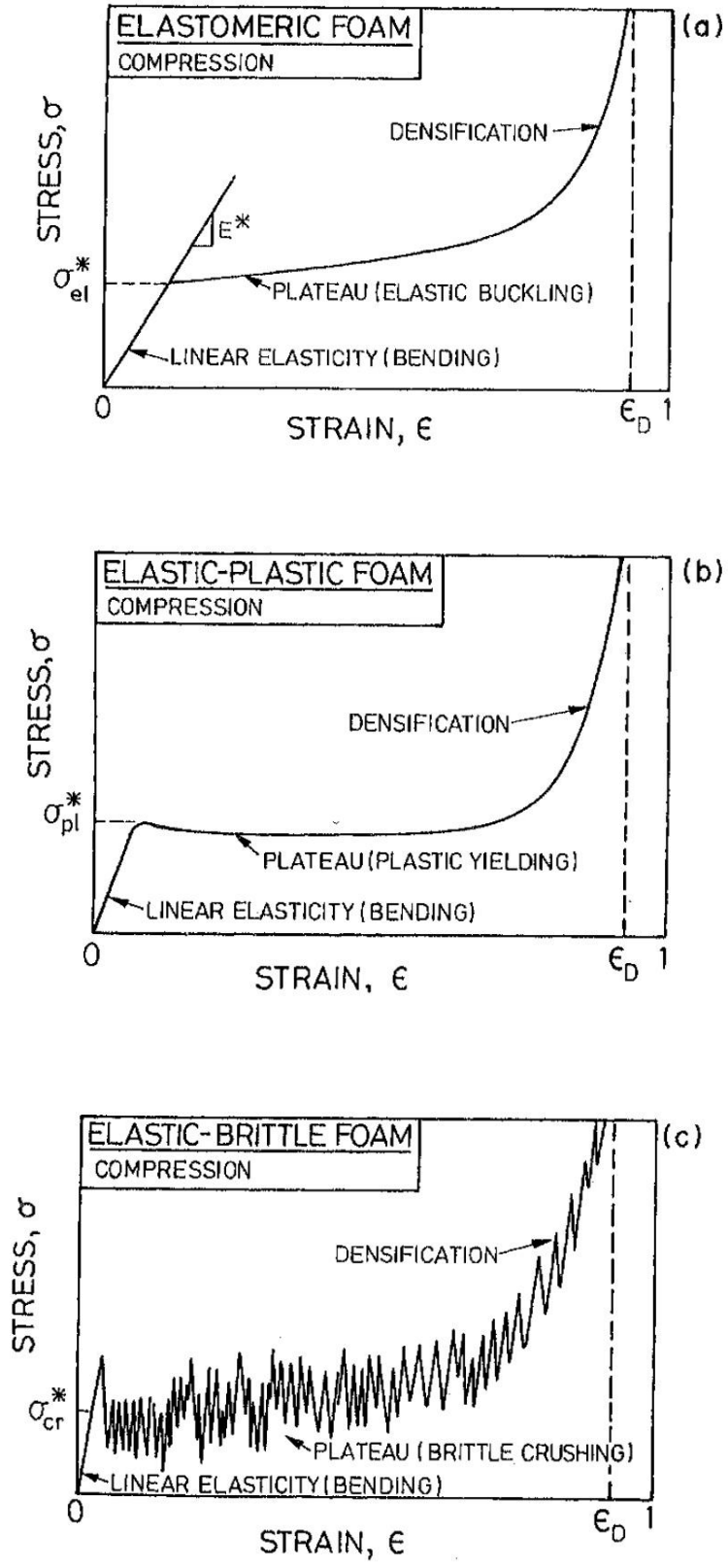

Figure 1.11: Schematic representation, as shown in Gibson and Ashby, of stress-strain curves for the compression of different types of foams (Gibson et al. 1997).

In these idealised curves, the three indicated areas (linear elasticity, plateau and densification) can be clearly distinguished. However, for real foams, especially metal foams, the stress-strain curves are usually more complex and the three regions might be more difficult to distinguish. When calculating properties such as Young's modulus and yield strength the region that is of interest is the linear region at low strain and before initial failure of the sample. The Young's modulus can be calculated by applying the following formula to the linear elastic region of the stress-strain curve:

Equation 1.1: $E_f = \frac{d\sigma}{d\varepsilon}$

In this formula E_f is the YM of the foam, σ is the stress and ε is the strain. The value for the YM can then be used to determine the point on the stress-strain curve at which the behaviour of the foam starts to deviate for the linear behaviour described by the YM and deformation starts to become irreversible. This point is called the yield point of a foam. There are several methods of defining the yield point of a structure. In the case of materials that have a yield point that appears as a clear angle of deviation from the linear portion of the stress-strain curve defining the yield point is unambiguous. If, however, the stress-strain curves of a certain material do not show this clear angle but start to deviate gradually from linear behaviour defining a yield point becomes more ambiguous. In this case there is the possibility to define the yield point as the point at which the difference between the predicted value (based on linear behaviour) and the actual value exceeds a certain limit. This difference is usually a strain percentage, for example 0.2%; this means that the 0.2% offset yield strength is defined as the stress at which the strain is 0.2% higher than what would be expected based on linear behaviour.

Determining theoretical values of the mechanical properties of a foam is virtually impossible without defining parameters for the architecture of the foam. However, several authors have described laws that limit the properties of foams. However, these laws usually rely on simplified representations of foams or are only applicably at, for example, very high or very low densities.

One law that can sometimes be used to describe the properties of foams is the so-called 'rule of mixtures' or 'slab model', which in its general form describes the behaviour of composites if the properties of the pure materials are known. It states that composites can be simplified to

a slab model whereby the base materials are represented as slabs that can be stacked to form a composite with the same overall composition. The range of possible values for the YM of the original composite can then be determined by calculating the YM of the slab model in longitudinal (lower limit) and transverse compression (upper limit).
This rule of mixtures in its general form only applies to composites. However, there is a second method to use the rule of mixtures to describe foams which is to consider the foam itself as a composite of metal and air. In this model a simplified form of the rule of mixtures can be used to define the maximum stiffness as a function of the relative density (equation 1.2). The equation for the lower limit as defined by the rule of mixtures is not relevant in this case as the Young's modulus for air is zero.

Equation 1.2: $E_f = \frac{\rho_f}{\rho_s} \times E_s$

In this equation E_f is the YM of the foam, E_s is the YM of the solid metal and ρ_f/ρ_s is the relative density of the foam. For foams made solely of Ti6Al4V this would limit the stiffness of the foam to the red line shown below (see figure 1.13 on p. 36) (Goodall et al. 2014).

The bounds given by the rule of mixtures are very broad and the given limits also describe extreme situations for structures that do not resemble a foam in any way. In the case of uniform foams several authors have tried to derive formulas to describe the mechanical behaviour of foams in more detail. However, due to the aforementioned difficulties these laws only aim to describe specific conditions.
A well-known and frequently used example of such a law is the formula given by Gibson and Ashby (G&A model) for the behaviour at low strain of foams that have a relative density smaller than 10% (Gibson et al. 1997). In that situation, they argue, the foam could be modelled by describing a pore as a cubic array of struts of length l and thickness t that are joined by the struts of other pores not in the corners of the pore but in the middle of the struts (figure 1.12).

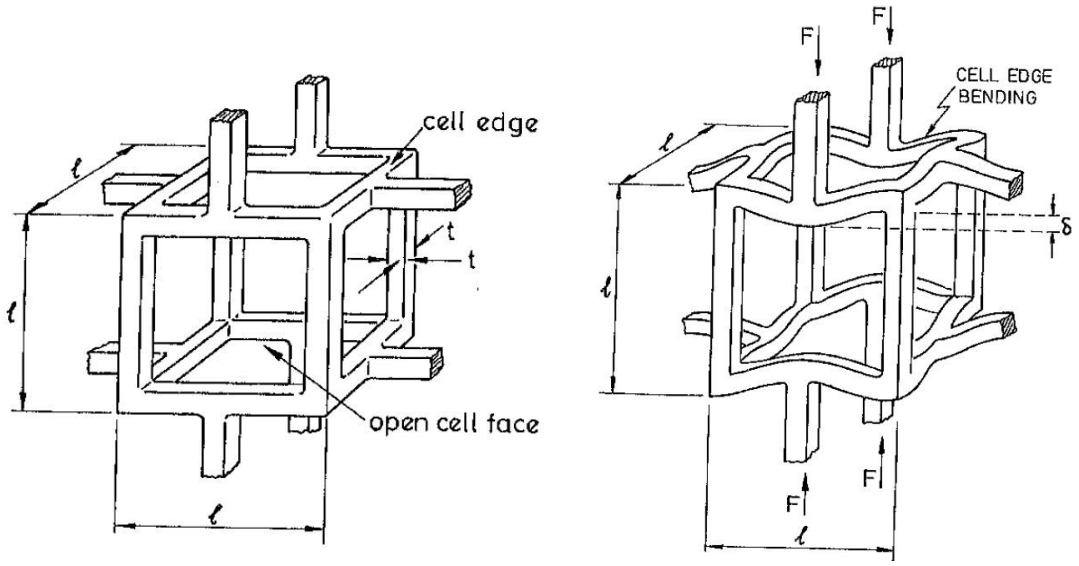

Figure 1.12: The model that was suggested by Gibson and Ashby for the mechanical behaviour of a low density open-cell foam at low strains (Gibson et al. 1997).

As the values for stress and strain are both related to the strut length l (by $F = \sigma \times l^2$ and $\varepsilon = \delta / l$, where F is the force on the foam and δ the deflection of the struts) Eq. 1.1 can be converted to:

Equation 1.3: $E_f = \frac{\sigma}{\varepsilon} = \frac{F}{l \times \delta}$

The deflection δ is given by standard beam theory as $d = (F \times^* l^3) / E_s \times I$, giving:

Equation 1.4: $E_f = \frac{I}{l^4} \times E_s$

where I is the second moment of area of a strut. Both the relative density ρ/ρ_0 and I are related to t and l (by $\rho/\rho_0 = (t / l)^2$ and $I = t^4$) which means that the equation for the relative Young's modulus E_f / E_s can be described as being proportional to the squared relative density as:

Equation 1.5: $\frac{E_f}{E_s} = C_1 \times \left(\frac{\rho_f}{\rho_s}\right)^2$

where C1 is a constant that includes all geometric constants of proportionality. An estimate of the YM of a foam as a function of the relative density is given by the blue line in figure 1.13.

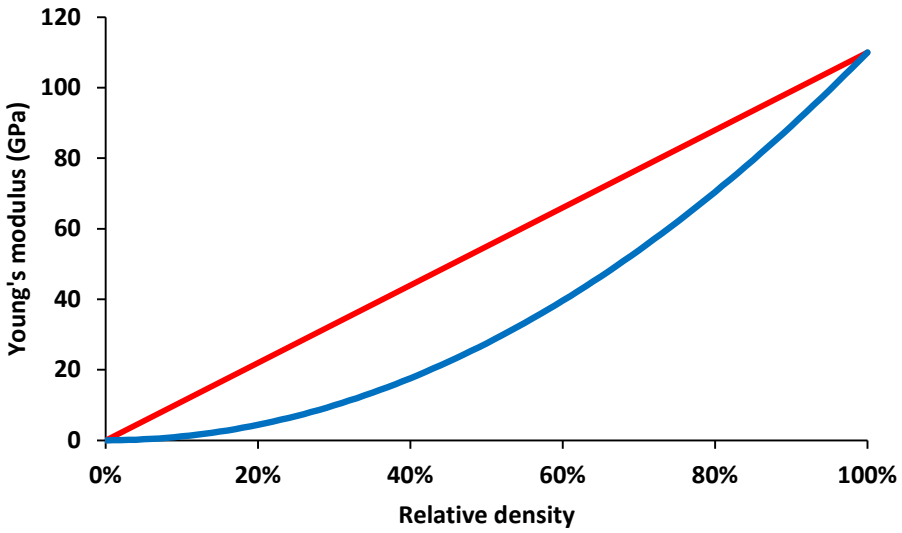

Figure 1.13: Upper bounds for the YM of Ti6Al4V given by the rule of mixtures (red) and the G&A model (blue) for materials of different relative densities.

The model shown in figure 1.12 can also be used to estimate other properties of low density foams. The plastic collapse strength, for example, is derived in a very similar method as a ratio of the solid metal. This ratio is given by:

Equation 1.6: $\frac{\sigma_{pl}}{\sigma_{ys}} = C \times \left(\frac{\rho_f}{\rho_s}\right)^{\frac{3}{2}}$

Although the Gibson and Ashby approach is a well known and frequently used method for estimating properties of foam there are many other theories have been developed over the years to look at other model geometries or other relative density ranges. An overview of the methods and models used can be found here (Mortensen et al. 2013; Goodall et al. 2014). One other approximation for the YM of foams that is relevant to the present study is the equation derived by Mortensen et al. for the behaviour of foams created by packing and compression of a removable phase (Mortensen et al. 2013).

Equation 1.7: $\frac{E_f}{E_s} = \frac{\left(1-2\left(\frac{1-V_m}{1-V_{m,c}}\right)^{\frac{2}{3}}+\left(\frac{1-V_m}{1-V_{m,c}}\right)^{\frac{4}{3}}\right)}{\left(1-2\left(\frac{1-V_{m,0}}{1-V_{m,c}}\right)^{\frac{2}{3}}+\left(\frac{1-V_{m,0}}{1-V_{m,c}}\right)^{\frac{4}{3}}\right)}$

In this equation $V_{m,0}$ is the maximum relative density that can be achieved by packing of spherical particles without compression and $V_{m,c}$ is the relative density at which compression leads to the disappearance of the initial struts.

1.3.3 Fabrication

A large number of fabrication methods exist for the production of porous metals, and the decision on which method to use will usually depend on many different specifications of the final product, such as density, base material, average pore size, pore size distribution, the presence of interconnections, etc. In the following section two different methods will be described which are relevant to the experimental chapter of this thesis. Both methods have the potential to be used for the production of porous metals for implant applications.

Space holder

Making porous metals using the so-called space holder technique is a specific case of the particle packing technique described earlier. In the case of 'normal' particle packing, porosity is introduced by spaces in between particles, whereas in case of a space holder based method a removable phase is packed in to the original mixture which is responsible for most of the porosity in the final product (figure 1.14).

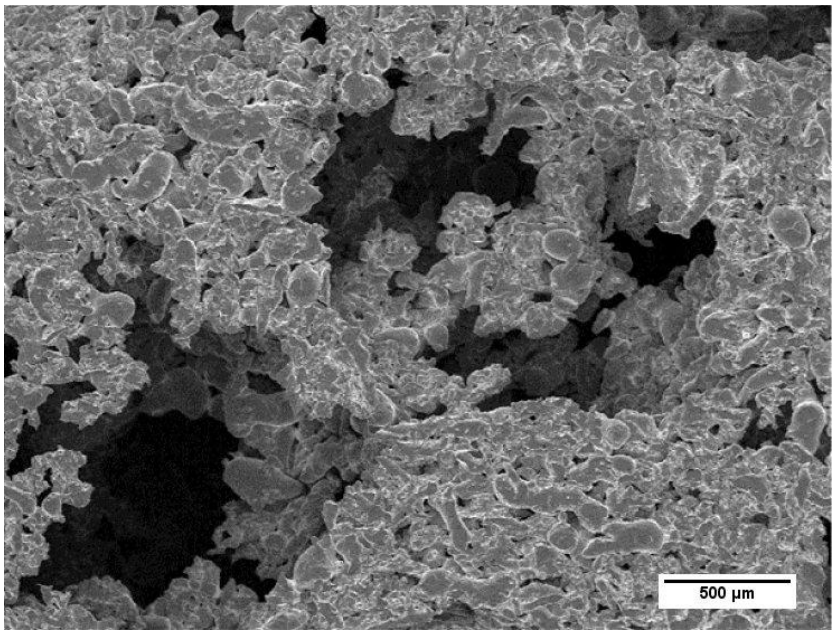

Figure 1.14: Image of a highly porous (70%) foam produced using the space holder technique (Bram et al. 2000). Powdered nickel-based superalloy (Inconel 600) was sintered at 1300 °C for 1 hour with carbamide acting as a space holder.

The density of a foam created by normal particle packing depends highly on the shape and uniformity of the particles, but some estimates can be made based on generalised situations. For example, in the case of spherical monodisperse particles the theoretical maximum of the density that can be achieved is 74%. However, in reality a packing with this level of order will not form and a value that is frequently used for the density of uniform spherical particles is 64%. When powders with a higher dispersity are used it is likely that the density of the system will increase; the use of non-spherical particles will usually lead to a lower relative density (Goodall et al. 2014).

When a space holder is used to give a foam its porous architecture the packing of the metal particles will be less important and the main factors to consider when designing a fabrication process will be the material, the shape and the size of the space holder.

The choice of a material to use as a space holder will be greatly influenced by the way the space holder will be removed from the metal. Although other methods exist, the most common techniques to remove the space holder from the final product are heating (burning, melting, evaporating) and dissolution. In case of space holder removal by dissolution commonly used materials are sugar and salt; if the space holder is removed by heating a wide range of materials can be used based on the desired processing temperature.

There are several reasons why a space holder method might be preferred over conventional particle packing. The most important reason is the control over the architecture of the pores; the space holder will usually be made of a material that is easier to process than the metal that will form the final product. Therefore, fabrication of complex architectures can be done using simple metal powder with a particle size which is much smaller than the features of the porosity.

Another important reason why a space holder might be used is because the metal used in the final product is difficult to process in its liquid form. This is mostly the case for metals and alloys with high melting points such as titanium (alloy), stainless steel and superalloys.

The use of a variety of space holder materials has been published. These materials are usually cheap, easy to process and easy to remove. Table salt (NaCl) is frequently used as a material as readily available in large quantities and can be removed by both heating to temperatures above 850 C and by dissolution. It can also easily be sieved to obtain the desired particle size range (Wen et al. 2001; Bansiddhi et al. 2008; Singh et al. 2009; Jha et al. 2013). Other materials that are frequently used are urea and ammonium hydrogen carbonate. These materials have the advantage that they can be removed at a relatively low temperature and therefore the possibility of the space holder reacting with the metal is minimised (Bram et al. 2000; Imwinkelried 2007). Fabrication of foams using magnesium (Esen et al. 2007) and polystyrene (Shimizu et al. 2012) space holders has also been reported.

Electron beam melting

A technique that has recently gained attention as a method for producing orthopaedic implants is Electron Beam Melting (EBM). EBM is a rapid prototyping technique for metals and alloys based on the principles of additive layer manufacturing.

The basic principle of EBM can be seen in figure 1.15 (Heinl et al. 2007). The fabrication of a 3D object takes place inside the build chamber of the EBM and starts with a solid metal base plate on which a thin layer (typically <100 μm) of metal powder is applied. This layer is then heated by a laser beam to a temperature which is not high enough to melt the particles completely, but does cause the particles to stick together into a semi-solid structure. In the next step a high-voltage electron beam is used to selectively hit areas of the powder according to a pre-determined Computer Aided Design (CAD) model. Unlike the laser, the electron beam does cause the temperature to rise above the melting point of the metal powder causing the particles of the semi-solid layer to fuse together completely.

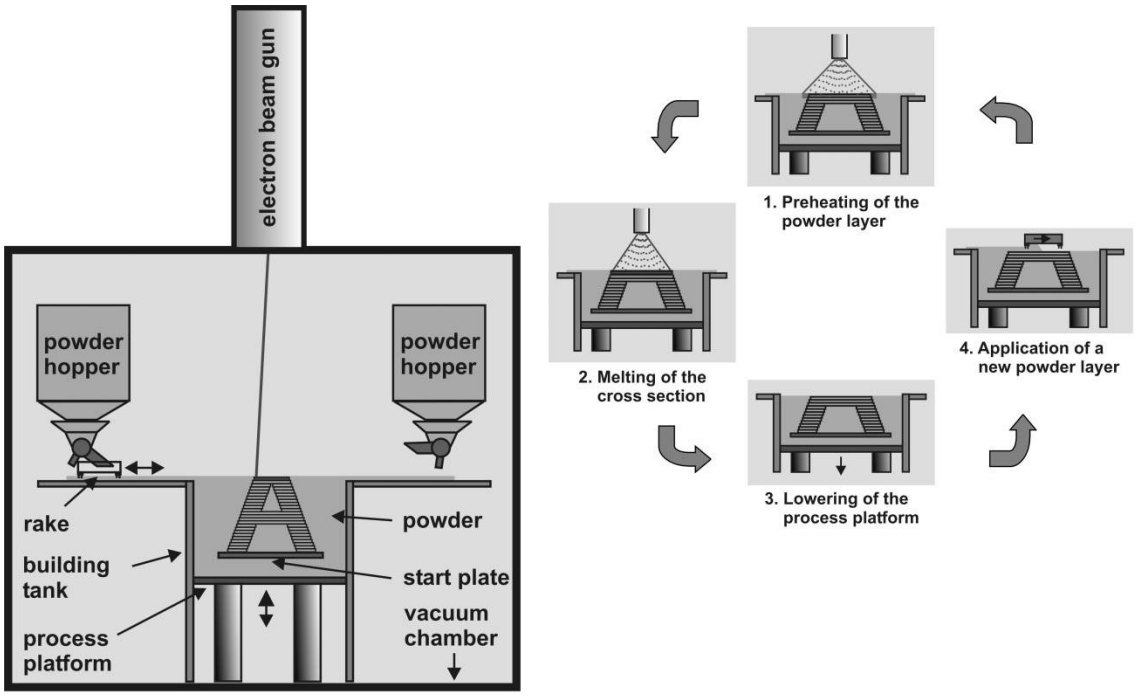

Figure 1.15: Overview of the repeated steps of the fabrication of metal components by electron beam melting (Heinl et al. 2007).

Once the electron beam has finished melting the 2D pattern of the layer the base plate is lowered and a rake is used to apply a fresh layer of powder. These steps can be repeated thousands of times to create structures of up to 20 cm, but ultimately limited only by the size of the build chamber (Heinl et al. 2007).

At the end of the process the semi-solid structure of particles can be removed in a so-called 'powder recycling system' where compressed air is used to blast the structure with metal particles of the same type as the build powder using metal particles as blasting medium, which can then be recycled. The entire building process is preformed at temperatures of around 700 °C and under vacuum in order to get optimal properties of the material in terms of strength and contaminations (Heinl et al. 2007).

The fabrication of 3D objects by EBM takes place under highly controlled conditions. Firstly, the entire fabrication process takes place under a high vacuum, as both the electron beam and the metal particles will be affected by the presence of gas molecules. Secondly, temperature control during the building process is also critical, because a temperature which is too low may lead to incomplete melting of the metal particles whereas too high temperature will lead to the 'melt pool' around the electron beam being too large leading to loss of resolution.

EBM technology was developed by Arcam AB (Stockholm, Sweden), founded in 1997. Since the early 2000s, the first peer reviewed articles have been published that used this technology. In 2004, Cormier et al. reported their research on the structural and mechanical properties of H13 steel samples produced by EBM. They described the properties of the materials as 'quite good' in terms of hardness and porosity (Cormier et al. 2004).

From 2007 onwards, Heinl et al. published a series of articles describing the potential use of EBM as a technique to create porous orthopaedic implants (Heinl et al. 2007; Heinl et al. 2008; Heinl et al. 2008). The fabrication of hatched and diamond-shaped structures was described, as well as a post-treatment with hydrochloric acid and sodium hydroxide aimed at improving the bioactivity of the surface. It was found that porous structures could be made with a stiffness that matches human cancellous bone.

1.4 Porous metals for bone implants

1.4.1 Timeline

The concept of using porous biomaterials to stabilise implants can be dated back to the early nineteenth century (Kienapfel et al. 1999). Its application in large implants, however, came shortly after the widespread introduction of TJA in the 1970s, when complications associated with cemented TJA emerged (Goldring et al. 1983; Kienapfel et al. 1999; Learmonth et al. 2007).

Initial experiments consisted mainly of porous-coated metals implanted in bone and maintained for different timepoints after which the implant was mechanically pushed out of the bone (push-out test) to determine the level of osseointegration over time (Welsh et al. 1971; Kienapfel et al. 1999). These experiments showed extensive bone ingrowth into the porous metal in animal experiments, but in human models mostly fibrous tissue was found at the bone-implant interface (Haddad et al. 2007).

The first porous-coated implants were used as early as the 1970s, but availability was limited and their performance is not extensively reported (Hungerford et al. 1982; Hungerford et al. 1983). In the 1980s, several manufacturers introduced implants that were either fully or proximally porous coated (usually produced by metal beads sintered together). Examples include AML (DePuy), Harris-Galante (Zimmer), Howmedica PCA (Howmedica), and Implant Technology LSF (Implant Technology) (Woolson et al. 1996; Haddad et al. 2007; Hennessy et al. 2009) (figure 1.16).

Figure 1.16: Image of a Howmedica porous coated anatomical stem, a first generation porous coated implant.

In 1987, Engh et al. reported clinical (2-year and 5-year follow-up) and histological results of a porous coated cobalt-chromium femoral implant that was used in their clinic since 1977 (Engh et al. 1987). Clinical evidence, such as radiographs and explanted femurs, showed excellent osseointegration in the majority of patients, but also evidence of fibrous interfaces (18%) and hip pain (12%) (Engh et al. 1987).

In the following years numerous studies have evaluated the short- and mid-term performance of porous-coated implants and increased pain near the implant was frequently observed. Evidence suggested that so-called stress shielding can be a major factor contributing to hip pain (Bugbee et al. 1997).

Stress shielding is a phenomenon that may occur when an implant with mechanical properties different to bone is implanted. An implant with a higher stiffness than the surrounding bone (due to a higher Young's modulus) will, when the whole joint is loaded, carry a larger proportion of the applied force. Thus the stress experienced by certain parts of the surrounding bone may be reduced (Haase et al. 2010).

As a result, the quality of the bone tissue in these areas will deteriorate due to functional remodelling of the bone. This process, often referred to as Wolff's law, encompasses changes to the rate of bone formation and bone resorption as a result of mechanical forces acting on

the tissue; high stresses on bone tissue will lead to a increase in bone mass whereas low mechanical loading (e.g. stress shielding) will cause a decrease. Consequently, osseointegration and bone ingrowth will be lower and the chance of loosening of the implant will increase in stress shielded tissues (Bugbee et al. 1997; Cowin 2004; Ruff et al. 2006).

In order to prevent stress shielding and its associated conditions a new generation of implants was developed with changes to the porous coating and the design of the stem specifically to address the problem of unequal loading of the femur.

One of these changes was to change in the design of the stem from the traditional cylindrical or tapered shape to an anatomical stem, i.e. having an anteroposterior curve following the natural shape of the bone; this change was thought to improve proximal loading, but the anatomical design resulted in higher incidence of distal thigh pain associated with stress shielding (Learmonth et al. 2007).

Another way to prevent bone resorption around the implant was to coat only specific areas of the stem. Normally, the whole intramedullary surface of the stem was coated in order to maximise osseointegration; in this case, however, only the proximal part – either half or one third – had a porous surface to increase loading around the proximal part of the femur (Learmonth et al. 2007).

To date, prostheses with both types of coating are commercially available. A recent study comparing modern fully-coated and proximally-coated implants found no significant differences in pain levels between the groups in follow-ups of up to 2 years (MacDonald et al. 2010).

1.4.2 Biological testing of porous metals

Bone implants are the main application for most research that is being published on porous metal for biomedical applications. Two important properties are often mentioned in the biological assessment of porous metals for bone implants: biocompatibility, sometimes referred to as osteoconduction, and bone ingrowth. Biocompatibility is the absence of an adverse response of cell or tissues and is in this case mainly a property of the bulk material. Bone ingrowth refers to bone formation inside the pores of the material.

Testing of the biocompatibility of a non-resorbable material is relatively straightforward and in many publications a simple cell culture experiment is used as evidence for good biocompatibility. A typical experiment involves the seeding of a relevant cell type onto the

surface of the material, investigation of cell survival and/or cell proliferation over time and analysis of the materials by light microscopy, immunohistochemistry or histology.

Measuring bone ingrowth however is far less straightforward; it requires a relevant animal model, the duration of an experiment is typically several months and variation between samples and experiments is usually higher due to the complexity of implanting the materials and the natural variation between animals. The following sections will discuss recent advances in these different types of tests.

In vitro

In recent years, several authors have described in vitro biocompatibility testing of a range of different titanium structures produced by EBM. Ponader et al. seeded human foetal osteoblasts on smooth, textured, and porous surfaces and investigated cell attachment, proliferation, and expression of osteogenic markers (Col1, OC, OP, ALP) as a result of exposure to a differentiation medium. It was found that cell attachment was significantly higher on smooth and compact surfaces, whereas the rough and porous surfaces showed low cell attachment or none at all. Significant upregulation of osteogenic markers was not observed (Ponader et al. 2008).

Haslauer et al. compared the biocompatibility of three different solid EBM discs with one porous disc (Haslauer et al. 2010). Attachment and proliferation of human adipose-derived stem cells (hASCs) was investigated as well as the release of the inflammatory cytokines interleukin 6 and 8 (IL-6 and IL-8). Cell viability assays showed normal proliferation and the release of IL-6 and IL-8 was not significantly higher for the porous disc then for the solid discs. These structures could, therefore, be acceptable as a coating for orthopaedic implants. However, whether these structures are likely to permit osseointegration and bone ingrowth after implantation was not discussed (Haslauer et al. 2010).

The ability of cells to differentiate when seeded on EBM structures (measured by the upregulation of bone specific markers) was investigated by De Peppo et al. (De Peppo et al. 2012). In this study, samples of Ti6Al4V and commercially pure titanium (cpTi) were seeded with human Embryonic Stem Cell-derived Mesenchymal Progenitor (hESMP) cells and analysed using Polymerase Chain Reaction (PCR) analysis. They found that the activity of osteogenic markers such as OC and OP increased over time but that there was no significant difference between the materials (figure 1.17).

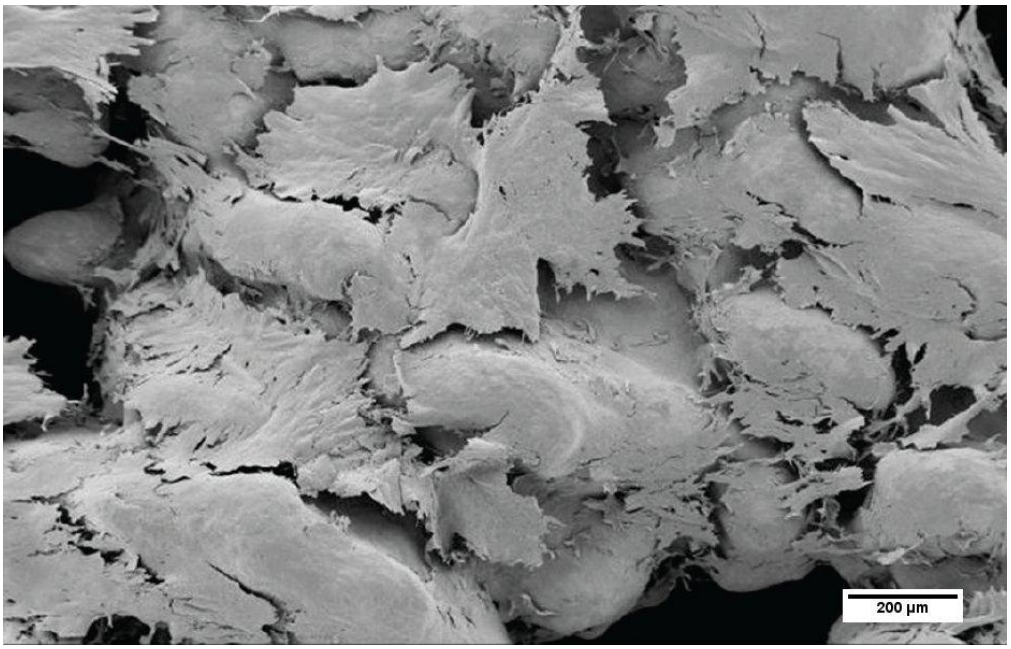

Figure 1.17: SEM image of cells on titanium (De Peppo et al. 2012).

An alternative method of assessing the biocompatibility of titanium structures was described by Heinl et al. (Heinl et al. 2008), who investigated bioactivity by immersion in simulated body fluid, a solution of different salts in the concentrations at which they are present in human blood plasma (Kokubo et al. 2006; Heinl et al. 2008). Samples were immersed for 6 days and the composition of the materials that were deposited on the surface by the simulated body fluid was measured. It was found to contain carbonated hydroxyapatite and phosphate groups, which was seen as an indication that there would be improved fixation and long term stability when used in vivo (Heinl et al. 2008). Although the use of simulated body fluid was recently described as a good method to predict osseointegration qualitatively and quantitatively (Kokubo et al. 2006), it does not provide any information about the ability of cells to attach a material and to form bone tissue.

Mechanical stimulation

A more advanced method of assessing the suitability of biomaterials in vitro is to subject cells to some form of mechanical stimulation when seeded onto the surface of a biomaterial. In the human body the fast majority of cells are constantly subjected to mechanical forces, either by stretching or compression of tissue or by fluid flow; it is well-known that these forces have many effects on the (biological) behaviour of cells.

Several different systems have been developed to mechanically stimulate cells in vitro (Bancroft et al. 2002); examples include rocking (Delaine-Smith et al. 2012; Delaine-Smith 2013), spinner flasks (Vunjak-Novakovic et al. 1998; Vunjak-Novakovic et al. 1999), rotating wall vessels (Qiu et al. 1998; Botchwey et al. 2001) and flow perfusion bioreactors (Bancroft et al. 2002).

In the case of bone cells, it has been shown that mechanical stimulation has a positive effect on bone matrix formation both in vivo (Bassey et al. 1994) and in vitro (Janmey et al. 2007; Delaine-Smith et al. 2012; Delaine-Smith 2013). For example, it has been shown that high impact exercise is associated with increased bone density in premenopausal women compared to low impact exercise (Bassey et al. 1994).

In vitro, bone cells can be stimulated in a more controlled manner and the effects of mechanical loading can be investigated earlier than in vivo. Delaine-Smith et al. investigated this effect by growing bone cells on 2D surfaces and stimulating the cells by fluid flow on a rocking platform (Delaine-Smith et al. 2012; Delaine-Smith 2013). It was shown that this simple stimulus resulted in an increase in the production of bone-like extracellular matrix. Mullender et al. found a similar effect by stimulating primary bone cells by pulsating fluid flow and cyclic strain and showing that both treatments led to an increase in the release of PGE2 and NO (Mullender et al. 2004; Sittichokechaiwut 2009; El Haj et al. 2010). The effect of perfusion culture on cells seeded on a titanium scaffold was investigated by Bancroft et al. and also confirmed the increase of production of ECM upon mechanical stimulation (Bancroft et al. 2002).

In vivo

Assessing bone ingrowth however is far less straightforward and to date no in vitro experiment has been developed that can adequately predict bone ingrowth in vivo. Therefore, the most frequently used experiments to predict the performance of porous metals for bone implants are based on animal models. In most cases a simple geometrical shape is implanted into a long bone for a period typically between 1 and 6 months. Its performance can be assessed by looking at the strength of the interface (usually by measuring the force required to pull the implant out of the bone) or by histological assessment. In case of histological assessment there are two parameters that are often measured. Firstly, total bone surface, which is the area that stains positive for bone divided by the total area of the pores in one particular cross section, and secondly the bone-implant contact which is the percentage of the implant surface in a cross section that is covered by bone.

Recently, several authors have reported the in vivo performance of porous metals produced by EBM (Thomsen et al. 2009; Ponader et al. 2010; Biemond et al. 2011; Biemond et al. 2011; Tarala et al. 2011; Bertollo et al. 2012; Biemond et al. 2012). The animal models described to date are goat (Biemond et al. 2011; Biemond et al. 2011; Tarala et al. 2011; Biemond et al. 2012), sheep (Bertollo et al. 2012), rabbit (Thomsen et al. 2009) and pig (Ponader et al. 2010).

Thomsen et al. investigated bone-implant contact of solid blocks of Ti6Al4V two weeks after endosseous implantation in rabbits and found no significant differences between Ti6Al4V prepared by EBM and by conventional methods; percentages of bone-implant contact between 29 and 41 percent were found (Thomsen et al. 2009). Bertollo et al. combined histological assessment with pull-out tests to measure the shear strength and the energy to failure of EBM and plasma sprayed titanium. They also investigated the effect of the 'fit' of the implant by implanting a straight cylindrical implant into a defect with varying radii. This created three types of fit which they called gap (implant smaller than defect), line-to-line (same size) and interference (implant larger than defect). This experiment showed a significant increase in bone ingrowth between week 4 and week 12, but the results on the effect of the fit on bone ingrowth were ambiguous (Bertollo et al. 2012).

In 2010, Ponader et al. were the first to report on the implantation of porous Ti6Al4V in the skulls of domestic pigs (Ponader et al. 2010). Bone ingrowth into the pores was clearly visible between day 14 and day 60, but bone-implant contact was scarce with only six percent of the surface of the implant covered after 60 days.

In an effort to improve the bone-implant contact Biemond et al. investigated the effect of several types of coatings and surface treatments of porous titanium structures produced by EBM (Biemond et al. 2011; Biemond et al. 2011; Tarala et al. 2011; Biemond et al. 2012) (figure 1.18). In these studies, a plasma sprayed titanium control was compared to the following EBM samples: uncoated titanium (Biemond et al. 2011), acid etched titanium (Biemond et al. 2012), hydroxyapatite coated titanium (Tarala et al. 2011) and brushite coated titanium (Biemond et al. 2011). These studies showed that structures produced by EBM showed significantly more bone ingrowth than plasma sprayed titanium controls and that coating EBM produced surfaces with hydroxyapatite or brushite further improved bone ingrowth depth but not pull out strength.

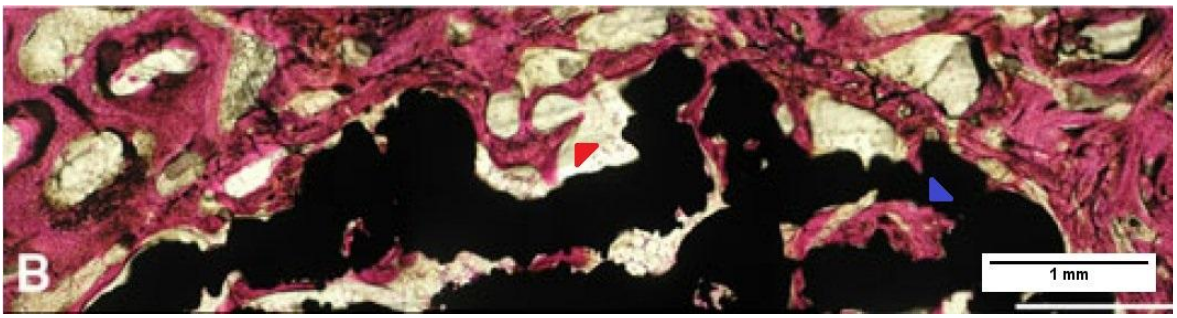

Figure 1.18: Light microscopy image of a histology section of bone ingrowth (shown by haematoxylin/eosin staining which stains bone tissue pink) into a titanium implant (black). White areas represent pores in the bone or the implant with no tissue present. Arrowheads show bone ingrowth with (blue) and without (red) good osseointegration and bone-implant contact (Biemond et al. 2011).

These studies show that there is a highly complex relationship between the properties of the surface of the implanted material and the osseointegration and bone ingrowth by the host tissue. It is also shown that bone-implant contact may be reduced over time, a process that could be seen as the opposite of osseointegration. It has been suggested that macromotion in the first days after implantation may be involved, but a clear rationale that explains the way in which mechanical forces affect osseointegration over time was not described (Ponader et al. 2010).

In summary, EBM is a versatile technique that can be used for the fabrication of high-value metal foams. Many researchers are developing titanium foams for medical applications using different designs, but many aspects regarding the question how the design and properties of a foam affect bone ingrowth and implant stability are unknown. In the experimental work described in the following chapters EBM, as well as the space holder technique, will be used to produce different types of porous metal and use structural, mechanical and well as biological characterisation to assess their suitability in bone implants.

2. Methods

For the experimental work of this thesis a wide range of experimental techniques and methods has been used. Some of these methods are very well known and their parameters and conditions are well described in the literature. Others, such as the space holder method for creating porous titanium and the design of a bioreactor, were specifically adapted for this project and have been modified based on initial findings during this study. Therefore, the more straightforward methods will be described in this chapter and the bespoke methods in the subsequent results chapters along with the initial observations that led to the 'fine-tuning' of those methods.

2.1 Electron Beam Melting

All Electron Beam Melting (EBM) manufacturing was performed on the Arcam EBM-S12 machine owned by the Mercury Centre of the University of Sheffield (figure 2.1). Many of the details of the manufacturing process have been developed and tested by the Mercury Centre based on the specifications of the individual builds.

Figure 2.1: The Arcam EBM-S12 (Al-Bermani 2011).

Equipment

For the basic day-to-day running of the EBM process four main pieces of equipment are required.

- The **EBM machine** itself, this is the place where actual fabrication takes place. It contains the build chamber, the column where the electron beam is generated as well as the computer with the software that controls the building process.
- Two **vacuum cleaners**, one that was exclusively used for the collection of uncontaminated titanium powder that could be recycled and one that was used to clean all other dirt as well as contaminated titanium powder.
- One **Powder Recycling System** (PRS); this is a chamber where unmelted powder can be removed from newly built EBM structures by blasting the build with titanium particles. Because the chamber is sealed and is kept free of contamination from outside the unsintered powder and the powder that was used as the blasting medium can be recycled.
- One compressed air driven **vibrating sieve**. After removing the powder from the PRS all the recovered powder was passed through this sieve to remove particles that were sintered together and other irregular-shaped particles; this was done keep the powder uniform and spherical as this is crucial to the EBM building process.

The build chamber

The build chamber is the part of the EBM machine where the melting of the powders takes place. Figure 2.2 shows an overview of the most important components of the build chamber.

Figure 2.2: The build chamber of the EBM-S12 (Al-Bermani 2011).

As the build chamber was under vacuum during the entire building process all moving parts were controlled by the EBM software. These components are:

- The **base plate**. This is a steel plate onto which the structure was built. As EBM structures were built up layer by layer the base plate was lowered after each melting step by a certain distance; this distance then became the thickness of the next layer. This distance could be varied, but for this powder the optimal layer thickness was found to be 70 μm.
- The **rake**. After the building platform was lowered the rake moves horizontally across the centre of the build chamber taking metal powder dispensed from one of the powder hoppers on the side to the centre of the chamber so that a new layer of powder forms on top of the layer that has just been melted.

Building

A typical EBM build will involve the following steps.

1. **Cleaning the build chamber**. Before each build the build chamber was cleaned on the inside; this prevents any dirt from being mixed with the powder which may affect future builds. The column of the electron beam and the vacuum seal were also cleaned.
2. **Loading the build chamber**. After cleaning the powder hoppers were inserted, the base plate was brought into position and the rake was tested to check that the powder is equally spread across the building platform.
3. **Preparing the build chamber**. Before the chamber was sealed a heat shield was placed over the building platform to reduce fluctuations in temperature during the build. The chamber was then depressurised to around 5 Pa and voltage of the electron beam was gradually increased to 60 kV. In the meantime an 'Arcam build file' of the product was uploaded to the computer. Immediately before building started, the temperature of the platform was raised to 760 °C.
4. **Building**. The building of each individual layer of the file started with the lowering of the platform and the rake applying a new layer of powder. All particles on the building platform were then partially sintered by a laser into a semi-solid structure to prevent the particles from being displaced by the charge of the electron beam. The beam then melted the layer according to the build file so that the semi-solid structure was melted into a fully dense structure and completely fused with the previous layer. The speed of the electron beam was set to 200 mm/s, the power of the beam was 102 W and the thickness of each layer was 70 µm.
5. **Cleaning the structure and powder recycling**. Once the structure was fully built the electron beam was switched off and the pressure was increased in order to assist cooling. Because of the reactivity of titanium with atmospheric gasses at high temperatures helium was pumped into the chamber first. Once the build had reached a safe temperature it was transferred to the PRS where the structure was blasted with titanium particles to break the semi-solid structure into a powder which could then be recycled along with the particles used for blasting.

2.2 Scanning electron microscopy

Scanning Electron Microscopy (SEM) was used to analyse the structure of the porous metals produced by EBM and the space holder technique. All SEM was performed on the Jeol JSM 6400 of the Sorby Centre of the University of Sheffield. All samples were conductive, so gold or carbon coating was not necessary.

All EBM samples were washed in alcohol in an ultrasonic bath and imaged without further processing. The samples made by the space holder technique were all cut in half on an Isomet-5000 precision saw (Buehler) and ground on SiC paper with decreasing roughness (p240, p400, p800 and p1200).

2.3 Shrinkage

Compressed, unsintered space holder samples (green bodies) are likely to undergo some degree of shrinkage during the heat treatment (i.e. a decrease in the overall volume of the structure, which is the volume of the titanium and the pores combined). This form of shrinkage is highly unpredictable, but it is expected that it will be affected by the type of powder used and by the percentage of titanium in the green body, and potentially also by the method of preparation of the green body.

A decrease in the overall volume of an irregular porous structure is less straightforward than measuring solid objects. Usually, a simple method for these kinds of measurement is to submerge the object in a liquid and measure the change in volume or alternatively to add liquid to the object up to set volume and measure the weight of the liquid after removal of the object. In case of a porous structure, a similar method can be used, but it is necessary to ensure that the pores are closed to prevent liquid entering the pores, as the aim is to include the volume of the pores in the overall volume.

In this experiment all the porous structures were immersed in liquid paraffin of around 60 °C for several minutes. Initially, the paraffin will form a solid layer around the (cold) structure, but gradually the paraffin will start to melt and penetrate the pores. When this starts to occur, the container was tapped several times to allow small air bubbles to escape. Finally, the structure is removed from the paraffin so that the remaining paraffin inside the pores solidifies. As the viscosity of the liquid paraffin is relatively low there is no formation of a solid paraffin layer around the structure that would affect its overall volume; any solidified paraffin droplets could easily be removed before measurement. After solidification the volume of the foams can be measured by immersing them in water.

2.4 Mechanical testing

Mechanical testing of all porous metals was done by uniaxial compression on a Hounsfield mechanical testing apparatus. For the measurement all samples were placed on the bottom plate of the machine and crushed at a speed of 0.25 mm/min until the height of the samples was reduced by 40% or until the force reached 90 kN. After each session the compliance of the equipment was measured by pressing the plates together with no sample present. The curve of the resulting force and displacement was used for compliance correction of each sample. After this correction the force-displacement curves were converted to stress-strain curves.

If a clear linear region could be observed in the initial part of the stress-strain curve the slope of this linear region was used to calculate the Young's Modulus (YM) of the sample using equation 1.1.

The same slope was also used to determine 0.2% offset Yield Strength (YS). This is defined as the stress as which the strain is more than 0.2% higher than what would be expected based on linear behaviour (figure 2.3).

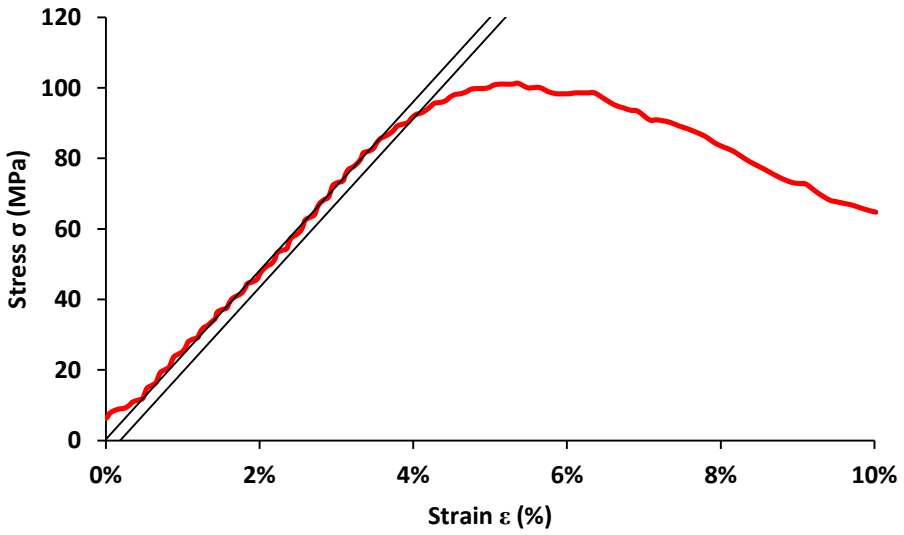

Figure 2.3: Compliance corrected stress-strain curve with the trend lines that were used to determine the Young's modulus and the 0.2% offset yield strength.

2.5 MicroCT

For a more detailed examination of the structure of the graded lattice, a Micro Computed Tomography (MicroCT) scan was undertaken. An example of a graded lattice was cleaned and scanned using a Skyscan 1172 MicroCT scanner over an angle of 360° with one image

taken every 0.7° on a camera of 2000 × 1000 pixels; the pixel size was 8.9 µm and the resolution was 25 µm. The images were taken at a voltage of 100 kV and a CuAl filter was used to improve beam quality.

2.6 Cell culture

All media, solvents and other chemicals were purchased from Sigma (Gillingham, Dorset, UK) unless stated otherwise.

The cell lines used for the experimental work of this thesis were the pre-osteoblastic cell line MG63 (Billiau et al. 1977) and the post-osteoblastic cell line MLO-A5 (Kato et al. 2001). The culture medium used for the MG63 cells was Dulbecco's Modified Eagle's Medium (DMEM, Biosera, East Sussex, UK) and the medium used for the MLO-A5 cells was Minimal Essential Medium-α (α-MEM, Lonza, Castleford, UK). Both media were supplemented with 10% Foetal Calf Serum (FCS), 1% L-Glutamine solution (0.2 M) and 1% Antibiotic solution containing penicillin (10,000 U/mL) and streptomycin (10 mg/mL). Both cell types were expanded in 2D in T75 tissue culture-treated polystyrene flasks and subcultured at a confluence of 80 - 90% using a 1 mM EDTA solution containing 0.25% trypsin.

To induce maturation and mineralisation cells were grown for up to three weeks in osteogenic medium. For the MG63 cell line osteogenic medium consisted of basic culture medium supplemented with Ascorbic Acid-2-Phosphate (AA, 0.2 mM), dexamethasone (dex, 10 nM) and β-glycerophosphate (β-GP, 5 mM). For the MLO-A5 cells the medium was also supplemented with AA and β-GP, but dex was not used.

2.7 Cell viability assay

To measure the viability of cells during culture an assay was used that relies on the metabolic activity of the culture as a whole. The metabolic activity can be shown by adding a non-toxic blue dye to the medium that is taken up into the cell, where it reacts at a rate that is proportional to the metabolic activity of the cell. This dye is called resazurin and it is commercially available in powder form as a sodium salt or in solution when it is commonly known under trademark names such as Alamar Blue.

Resazurin can be used to measure cell viability with two different methods that both rely on the reduction of resazurin to resorufin. As resazurin is blue and resorufin is purple the

progress of the reaction can be easily observed with the naked eye or quantified by measuring the absorbance of the medium at a wavelength of around 570 nm. Another difference between resazurin and resorufin is that resorufin is highly fluorescent when excited with green or yellow light (540-570 nm) where it emits red light (peak emission is at 585 nm). Therefore, the progress of the reaction can also be measured using a fluorescent spectrophotometer. For the experimental work of the current project the reduction of resazurin was always measured by fluorescence.

A typical cell viability measurement was carried out as follows. A resazurin working solution was made by making a solution of resazurin sodium salt in PBS at a concentration of 0.269 g/L. The working solution was filter sterilised and was stored at 4 °C in the dark for up to 1 month. Before each assay resazurin-containing medium was prepared consisting of 10% working solution and 90% of the appropriate culture medium. The old culture medium was then replaced by 7 mL of resazurin-containing medium and incubated for 4 hours protected from light. After the incubation period the colour change was assessed by eye and fluorescence was measured by transferring three times 200 µL of each sample to a 96-well plate and measuring the emission at 635 nm with an excitation wavelength of 540 nm. The negative control consisted of resazurin-containing medium incubated with no cells present; results are presented as fluorescence intensity units or as a percentage of a positive control. Cell viability graphs represent triplicates unless stated otherwise.

Statistical analysis for this assay and for the assays described below was carried out using GraphPad InStat. Statistical significance between groups was determined by the student T-Test in case of two groups and by the one-way ANOVA with Tukey post-test in case of three or more groups. Groups were considered statistically significant if $p < 0.05$ and significance was indicated on graphs as * for $p < 0.05$, ** for $p < 0.01$ or *** for $p < 0.001$.

2.8 Calcium and collagen staining

After culturing cells on a biomaterial or in 2D cells can be fixed and the extracellular matrix that was produced by the cell can be analysed. Two components of the extracellular matrix were considered to be the most relevant to the present work: total collagen content and calcium content.

Calcium, which is present in large quantities in bone-like extracellular matrix as a component of the bone mineral hydroxyapatite, can be analysed with Alizarin red S. This is a dark red

dye that strongly binds to calcium containing minerals. To measure the total collagen content of the extracellular matrix a dye called Sirius red was used. These two assays can be performed on the same samples, however it is recommended that the calcium assay is performed first as the substances used in this assay are less likely to have an effect on the collagen present in the extracellular matrix.

A working solution of Alizarin red S was prepared by dissolving Alizarin red S powder in distilled water at 5 g/L and adjusting the pH to 4.1 using a solution of ammonium hydroxide. To prepare the Picro-sirius red working solution Sirius red powder was dissolved in saturated picric acid at a concentration of 1 g/L.

After cell culture the medium was removed and the material or the well plate (hereafter 'the sample') was washed with PBS and fixed in a 3.7wt% solution of formalin in distilled water for 40 minutes. The formalin solution was then removed and the samples were washed in distilled water three times to ensure that there was no dissolved calcium present in the samples. Alizarin working solution was added to the samples until they were fully covered; the samples were then placed on a rocking platform. After 30 minutes the working solution was removed and the samples were washed in distilled water for a minimum of three times, but washing was continued until no trace of red colour was present in the washes.
For quantitative analysis 1 mL of de-staining solution (5% perchloric acid in distilled water) was added to the samples. This solution lowers the pH of the samples to below 2 and causes the calcium-Alizarin complex to dissolve and change colour from red to yellow. If the sample was a 3D metal structure the sample was transferred to a smaller container beforehand to ensure that the structure was completely submerged by 1 mL of de-staining solution. The de-staining solution was pipetted over or through the sample several times in order to allow all mineral to dissolve. Finally, three times 200 µL of the de-staining solution was transferred to a 96-well plate and a spectrophotometer was used to measure the optical density (O.D., given in arbitrary units, a.u.) at 405 nm. Blanks consisted of de-staining solution with no mineral present.

After the calcium assay all samples were washed in distilled water, 4 mL of Picro-sirius red working solution was added and the samples were left on a rocking platform for at least 12 hours. The working solution was removed and, similar to the calcium assay, the samples were washed in distilled water until no trace of the Sirius red was present in the washes. The

samples were then de-stained using a mixture consisting of 50% methanol and 50% 0.2 M sodium hydroxide solution. Three times 200 µL of each sample was transferred to a 96-well plate and the O.D. was measured at 490 nm. Blanks consisted of pure de-staining solution with no collagen present. Graphs showing the results of calcium and collagen assays represent triplicates unless stated otherwise.

2.9 In vivo bone ingrowth

To assess bone ingrowth into the graded titanium lattices in vivo 6 × 6 × 10 mm metal implants were implanted in a rabbit femoral defect. This study was carried out in collaboration with the Medical Institute of Sumy State University. 6 months old rabbits of the chinchilla breed with a body weight of between 3 and 3.5 kg were kept at the Medical Institute of Sumy State Universtity (Sumy, Ukraine). Husbandry and experimental conditions complied with the 'European Convention for the Protection of Vertebrate Animals used for Experimental and Other Scientific Purposes' (1986), 'Directive 2010/63/EU' of the European Parliament and of the Council on the protection of animals used for scientific purposes (2010) and national legislation ('General Ethical Principles for Experiments on Animals', Kyiv, 2001). Local approval (#14/65) was granted on 28-03-2013.

Animals were divided into 3 groups:
Negative control (7 animals) – Solid implant: Solid Ti6Al4V produced by EBM using the same method as the porous lattices.
Graded lattices (10 animals) – Graded porous lattice: porous lattices with the architecture described in chapter 4, but with a smaller overall size (6 × 6 × 10 mm) to fit the defect.
Positive control (8 animals) – Commercially available porous metal optimised for bone ingrowth: porous tantalum produced by carbon fibre deposition (Trabecular metal, Zimmer).

Under general anaesthesia, the right leg was shaved from the hip joint to the knee. The surgical site was treated with C-4 solution and a longitudinal incision was made 2 cm below the hip joint to 1 cm above knee joint on lateral side of the thigh. The skin and muscles were retracted in order to access the femur.
On the middle third of femur the periosteum was separated in a lateral direction with a bone rasp and a longitudinal defect of the femur corresponding to the size of the implant was made using a dental drill and Liston's forceps. The implant was then placed into the defect and the

muscle was sewn using atraumatic sutures. Finally, the wound was closed with simple interrupted sutures and an aseptic dressing was applied.
All animals were euthanised by overdose of anaesthetic (ketamine, 100 mg per kg of animal weight) either 4 weeks or 12 weeks after the implantation. The femur was removed and fixed in 4% paraformaldehyde for 48 hours followed by dehydration in ethanol solutions. Femurs were infiltrated with liquid methylmethacrylate (MMA) at 4 °C overnight and transferred to fresh MMA and left at 4 °C for 2 days. Finally, the samples were embedded by polymerisation in fresh MMA.

The numbers of animals per timepoint were as follows:
Negative control: 4 weeks – 3 animals, 12 weeks – 4 animals
Positive control: 4 weeks – 3 animals, 12 weeks – 5 animals
Graded lattice: 4 weeks – 5 animals, 12 weeks – 5 animals

Before the specimens were sectioned, an etching solution and two staining solutions were prepared. The etching solution was prepared by mixing ethanol with 1N HCl in a ratio of 100:1. A methylene blue staining solution was prepared by dissolving 1 g of methylene blue powder in 100 mL of a 1M borax solution and lowering the pH to 8.5 with an HCl solution. Finally, a basic fuchsin solution was prepared by mixing 0.3 g of basic fuchsin powder in 100 mL of distilled water and boiling the mixture in order to improve dissolution of the powder. Both staining solutions were filtered before use.
After embedding the tissue containing the implant was cut open and sectioned using a Leica SP1600 saw. After each cut the newly exposed surface was etched for 1 min using a few drops of etching solution, the surface was then washed with distilled water, stained with methylene blue for 1 min, washed again and stained with basic fuchsin for 45 s. Finally, the surface was washed again, dried completely, glued to a coverslip using UV sensitive glue and cured for 1 min. The specimen was then raised by a distance of 310 µm and cut. As the thickness of the blade is 300 µm the thickness of the section will be approximately 10 µm. The section was glued to a microscopy slide and images were taken using an optical microscope at 40× and 100× magnifications.

3. Space holder

As described in the introduction a common way to fabricate a porous metal scaffold is the space holder method. This chapter describes the development of a protocol for synthesising porous metal samples using the space holder method and the results of the structural and mechanical characterisation of these samples.

3.1 Fabrication

Many different fabrication methods for porous metals have been suggested in the literature over time, but one of the most favourable ones in terms of cost and ease of processing is the use of a removable phase to introduce porosity. The reason for this is that that the materials required are relatively inexpensive and that the equipment required for processing (press, furnace) are widely available.

Despite being relatively straightforward and inexpensive the method is highly versatile because a range of metal powders and processing temperatures can be used and because of the versatility of the removable phase.

For the production of space holder foams, table salt (Sainsbury, Sheffield, UK) was manually mixed with powdered Ti6Al4V with the salt content varying between 60% and 80% by volume. The salt was sieved to obtain a powder with a particle size range of 250 to 500 µm. Two different titanium powders were used; one was spherical with a powder diameter of 45-100 µm (Arcam, Mölndal, Sweden), which is the same powder that was used for the EBM process. The other powder was irregular-shaped with a diameter similar to the EBM powder (Goodfellow, Cambridge, UK) (figure 3.1).

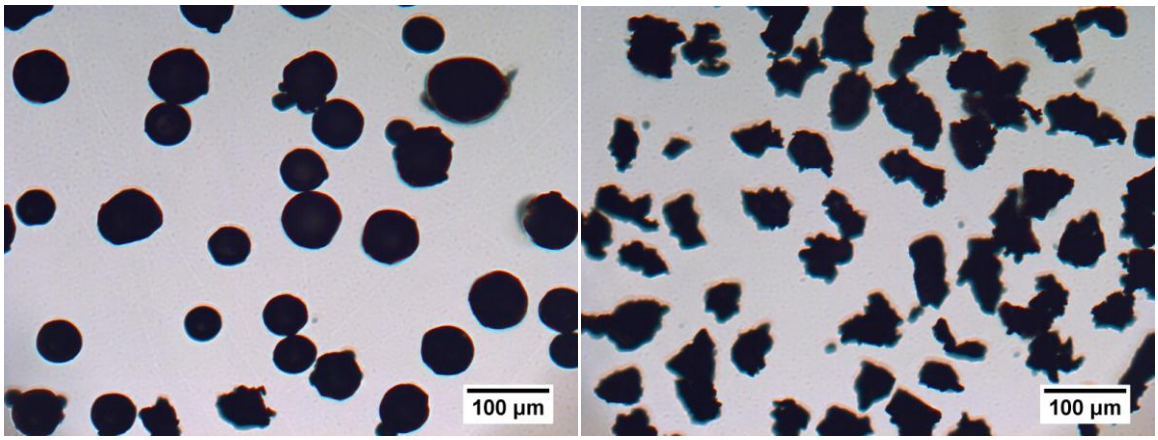

Figure 3.1: Ti6Al4V powders used for the fabrication of the space holder foams: spherical particles (left), irregular-shaped particles (right).

These mixtures were compressed inside a steel die to obtain a solid cylindrical structure (green body). The first green bodies that were produced using the space holder method were relatively large samples for which the sum of the volumes of the titanium and the salt was 6 cm^3 (see box). However, even though the mixtures appeared homogeneous on visual inspection before compression, there was a higher concentration of titanium particles at the bottom of the sample after compression (Figure 3.2). The titanium particles are smaller and of higher density (density NaCl = 2165 kg/m^3, density Ti = 4420 kg/m^3), and so are more likely to concentrate at the bottom.

Not only does separation before sintering lead to inhomogeneous foams, it also causes the green bodies to be extremely fragile at places where the titanium content is low. There is very little movement of the powder after the mixing step. Therefore, if this separation is the cause of the problem, then it is likely to be a very difficult challenge for this processing method to overcome.

Box: Volume

All volumes of space holder samples in this chapter are given in mL and this volume is defined as the sum of the volume of the salt and the volume of the titanium powder, ignoring any pores or open spaces in the compact. This initial volume changes slightly when the powders are mixed and again when compressed. When further shrinkage during sintering was measured this will refer to the ratio between green body and sintered product.

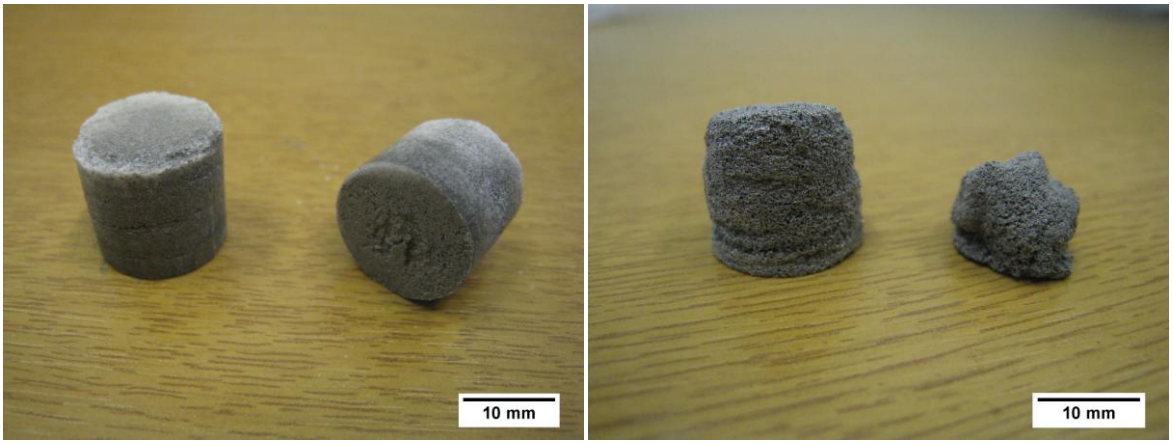

Figure 3.2: Photograph of a large (6 mL) space holder foam at the green body stage (left) and after sintering (right).

Probably as a result of both factors mentioned above, the sintering of the green bodies resulted in high shrinkage and very irregular foams. Therefore, it was decided not to investigate these particular samples further and to reduce the total volume of the components to 2 mL. Furthermore, it was decided to use two different methods to mix the powders together; the normal (dry) mixing method and a method whereby after the initial mixing step several drops of hexane were added to the mixture which was then stirred again (wet method). Using this wet mixing method the powders would readily stick together and therefore separation of the powders between the mixing and the compression step was less likely to occur.

Using a volume of 2 mL it was attempted to produce twenty different types of space holder foams following the method described above, with the processing conditions specified below. However, due to the low levels of titanium in some of the green bodies it was difficult to produce consistent foams. Therefore, three samples of each type were produced. One of the repeats was soaked in liquid paraffin to measure shrinkage (see section 2.3). A second one was cut in half on the Isomet-5000 and polished so that the inner architecture of the pores could be imaged by SEM. The third one was compressed to investigate the influence of the different fabrication methods and the metal content of the foams on the mechanical properties of the foams. Based on the data from these experiments four foams were then selected and three more samples of each of these foams were then produced to repeat the compression tests. Table 1 shows a schematic overview of all the different foams that were produced. Figure 3.3 shows several examples of green bodies and the resulting foams.

Table 3.1: Overview of the different foams produced using the space holder method. In total 20 different foams were produced; foams marked with an '×' were considered the most promising after preliminary examination and were used for mechanical testing as well.

Powder	Mixing	Titanium content (%)				
		20	25	30	35	40
Irregular	Dry	-	-	-	×	×
Irregular	Wet	-	-	-	×	×
Spherical	Dry	-	-	-	-	-
Spherical	Wet	-	-	-	-	-

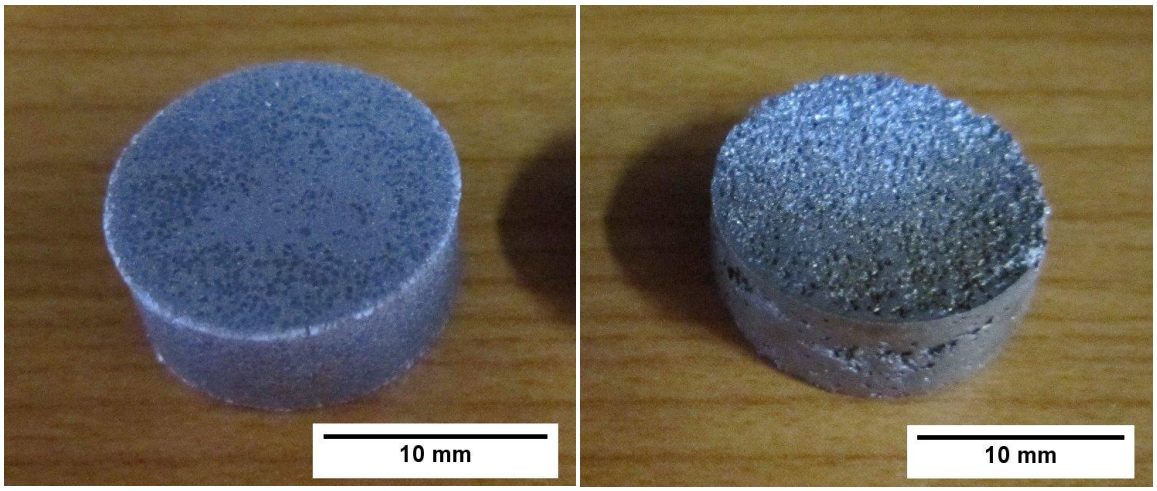

Figure 3.3: Photograph of a small (2 mL) space holder foam at the green body stage (left) and after sintering (right).

3.2 Salt removal

The efficiency of salt removal by the heat treatment was assessed by weighing the samples after the heat treatment and after the washing step, and by comparing these values with the original and the theoretical final weight; the result is shown below (figure 3.4).

These results show that although the heat treatment at 1100 °C is sufficient to sinter the metal particles together, it does not effectively remove the space holder. This can be explained by the fact that although 1100 °C is considerably higher than the melting point of sodium chloride (800 °C) and there is some evaporation of salt from the liquid, this temperature is lower than its boiling point (1400 °C). Therefore, it is unlikely that all the liquid leaches out of the small pores (it will be impeded by capillary action, for example). This means that a washing step is essential for further tests on these foams.

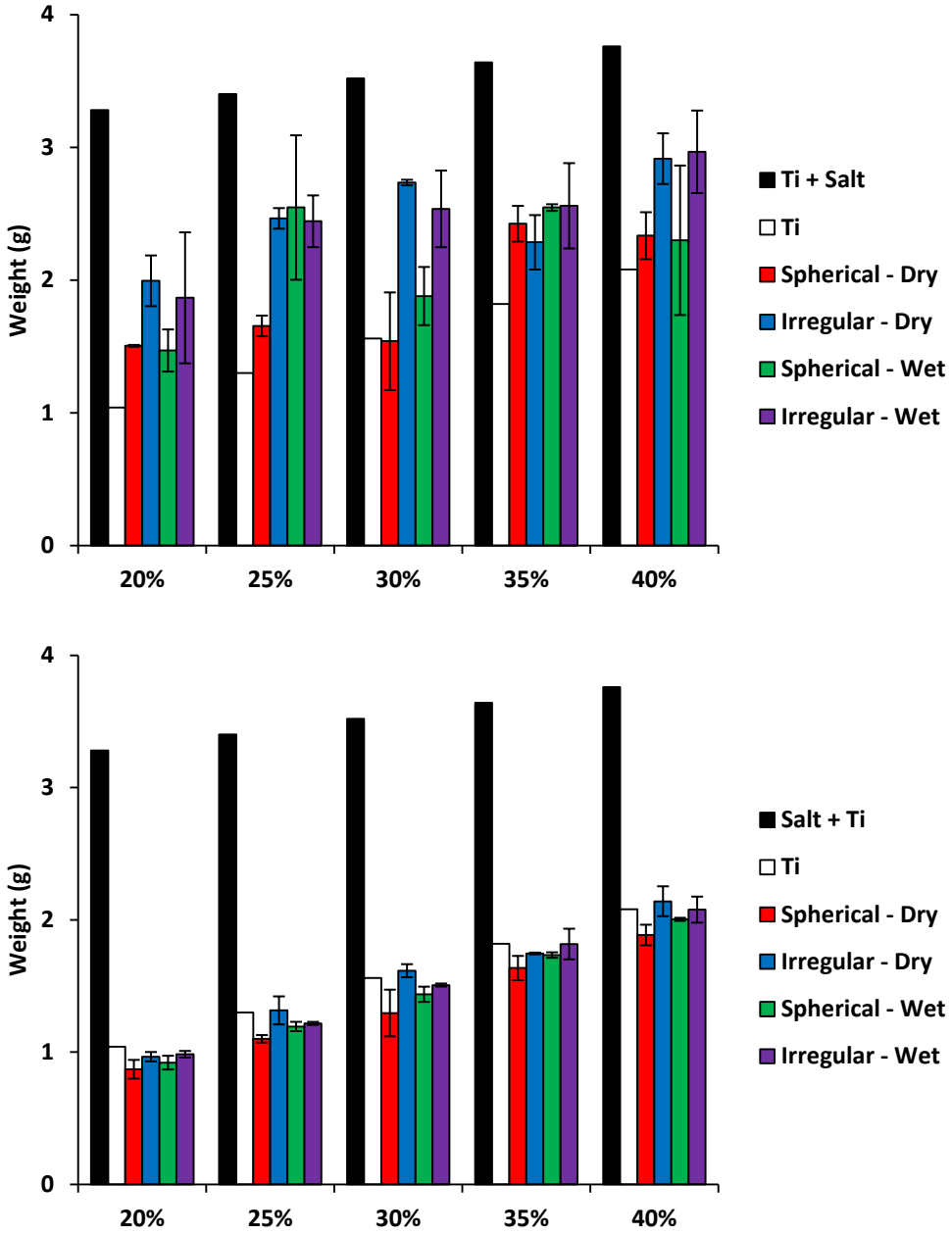

Figure 3.4: Bar chart showing the weight of the space holder foams after the sintering step (a) and after the washing step (b). The black bar represents the theoretical weight of the salt and the titanium combined; the white bar represents the theoretical weight of the titanium alone.

3.3 Shrinkage

A shrinkage test was performed on one sample of each composition (see methods); the results are represented below (figure 3.5).

All samples undergo shrinkage during sintering, although the extent of the shrinkage varies from roughly 5% to 50%. Shrinkage was significantly ($P < 0.05$) lower for samples produced

with irregular-shaped powder Ti6Al4V; the addition of hexane (explored as an aid to improve blending of the powders) during mixing had no significant effect on shrinkage. These trends are to be expected, the smaller surface area to unit volume of the larger powder means that the driving force for sintering (the reduction in surface area to minimise the energy of the system) will be lower.

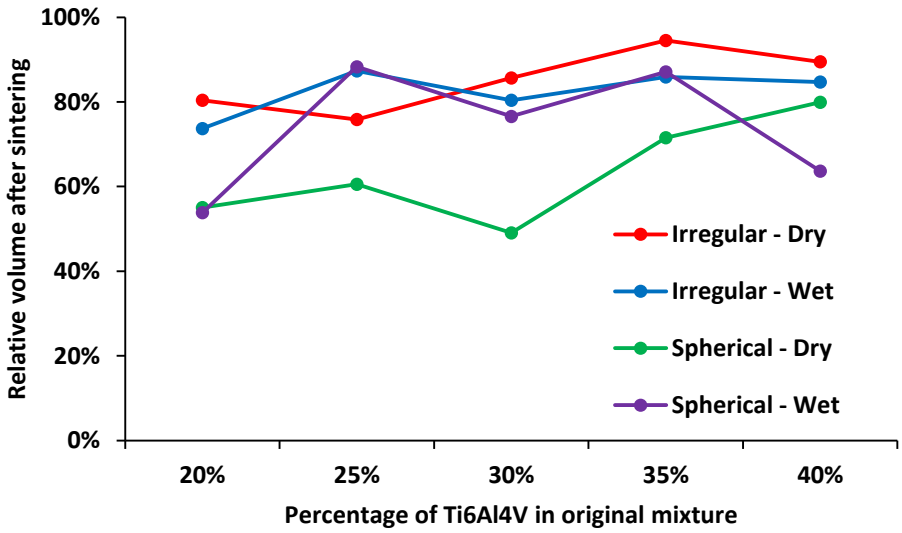

Figure 3.5: Bar chart showing the reduction in gross volume of the foam during sintering. Values represent the gross volume of the foam after sintering and cleaning divided by the volume of the green body.

3.4 Scanning Electron Microscopy

SEM was used to examine the porosity and interconnections of the space holder and the EBM samples. The space holder samples that were prepared using hexane during the mixing step are shown in figure 3.6 and 3.7; figure 3.8 shows a comparison between samples made with the dry and the wet method.

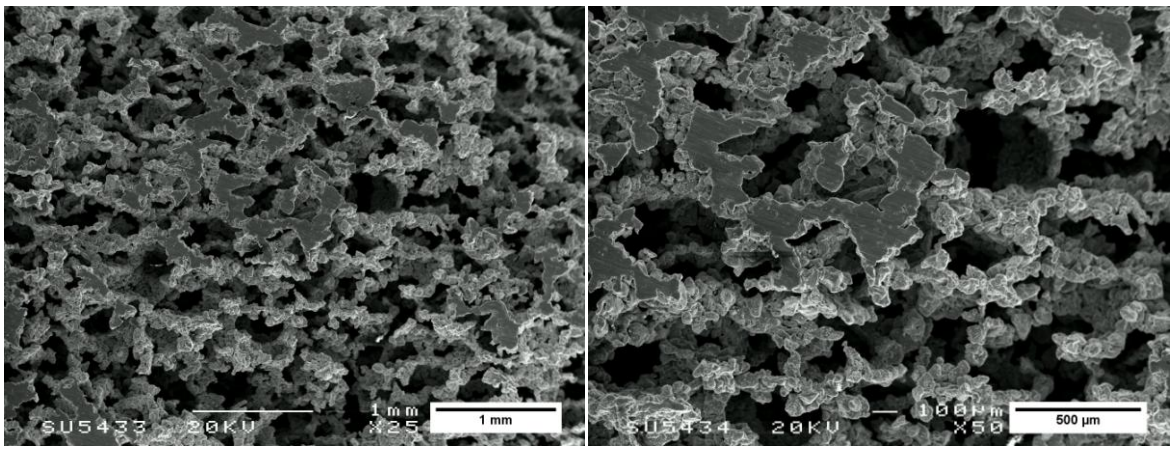
SU5433 20KV
1mm
X25
1 mm
SU5434 20KV
100µm
X50
500 µm

20%

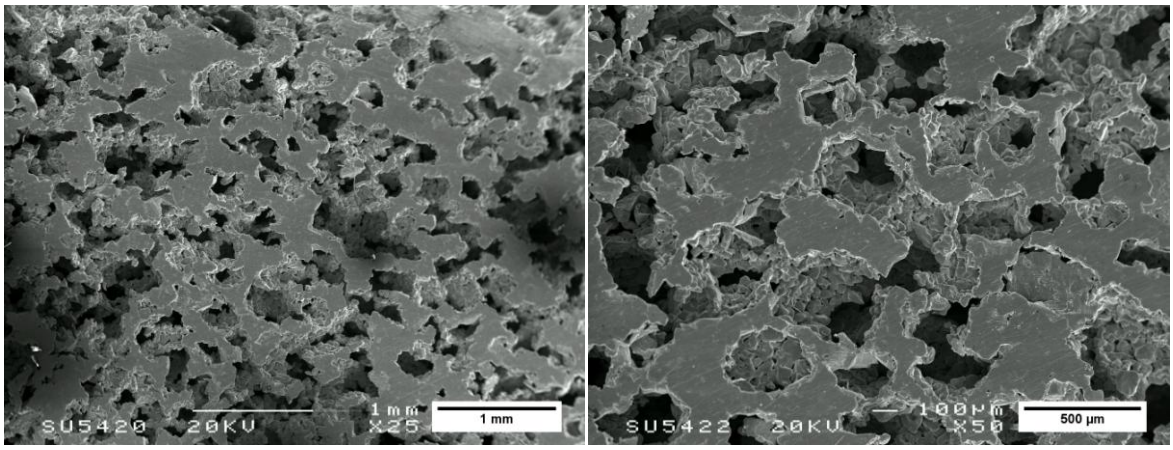
SU5420 20KV
1mm
X25
1 mm
SU5422 20KV
100µm
X50
500 µm

25%

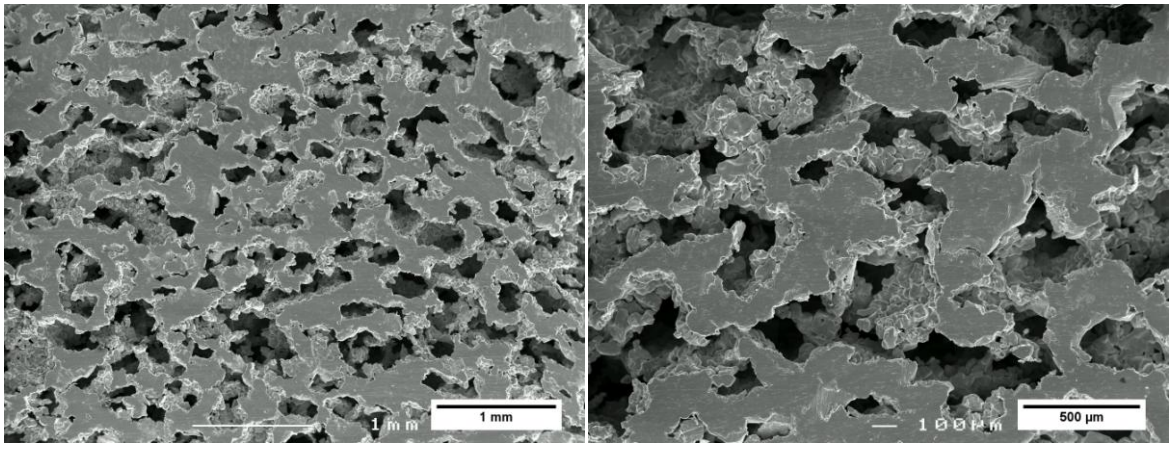
1mm
1 mm
100µm
500 µm

30%

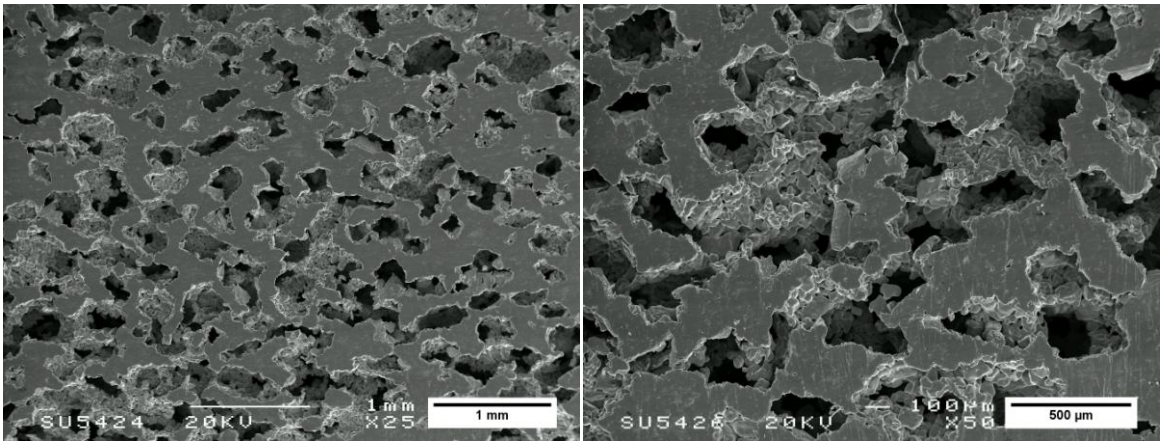

35%

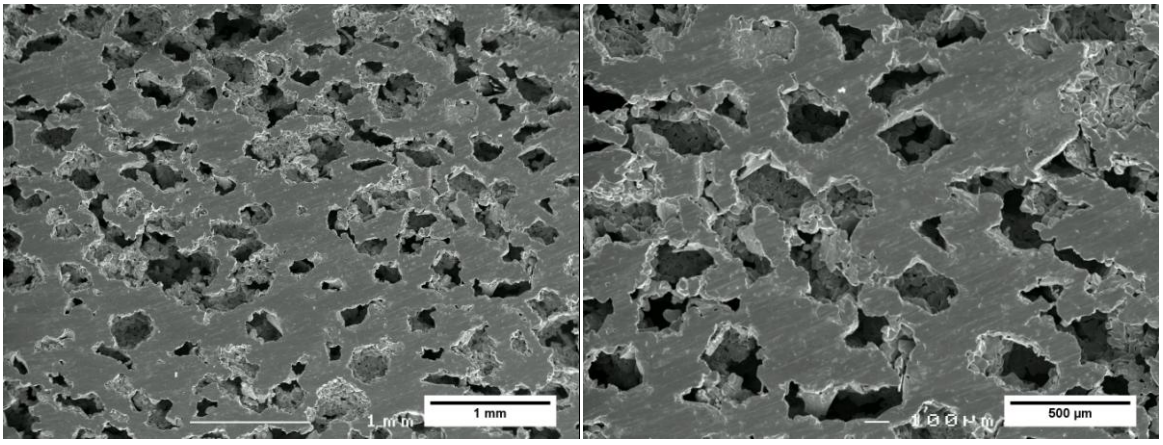

40%

Figure 3.6: SEM images made from the irregular-shaped Ti6Al4V powder using the wet mixing method shown at 25× magnification (left) and 50× magnification (right). The percentages of Ti6Al4V in the original mixture were (from top to bottom): 20%, 25%, 30%, 35% and 40%. Note that in all of these images the areas that show parallel marks from machining represent the areas where structure has been cut.

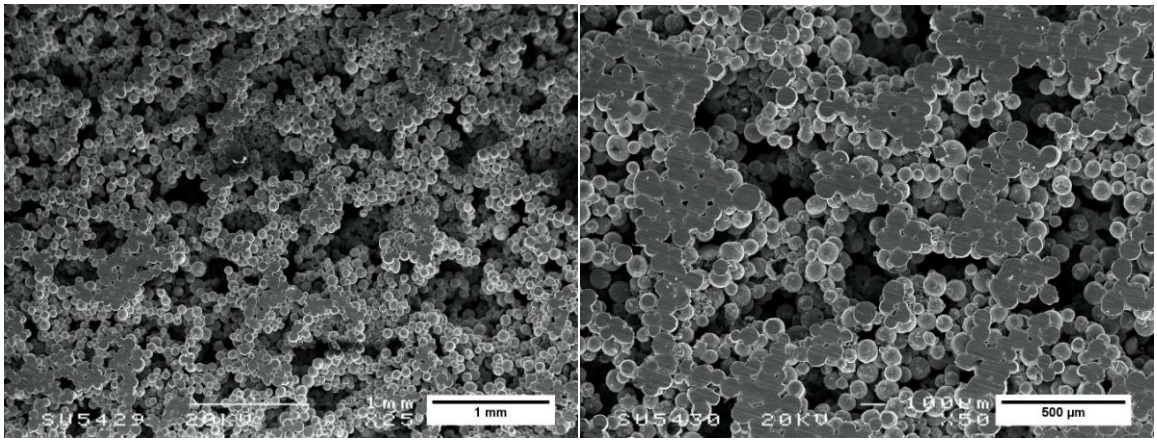

20%

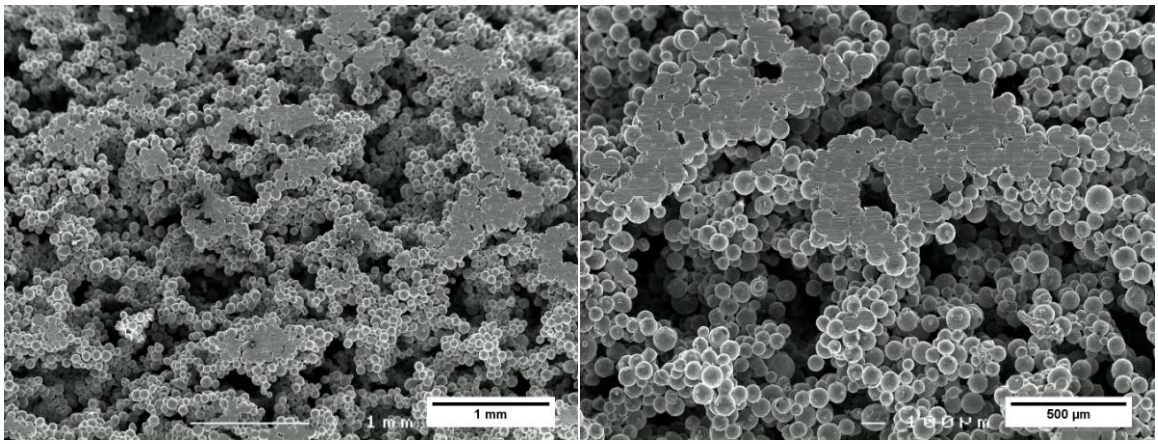

25%

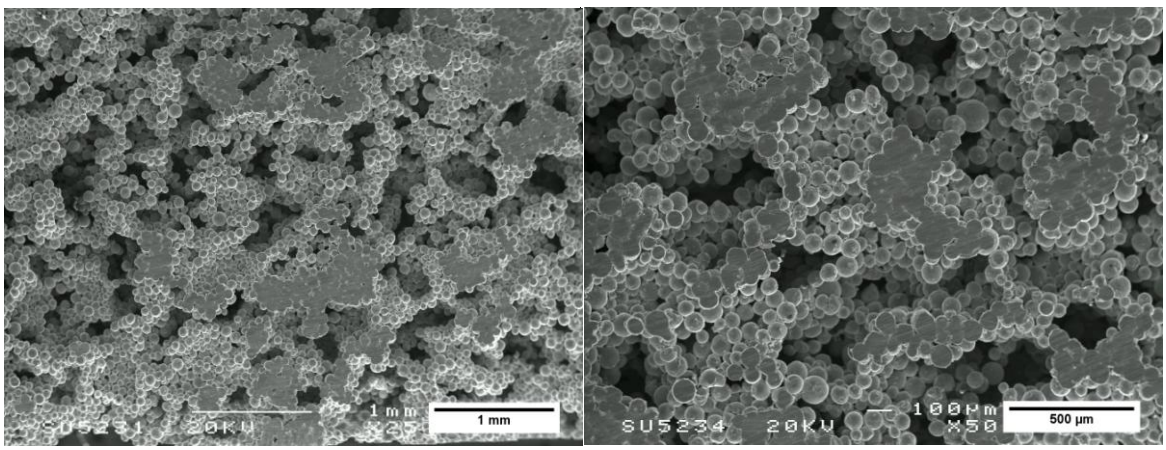

30%

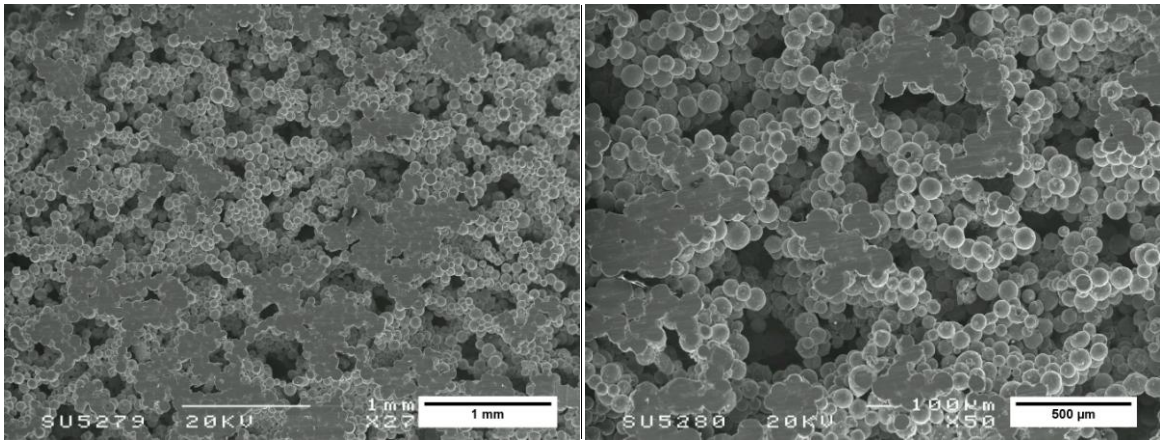

35%

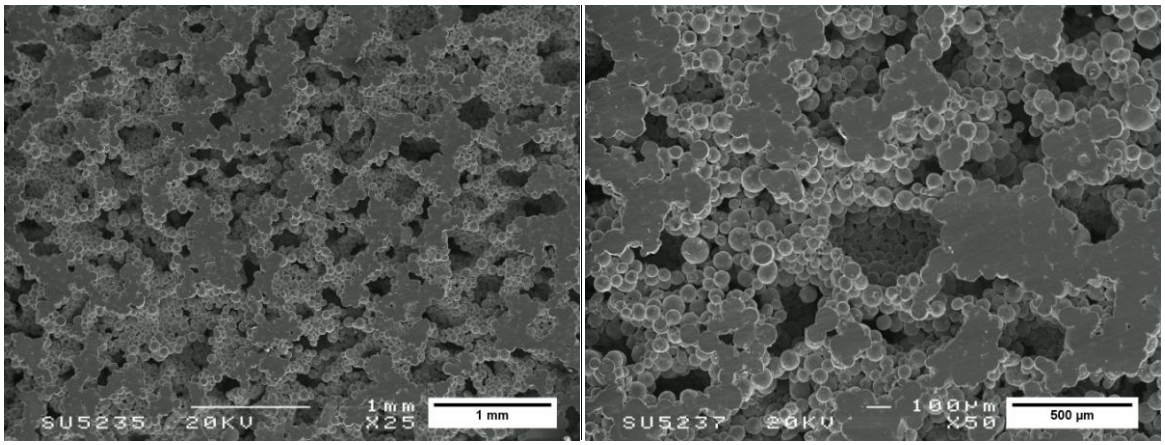

40%.

Figure 3.7: SEM images of foams made from the spherical Ti6Al4V powder using the wet mixing method shown at 25× magnification (left) and 50× magnification (right). The percentages of Ti6Al4V in the original mixture were (from top to bottom): 20%, 25%, 30%, 35% and 40%.

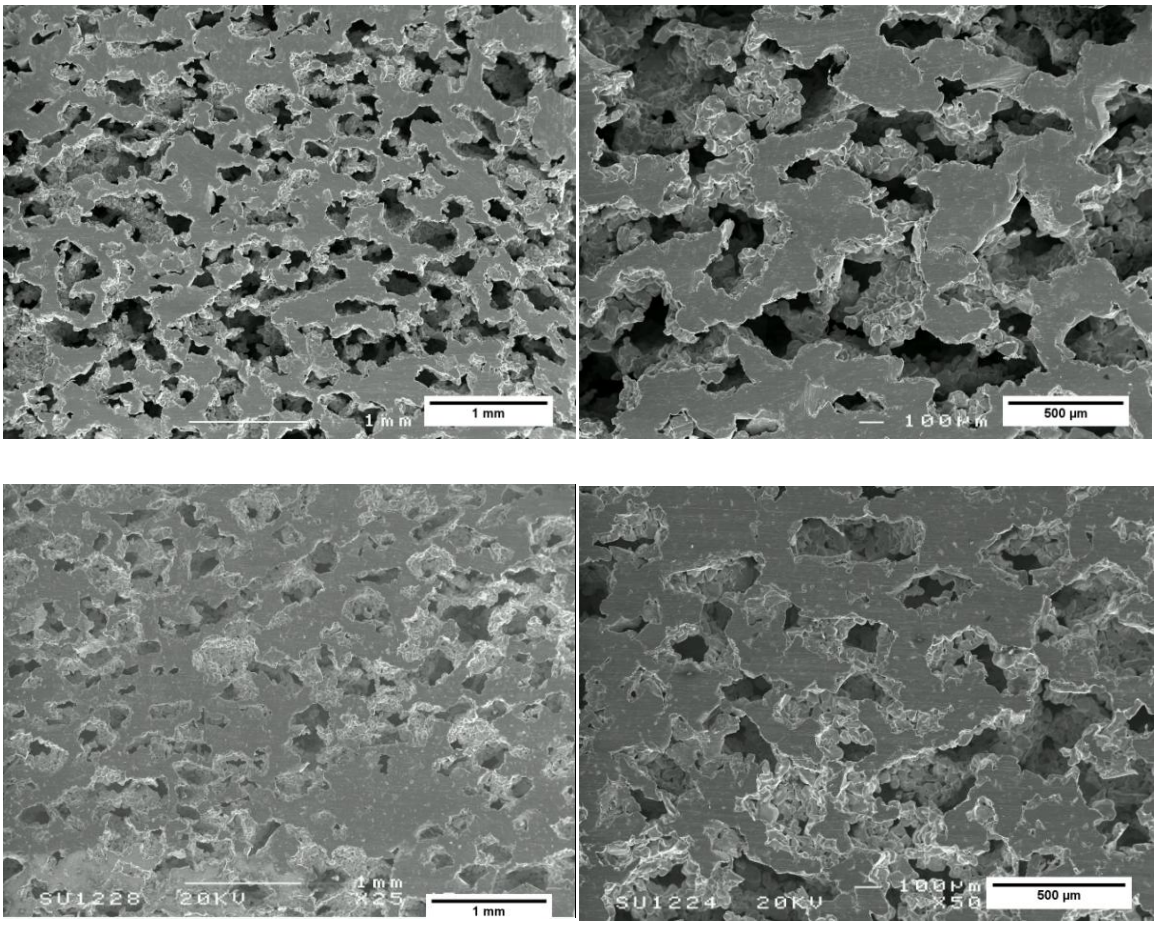

Figure 3.8: Comparison between foams produced using the wet and the dry mixing method shown at 25× magnification (top) and 50× magnification (bottom). The images of the wet method are shown on the left and the images of the dry method are shown on the right. All images show a sample made of the large powder with 30% metal content.

Figure 3.6 and 3.7 show the clear difference in structure when different titanium powders are used. The spherical particles in figure 3.7 are still clearly visible while the irregular-shaped particles in figure 3.6 appear to have fused much better into solid struts with less microporosity. The more efficient packing of the irregular-shaped particles seems inconsistent with the lower shrinkage of these foams, but it is expected that shrinkage of the foams is mainly due to failing struts (which is more likely to occur in struts where the particle packing is inefficient and where microporosity is present) and that the effect of shrinkage due to more efficient packing of the powder is much smaller.

The figures also show the effect of increasing Ti6Al4V content on the porosity of the samples. Most images show foams which still contain the shapes of pores formed by

individual salt particles (250-500 μm), but with decreasing Ti6Al4V content more interconnections appear and the overall structure becomes more open.

Figure 3.8 shows a comparison between foams produced using the wet and the dry method at different magnifications. These, and other samples that were compared by SEM, show no clear differences in the structure of the foam or the sizes or interconnections of the foams.

3.5 Mechanical testing

In the initial mechanical test one sample of all 20 compositions was compressed and the resulting forces were plotted as stress strain curves. Figure 3.9 shows these stress-strain curves which are grouped by powder type and fabrication method (different salt to metal ratios are shown in one graph).

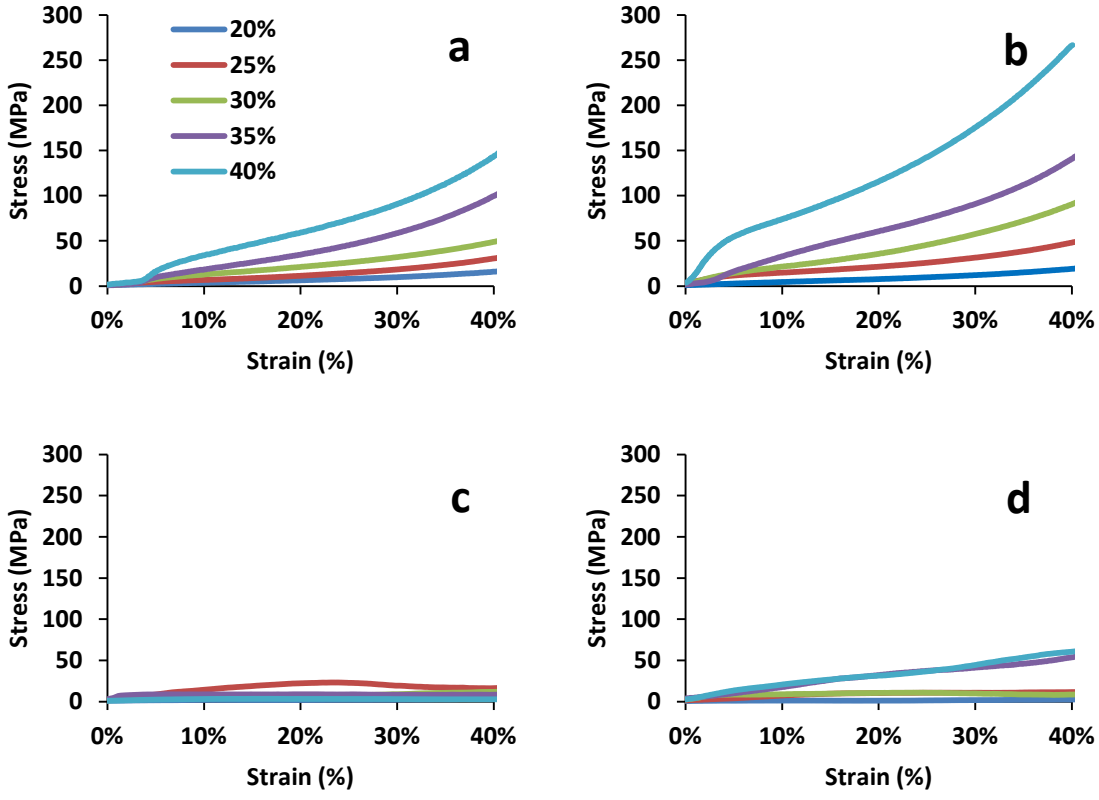

Figure 3.9: Compliance corrected stress-strain curves for the compression of metal foams. a: Irregular – Wet, b: Irregular – Dry, c: Spherical – Wet d: Spherical – Dry.

From these graphs it can been seen that all foams made by the spherical particles are very weak; in many cases it was not possible to identify a region of the stress strain curve that could be used to calculate a Young's modulus indicating that the foams show permanent

deformation from the onset of loading, they crumble rather than undergo elastic deformation. The behaviour of the foams produced by the large irregular-shaped particles was better, but also for these foams there was sometimes little evidence of elastic deformation, especially the foams with a lower metal content. Therefore, the compression test was repeated only with the 35% and the 40% large particle foams produced either by the wet or the dry method (figure 3.10).

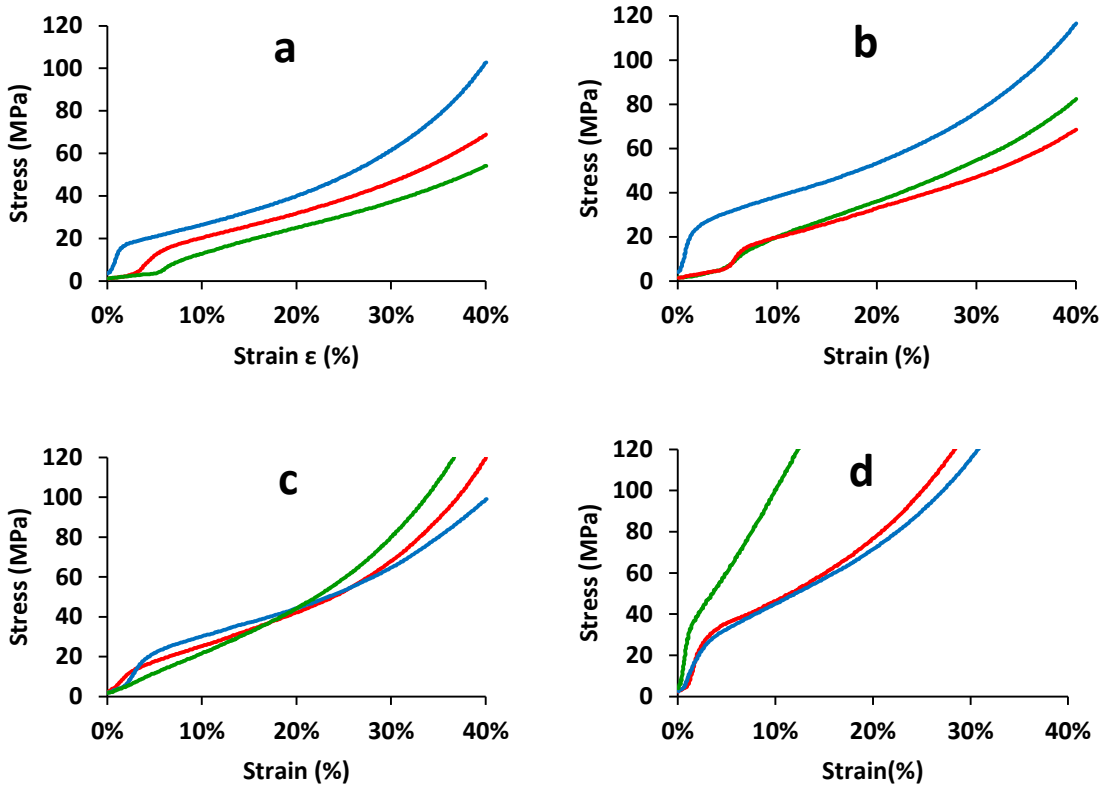

Figure 3.10: Triplicate tests of the four most promising space holder samples, all made using the irregular-shaped powder. a: wet - 35%, b: wet - 40%, c: dry - 35%, d: dry 40%.

From these graphs it can be seen that there are large differences in the behaviour under compression between the different fabrication methods, but also between different samples made by the same method. The crosshead position at which the force exceeded 100 N was defined as 0% strain; however, due to the fact that some of the space holder samples were not entirely flat the linear regions do not always start at 0% strain. In these samples there is a zero error contained in the strain, but this has not been corrected further due to the ambiguity in where the true zero point should lie, and the fact that this is produced due to the inconsistency in dimensions introduced by the technique.

The slope of the linear region of each of the curves was used to determine the Young's modulus of the materials. The results are plotted in figure 3.11.

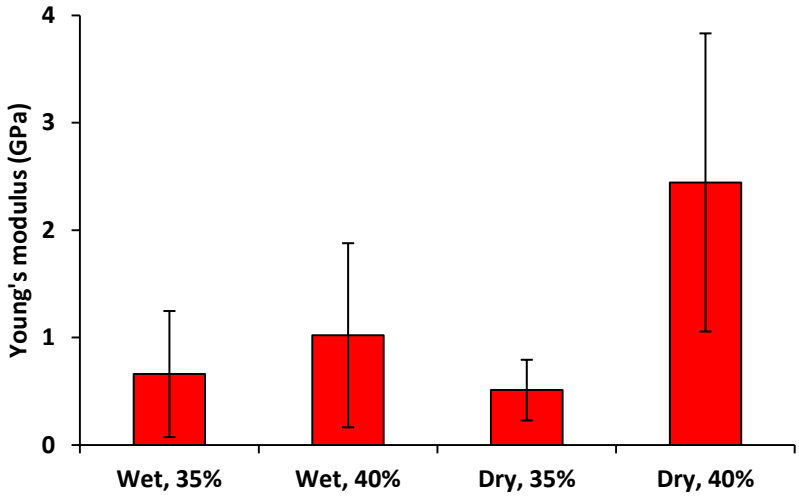

Figure 3.11: Young's moduli of the four selected space holder foams. Bars represent mean ± SD (n=3).

All samples made by the space holder technique showed a large variability and a very short or no linear region. The calculated Young's moduli were analysed by an ANOVA-test. This test showed a p-value higher than 0.05 which indicates that the differences between the groups were not statistically significant.

In summary, these results have shown that although the space holder method is a simple and versatile method to produce metal foams, the consistency of the properties of the foams using the current protocol is likely to have a negative effect on its potential applications. Therefore it was decided not to use these foams in the biological tests described in chapter 5, but instead focus the effort on other, more consistent foams.

4. Electron Beam Melting

In this chapter the results of the work related to EBM are described; it describes the structures that were designed and built and the structural and mechanical properties the most interesting samples. A thorough discussion of these results can be found in chapter 5. The highlights of this chapter have recently been published (Van Grunsven et al. 2014).

4.1 Prototype

The first structure built using the EBM process was a prototype that was designed to investigate some of the limitations of the EBM process such as feature size, pore size and powder removal depth. The model of the structure consisted of a solid base (10 × 10 × 2 mm) and a porous layer (10 × 10 × 4 mm) on top. The porous layer was made up of diamond unit cells (see figure 4.1) with a unit cell size of 2 × 2 × 2 mm and a strut thickness of 500 µm. The diamond structure is the most commonly used form of lattice (Heinl et al. 2007; Heinl et al. 2008), and this was selected to allow comparison to other work. This model was designed in Netfabb as an STL-file and later converted to an ABF; this is a format that represents 3D models as layer-by-layer information. The model is shown in figure 4.2.

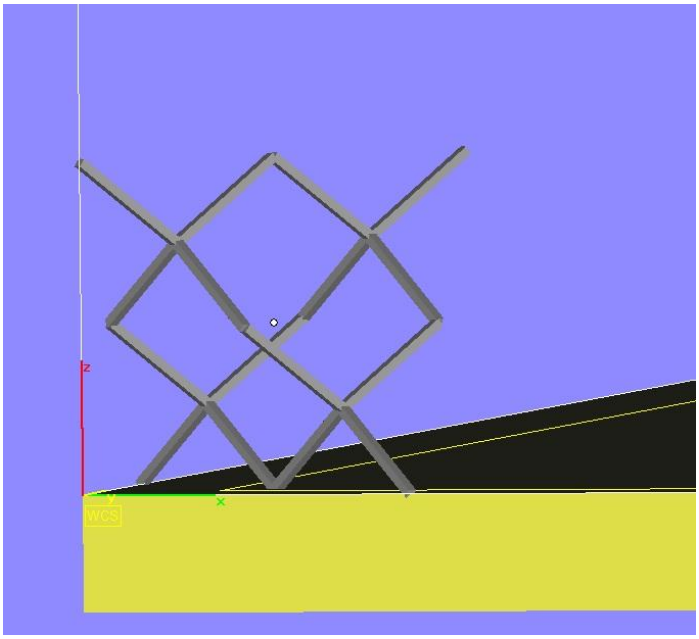

Figure 4.1: The diamond unit cell.

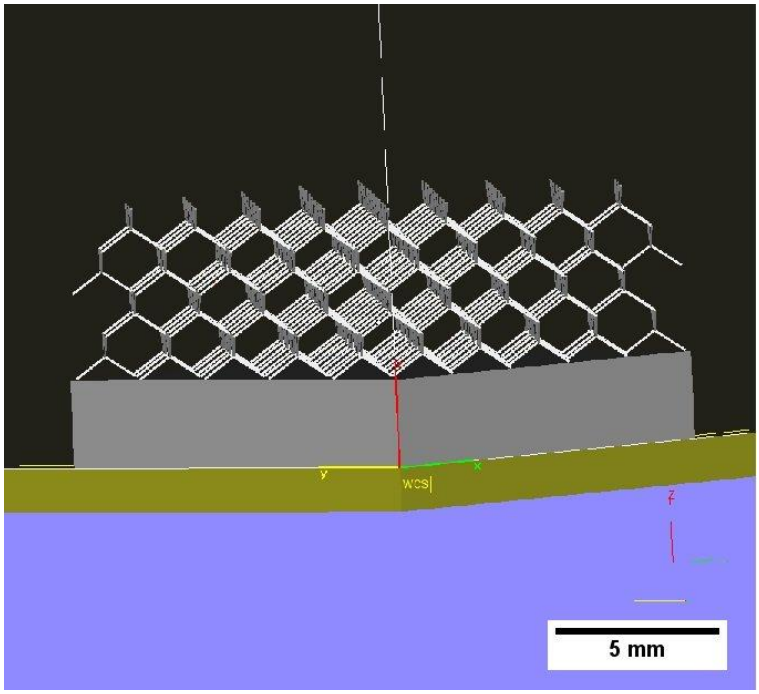

Figure 4.2: The CAD model of the prototype shown in Netfabb.

During the cleaning of these prototypes in the PRS it became clear that it was possible to remove the powder from all the pores of the prototype, but that cleaning of these porous structures takes considerably longer than flat surfaces (cleaning the prototype structure took approximately 10 minutes). Furthermore it was noticed that to remove all the powder from this structure the blasting particles only had to penetrate around 7 mm into the structure and that cleaning larger structures, even with the same pore size and architecture, might be considerably more difficult.

After cleaning, these prototypes were examined by SEM to determine the accuracy with which the diamond structure was reproduced and the properties of the surfaces in more detail (figure 4.3).

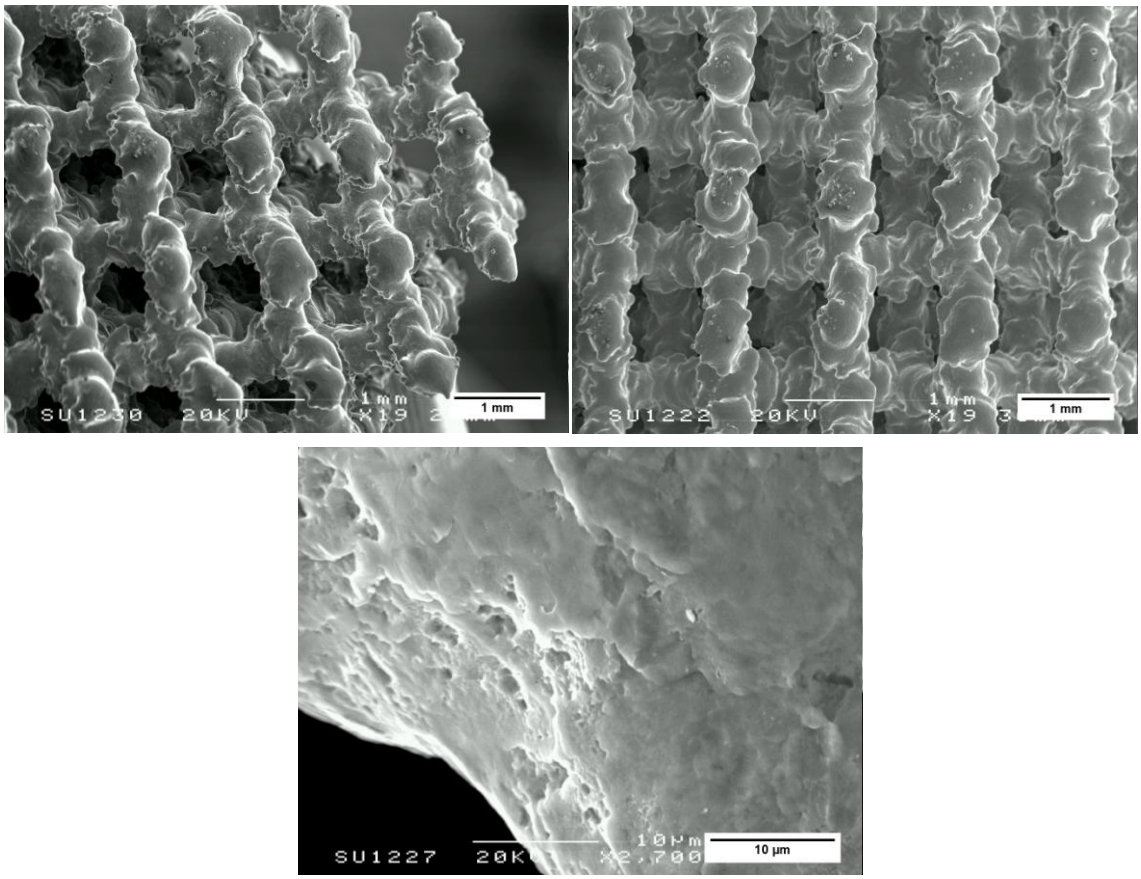

Figure 4.3: SEM images of the prototype structure.

4.2 Unit cell size

The possibility of removing powder from smaller pores was investigated by producing three lattices with roughly the same overall size but different unit cell sizes. The unit cell sizes of these new structures were 2.0 mm, 1.5 mm and 1.0 mm (figure 4.4). In the case of the 2.0 mm unit cells it was difficult to remove all the powder from the inner pores but it was possible to do so. For the 1.5 mm unit cell size it was possible to remove most of the powder from the outside few cells of the lattice, but even after prolonged cleaning a solid core of powder remained at depths of more than 2-3 cells. Powder removal from the lattice with the 1.0 mm unit cell was not possible; the blasting particles penetrated less than 1 mm into the lattice. In order to investigate how deep particles penetrated into the 1.5 mm lattice one lattice that was cleaned as well as could be achieved was embedded in resin and cut in half (figure 4.5). From this image it can be seen that the penetration depth of the powder depends slightly on the orientation of the lattice (where along some orientations there is less obstruction by the struts), but lies mostly between 5 and 6 mm.

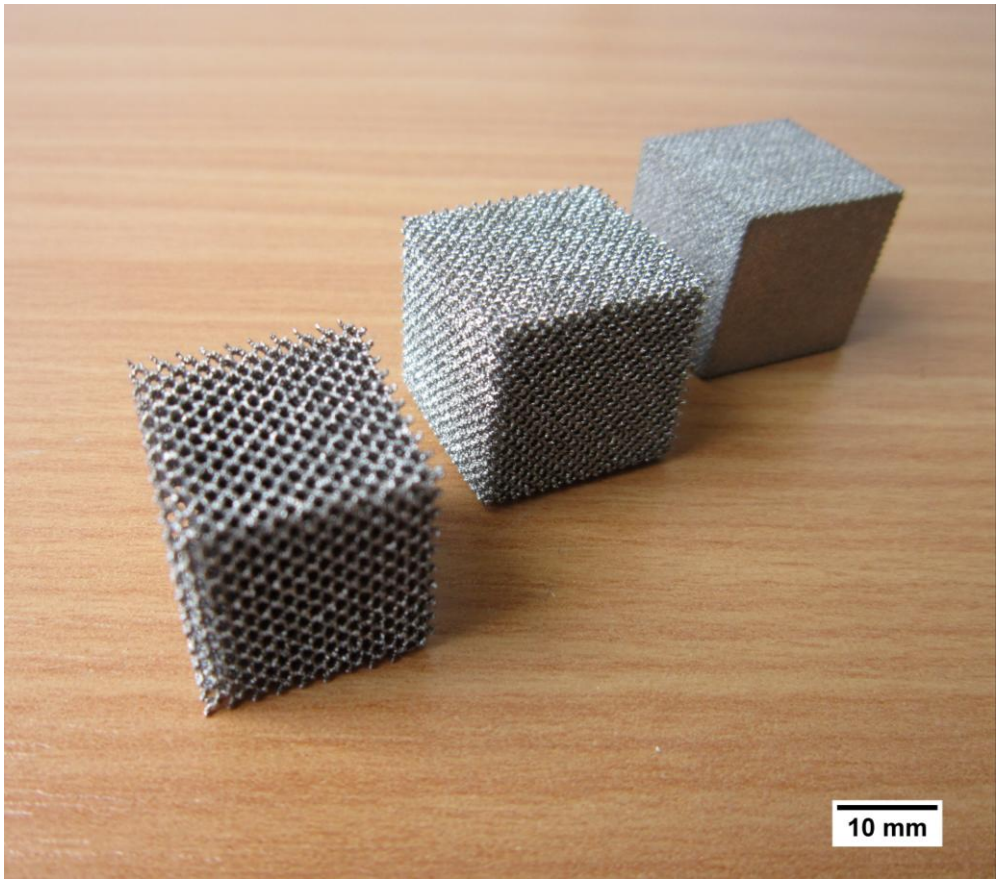

Figure 4.4: Photograph of the three lattices with different unit cell size. From left to right: 2.0 mm, 1.5 mm and 1.0 mm.

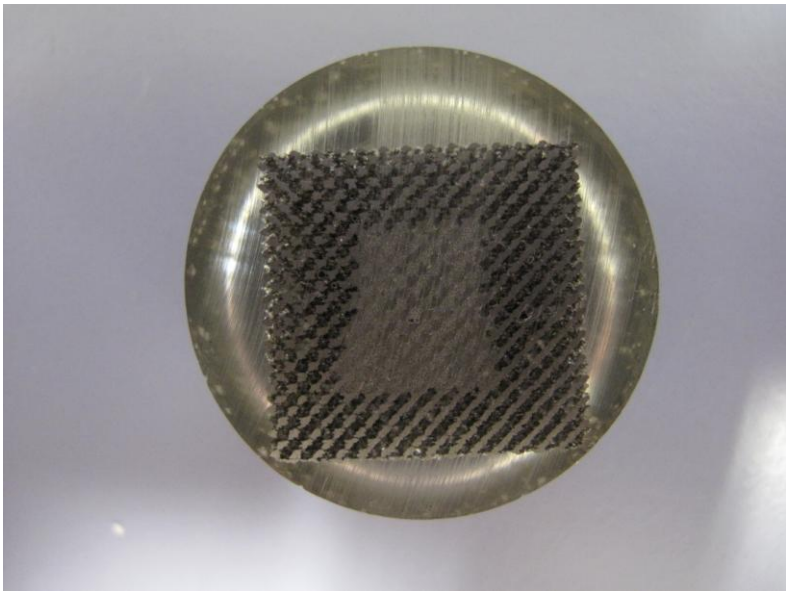

Figure 4.5: Photograph of a lattice with a unit cell size of 1.5 mm that was cleaned embedded in resin and cut in half. The solid grey core is the un-melted powder that could not be removed in the PRS.

In order to investigate the properties of lattices with a unit cell size of 1.5 mm without a solid core of un-melted powder in the middle, new lattices were designed with the same unit cell size, but a smaller overall size. Two new lattices were built one with dimensions of 15 × 15 × 15 mm (i.e. 10 unit cells in each dimension) and one of 9 × 9 × 9 (6 unit cells in each dimension).

After building it was attempted to remove all the powder from the centre of the lattice. As with the previous (20 mm) structure the powder was only able to penetrate around 6 mm into the lattice; in this case this was sufficient to clean the small (9 mm) structure but not to clean the larger (15 mm) one.

In order to compare the porosity of the lattices with the different unit cell sizes comparable images were taken with SEM which were then used to measure pore diameter and strut thickness (figure 4.6 a). The two structures were also compared to each other in terms of density by weighing and measuring the overall volume (figure 4.6 b).

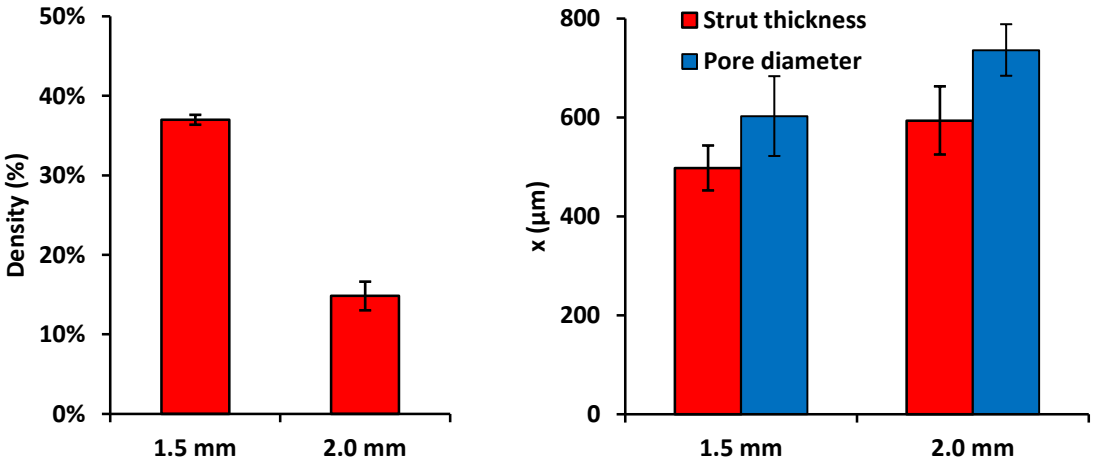

Figure 4.6: Comparison of the density (a) and the average strut thickness and pore diameter (b) of the two different unit cell sizes.

For mechanical testing all samples were placed in a Hounsfield mechanical testing apparatus and compressed at a speed of 0.25 mm/min to around 50% of the original size. The curves were corrected for the compliance of the equipment, and converted to stress-strain curves, based on the original lattice dimensions. The force-displacement curves as well as the stress-strain curves are shown below (figure 4.7).

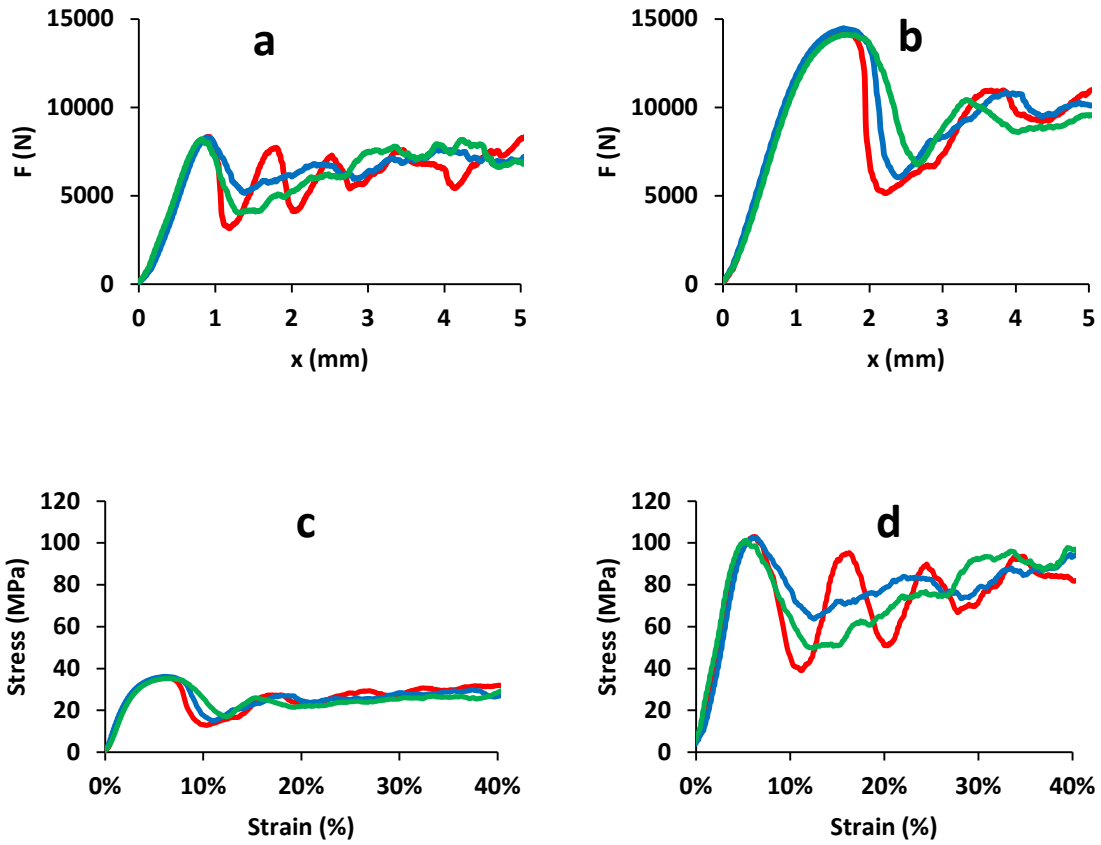

Figure 4.7: Force displacement curves (a-b) and stress-strain curves (c-d) obtained by compression of the two lattices; left: 2.0 mm, right: 1.5 mm.

The resulting curves were used to determine the Young's modulus and the 0.2% offset yield strength (figure 4.8).

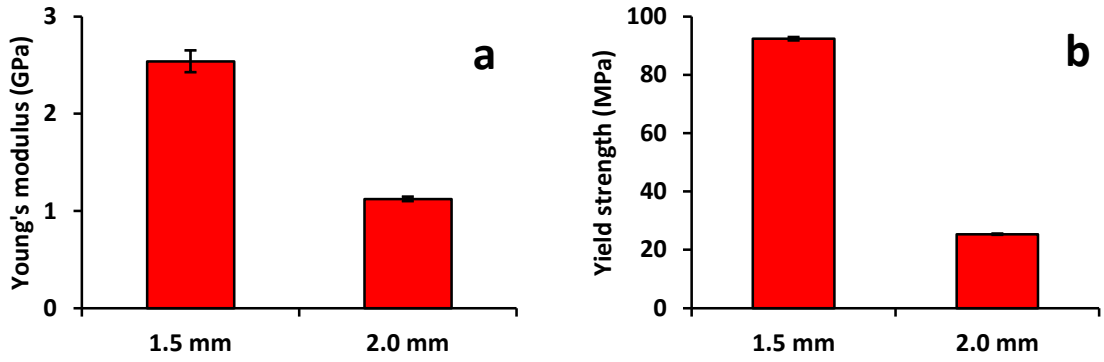

Figure 4.8: Comparison of the stiffness (a) and the yield strength (b) of the two lattices.

4.3 Graded structure

The next step in the project was to design and build a graded structure where the properties of the lattice vary depending on the vertical position. One way of designing a graded lattice is to design different layers of unit cells with the same cell size but a different strut thickness. These layers can then easily be merged to one CAD file so that the model can be built as one single structure.

It was decided to build a graded structure consisting of three layers with the strut thickness as the only variable. These three layers consisted of 2 mm unit cells with each layer having five unit cells in the x and y direction. The modelled strut thicknesses of the three layers were 200, 500 and 800 µm.

In order to compare this structure to non-graded lattices three more lattices were built each having the same strut thickness as one of the layers of the graded lattice. These structures all had dimensions of 8 × 8 × 4 mm and could be used to compare density, stiffness and yield strength.

The graded structure was built using the same parameters as for the previous builds; it was then cleaned and examined using SEM (figure 4.9) and MicroCT to examine to what extent the physical structure produced matched the model. After scanning the graded lattice with MicroCT the obtained scans (figure 4.10 a) were first converted to a series of 2D images representing a slice through the samples in the x-y plane (figure 4.10 b-c). This set of images could then be smoothed (figure 4.10 d-e) and converted to a 3D model of the entire structure (figure 4.11).

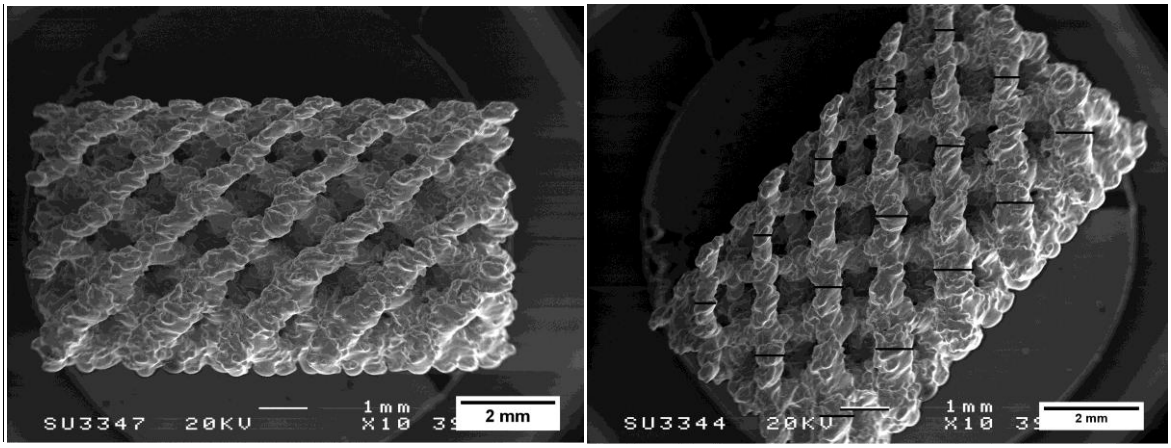

Figure 4.9: SEM images showing the surface of the graded lattice.

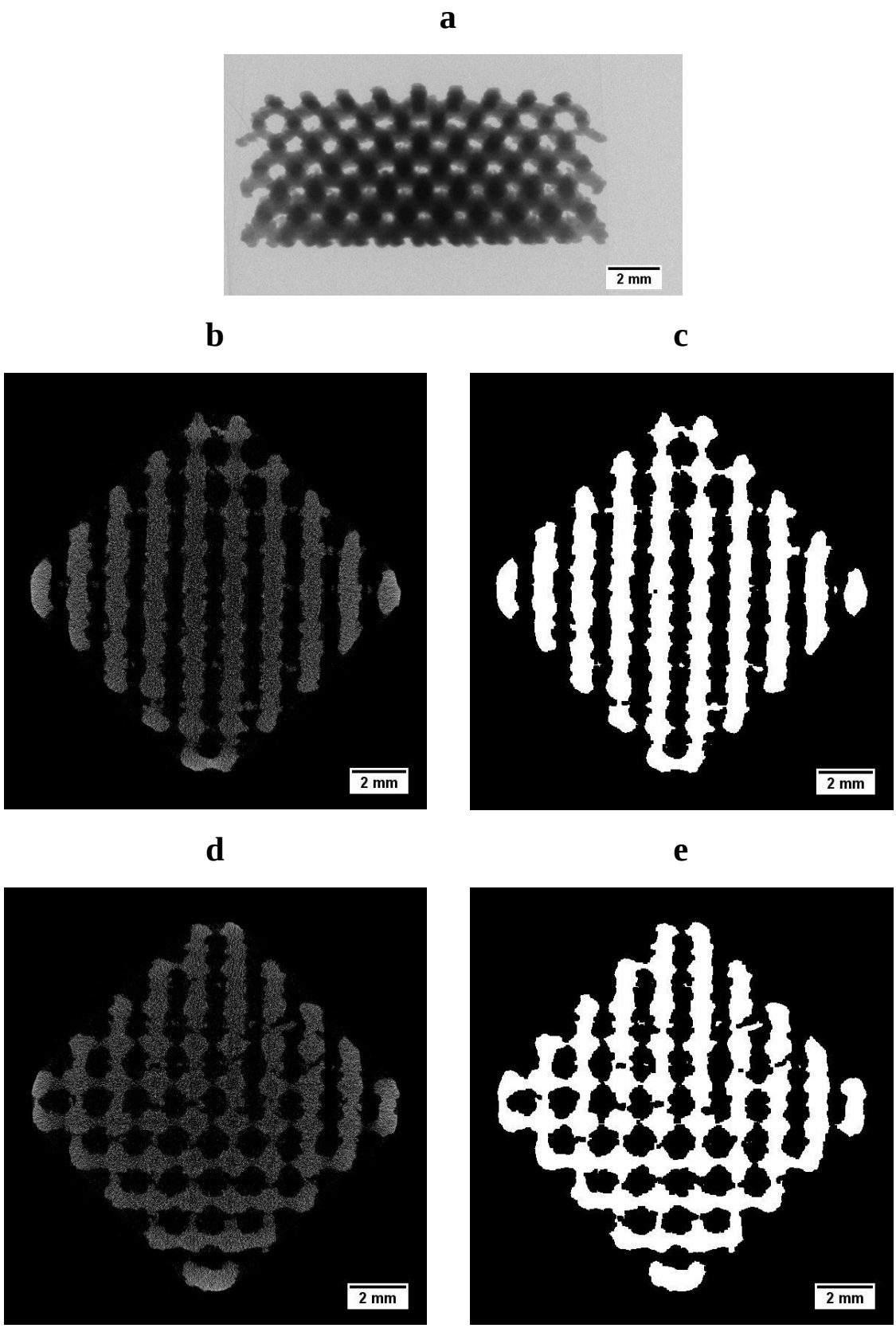

Figure 4.10: A single transmission x-ray image as an example of the images used in the MicroCT reconstruction (a), 2D images obtained by MicroCT in greyscale (b,d) and binary (c,e) that represent slices of the graded lattice.

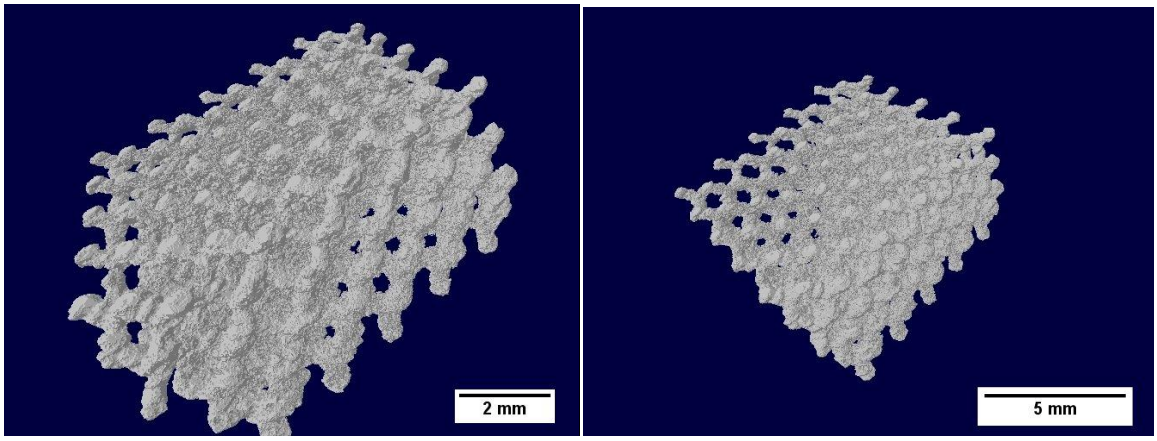

Figure 4.11: 3D reconstruction of the graded lattice based on the set of slice images.

Both SEM and MicroCT images confirmed that the structures had a highly regular and interconnected porosity (Table 4.1). When the designed strut size was 800 μm there was no significant difference between the CAD model and the product, but for the smaller designed strut sizes (500 or 200 μm) those in the product were significantly higher than the CAD model ($p<0.05$). This discrepancy occurs because when trying to build small features with sizes similar to the melted volume, the energy parameters of the beam (e.g. beam speed and beam current) become more important in determining the shape of the product than the original CAD file.

The average strut spacing of the three different layers is closely related to the thickness of the struts and measurements from SEM images showed a narrow distribution in all layers. These differences in strut thickness gave three different relative densities, varying from 21% at a model strut thickness of 200 μm to 43% at 800 μm.

The graded lattices were tested in uniaxial compression (figure 4.12). The lattices behave in a highly reproducible way under compression, even after the initial failure. Three near-linear regions can be clearly distinguished, all followed by a point of failure and a significant, but temporary, reduction in the stress required for further compression. Visual observations during the tests confirm that the three stress maxima correspond to the collapse of individual layers in the lattice, with the layer with the thinnest struts collapsing first.

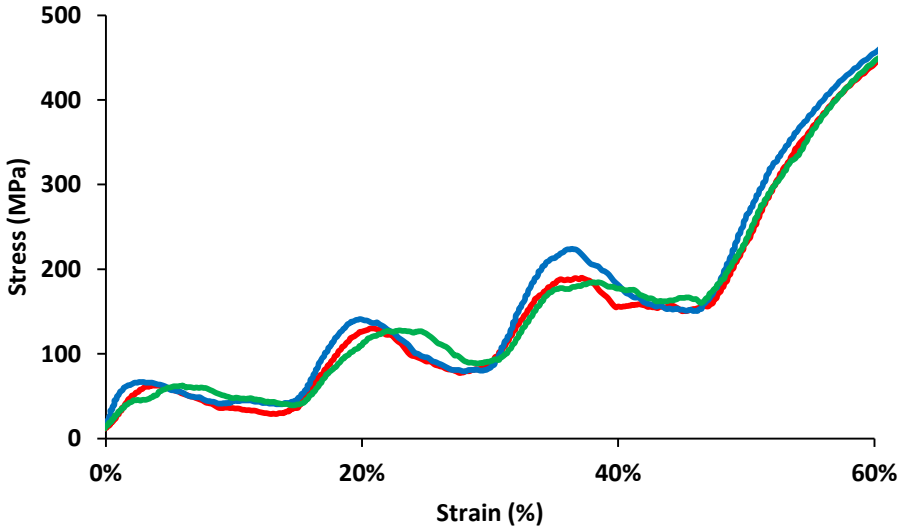

Figure 4.12: Stress-strain curves of three graded lattices under compressive loading. All curves clearly show the collapse of the individual layers and the increasing stress required to further crush the structure.

These curves were then compared to curves recorded for the three uniform lattices to see how the properties of these lattices compare to those of the graded structure. All the uniform lattices were also measured in triplicate and the results are shown below (figure 4.13)

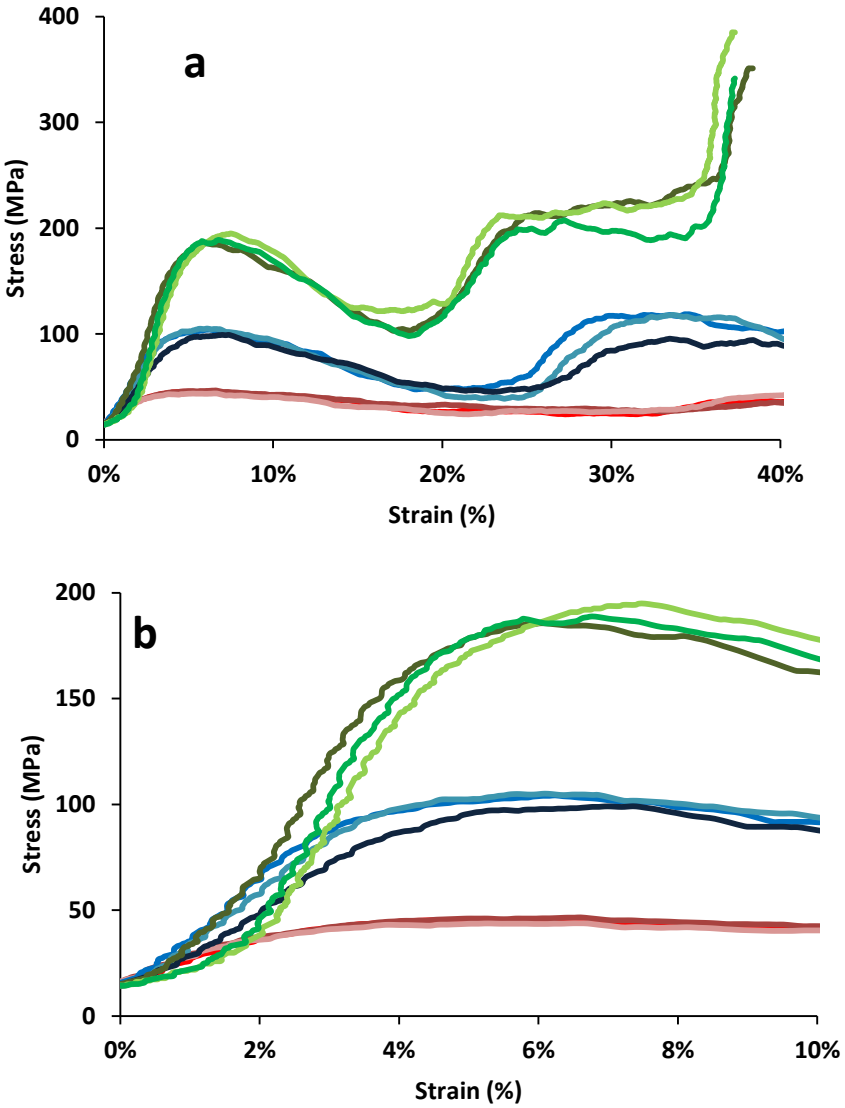

Figure 4.13: Stress-strain curves for the three uniform lattices that had the same strut thickness as the layers of the graded lattice. Top layer: red, middle layer: blue, bottom layer: green; a: full stress-strain curve showing the collapse of all layers, b: low-strain values showing the elastic region of the lattices.

The mechanical data obtained from these curves and the density values were combined with the data from the graded lattice and are shown below (table 4.1, figure 4.14).

Table 4.1: Structural and mechanical properties of strut thicknesses (Mean ± SD).

Model strut thickness (µm)	Strut thickness (µm)	Strut spacing (µm)	Relative density (%)	Young's modulus (GPa)	Yield strength (MPa)
200	398 ± 37	827 ± 49	21 ± 0.6	1.13 ± 0.03	37 ± 1
500	600 ± 60	593 ± 57	31 ± 0.4	2.48 ± 0.40	89 ± 4
800	769 ± 42	556 ± 51	43 ± 0.1	5.38 ± 0.37	160 ± 2
Graded	-	-	33 ± 0.3	2.28 ± 0.84	46 ± 5

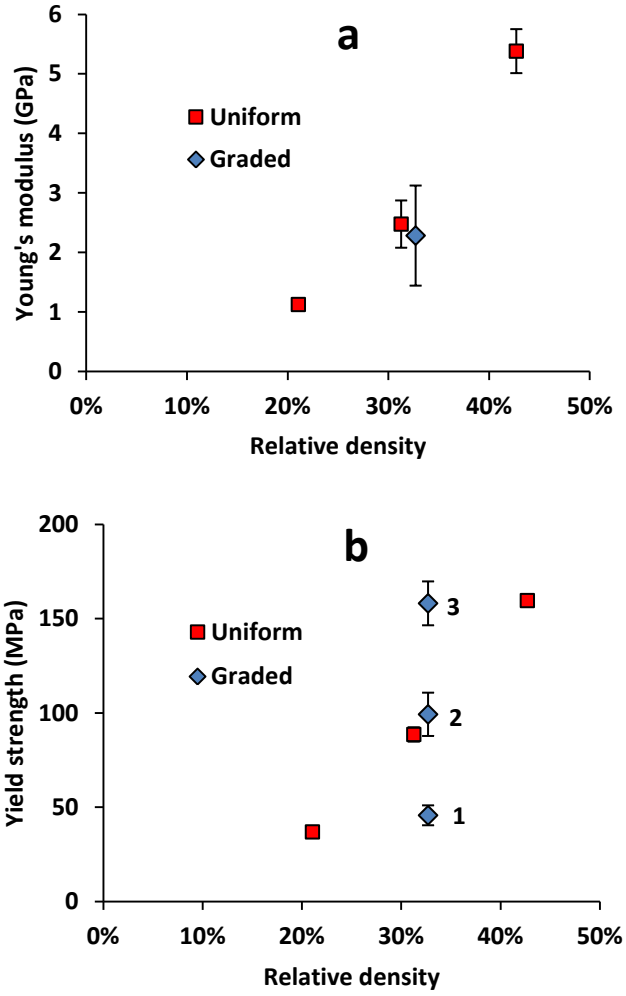

Figure 4.14: Comparison of the mechanical properties of the graded and uniform lattices against relative density; a) Young's modulus, b) yield strength. The values of the three stress peaks are shown for the graded lattice.

As expected there is an increase in Young's modulus of the uniform lattices with increasing strut thickness (figure 4.14). Statistical analysis indicated that there is a significant difference ($p<0.05$) between all the uniform lattices and also between the graded lattice and the 800 µm uniform lattice.

The 0.2% offset yield strength was determined and was significantly higher at a higher strut thickness for the uniform lattices. The yield strengths of the three layers of the graded lattice were also assessed and found to be not significantly different from the corresponding uniform lattices.

5. Biological assessment

This chapter describes the results the tests that were performed on different titanium lattices to investigate the biological response to the EBM produced structures. More specifically, it was aimed to investigate cell attachment, cell proliferation, production of ECM, and bone ingrowth. A discussion of the results can be found in chapter 6.

5.1 Resazurin reduction assay

One of the most commonly used tests used to obtain data for the in vitro cell culture experiments is the resazurin reduction assay for cell viability. Before using this assay for viability testing on materials the assay was tested on a range of known concentrations of cells to confirm that the assay is linear and to get an idea of the concentration and incubation time suitable for testing titanium lattices.

In this experiment MG63 cells were seeded in six concentrations ranging from 2,500 to 15,000 cells, allowed to attach overnight and then incubated in 500 µL of resazurin-containing medium for 6 hours. After the incubation two 200 µL samples of each density as well as two negative controls were transferred to a 96-well plate (figure 5.1).

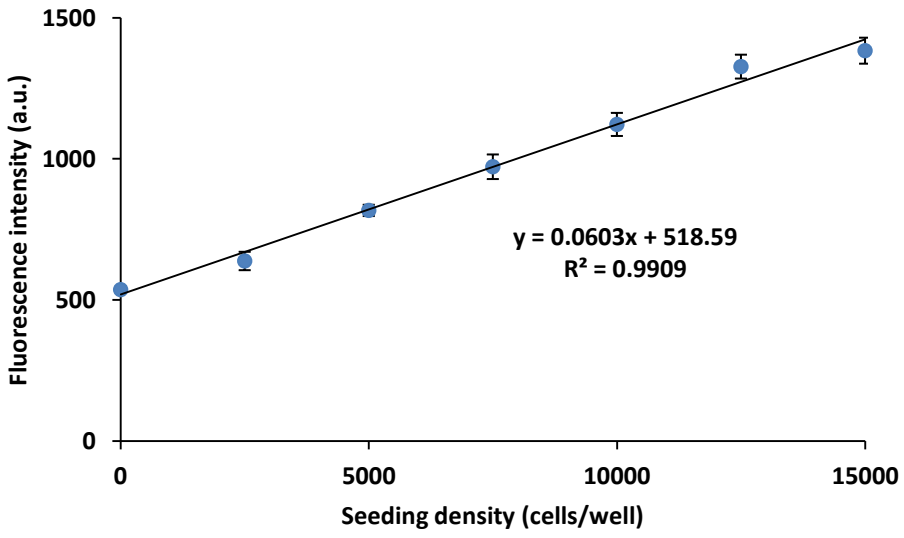

Figure 5.1: Graph showing the fluorescence intensity measured on different cell numbers.

There is a linear relationship between cell number and fluorescence intensity (Figure 5.1). There is also a 'background' fluorescence intensity which is the fluorescence intensity

measured with no cells present. This effect might occur either because the unreacted dye is also slightly fluorescent at the measured wavelength or because of slow spontaneous degradation of the resazurin. From these and other experiments it was seen that this background value can vary depending on the stock solution that is used. Therefore, all the viability measurements were done with individual negative controls to compensate for this effect (O'Brien et al. 2000).

The output of the plate reader that was used to measure the fluorescence intensity of the medium is given in arbitrary units, but using this curve an estimate can be made of cell number based on the following equation.

Equation 5.1: $CN = C \times I$

In this equation CN in the cell number, C is a constant based on the standard curve and I is the fluorescence intensity. This equation, however, relies on the assumption that the metabolic rate of each cell is the same and constant over time. As this may not always be the case another option is to present data as a percentage of a positive control (Mallick et al. 2012).

5.2 Cell seeding

The next step in the project was to investigate the effect of seeding method on the efficiency and the consistency of the seeding. Many cell viability tests for biomaterials are carried out by simply putting a material in a culture plate and pipetting a cell containing medium onto the material (‘high volume’ method). Over time cells will sink to the bottom of the well and spread equally on the materials. In case of a highly porous material or a material that is much smaller than the plate in which it is cultured this method may lead to a low seeding density or a highly inhomogeneous coverage of the surface as most cells will ‘land’ on the top surface of the materials and relatively few cells will enter the pores of the material. In this case a method whereby a small amount of medium is added could be a better option. This method involves adding the cells suspended in an amount of medium that is large enough to keep the cells alive until they have attached and small enough for all the liquid to be contained inside the pores of the material without leaking (‘low volume’ method). The size of this volume depends highly on the type of material and the pore size.

A third method that can be used to seed cells onto a porous material is to seed cells in a small volume of medium with a natural clotting agent, such as fibrinogen, added to it. This allows the cells to be seeded in liquid medium which then coagulates after seeding leaving a clot that is, in an ideal situation, strong enough to keep the cell suspension in place but also allows cells to attach to a surface and nutrients to diffuse. In the case of square highly porous metal samples the large volume method is impractical so for these samples only the low volume method and the clot-based method were compared.

In the low volume method, 100,000 cells (MG63) were suspended in 100 µL of basic medium and transferred to a 6-well plate. The plate was then placed in an incubator for 2 hours before more medium was added.

To make the fibrin clot 100,000 cells were suspended in 50 µL of medium to which 5 µL of a 50 U/mL thrombin solution was added. Immediately before seeding the cell suspension was mixed with 45 µL of a 10 mg/mL fibrinogen solution and also transferred to a 6-well plate. The samples were then placed in an incubator for 15 minutes before more medium was added. 4 hours and 20 hours after seeding cell viability was measured for both conditions (figure 5.2).

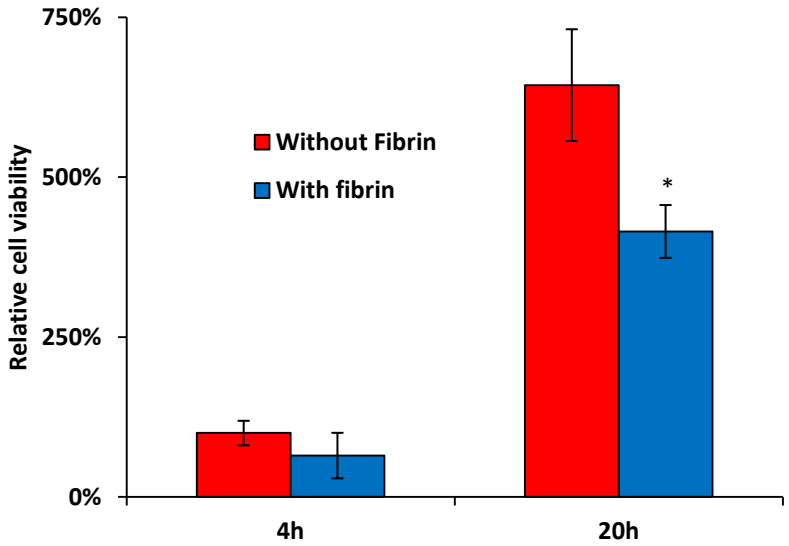

Figure 5.2: Effect of the seeding method of cell attachment and proliferation.

From figure 5.2 it becomes clear that cell viability is lower in the absence of a fibrin clot either because cell containing medium leaks out or because in the low volume method there is cell damage due to evaporation. It seems more likely that the fibrin clot reduces the ability of the cells to attach as the viability after 20 hours is significantly lower than the non-fibrin

samples. Furthermore, in separate tests where liquid without cells was added to metal lattices it was shown that 100 µL of liquid could be contained relatively easily inside the pores without a high risk of leaking. Therefore, it was decided to perform all cell seeding using the following conditions.

- Seeding density of 100,000 cells per sample
- Seeding volume of 100 µL
- Dropwise adding of the medium to ensure optimal cell distribution
- Handling plates with great care to prevent shocks that could lead to leakage
- 2 hours incubation before adding more medium

5.3 Prototypes

The first cell culture experiment on EBM titanium was done to see whether sterilisation had an effect on the seeding efficiency, to get an idea of the growth rate of cells on titanium and to see whether cell number reaches a plateau after three weeks of culture. Cells were seeded according to the conditions mentioned above and cultured for three weeks in osteogenic medium. Cell viability tests were performed on day 1, 3, 7, 14 and 21. Results were compared to a 2D tissue culture plastic control (figure 5.3).

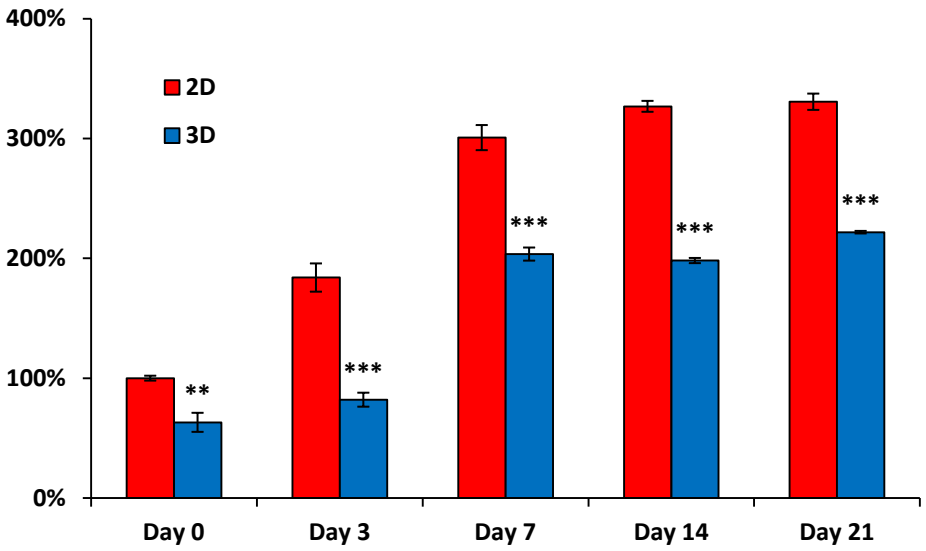

Figure 5.3: Cell viability over time for cells seeded on the prototypes titanium lattices.

The cell viability data on day 1 confirmed that the use of a fibrin clot is not necessary to achieve a high and a reproducible seeding efficiency. Under the assumption that all cells have

attached in the 2D control the seeding efficiency was 63% ± 8%. When these values are compared to the later timepoints it was also clear that the cell viability shows a highly regular increase over time. It is also likely the both conditions have reached a plateau after three weeks of culture; in the 3D group there were no significant differences between the cell viability values on day 7, 14 and 21 and for the 2D the difference between day 7 and 21 is statistically significant, but the difference between day 7 and 14 and between day 14 and 21 was not.

Only a small number of prototypes were produced; in the following experiments only fully porous lattices are used.

5.4 Assembly of the bioreactor

The next step in this project was to develop the in vitro cell culture further in order to get a more realistic model of the conditions that bone cells will experience in vivo. As discussed previously bone cells in a healthy human body experience a multitude of mechanical forces and their behaviour is highly determined by these forces. Therefore, testing of cell-biomaterial interactions would resemble the in vivo situation better if these forces would be applied as an experimental condition.

One of the most common methods of applying force to cells is to subject cells to fluid flow; this is also the way in which many cell types experience forces in vivo (Malone et al. 2007). There are many ways in which fluid flow can be applied during cell culture experiments (see 1.4.2). In the case of these titanium structures it was decided to develop a new simple bioreactor system that used a peristaltic pump to generate fluid flow.

The compartments where the metal structures were to be placed were made from 10 × 10 × 40 mm polystyrene cuvettes (Sigma) normally used for absorbance measurements. The bottom of the cuvette was then cut off so that a structure could be placed inside.

To close the compartment and to be able to connect it to the pump the standard cuvette lids were used on each side in which a round 4 mm diameter holes were made. The compartment could then be connected to the pump using 5 mm (4 mm bore) silicone tubing and a series of plastic connectors (figure 5.4).

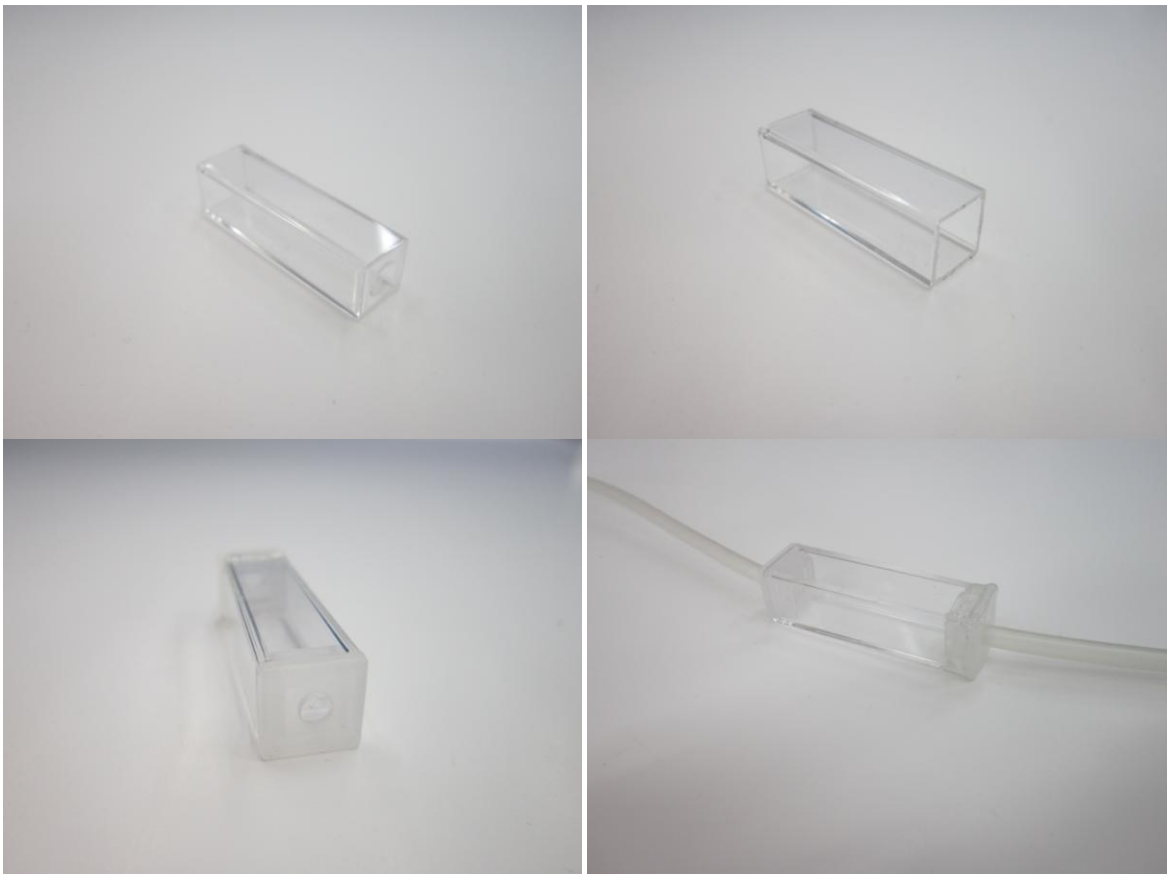

Figure 5.4: Assembly of the bioreactor: the bottom of a polystyrene cuvette (inner dimensions: 10 × 10 × 40 mm) is cut off, lids are applied on either side and tubes are inserted through narrow openings in the lids.

When the entire system was assembled and filled with liquid a lot of liquid leaked out between the lids and the compartment containing the sample. To prevent leakage this part of the system was wrapped in parafilm; this appeared to stop the leaking completely, however, after longer periods of pumping it appeared that there were still small amounts of liquid leaking which raised concerns about the possibility of keeping the system sterile for long periods of culture. Therefore it was decided to use a two-component fast-hardening epoxy resin (Wilkinson, Sheffield, UK) to seal the bioreactor.

Using resin to seal the bioreactor before use does create problems with sterilisation and sample removal. As it is not possible to assemble the bioreactor in a sterile manner there is the necessity to sterilise the inside of the bioreactor and the tubing after assembly. The fact that it is not possible to remove the sample means that the cells have to be put on the materials after the bioreactor is sealed, as the bioreactor requires sterilisation after sealing. It also means that tests on the materials all have to be done after the culture period in the bioreactor and that measurements during culture in the bioreactor (such as viability testing) are not possible.

Apart from the bioreactor and the tubing the flow system consisted of a medium reservoir, which is a sterile 250 mL glass bottle with a plastic lid with three openings with an external screw thread. These openings can be capped with a cap with tube though it. Two of these openings were used for long tubes that served as the medium in- and outlet; the third one was capped with a short tube connected to a 0.2 µm filter for gas exchange. The medium outlet can be connected to a tube that is fixed in a cassette that can be clicked into the peristaltic pump. The entire system is shown in figure 5.5.

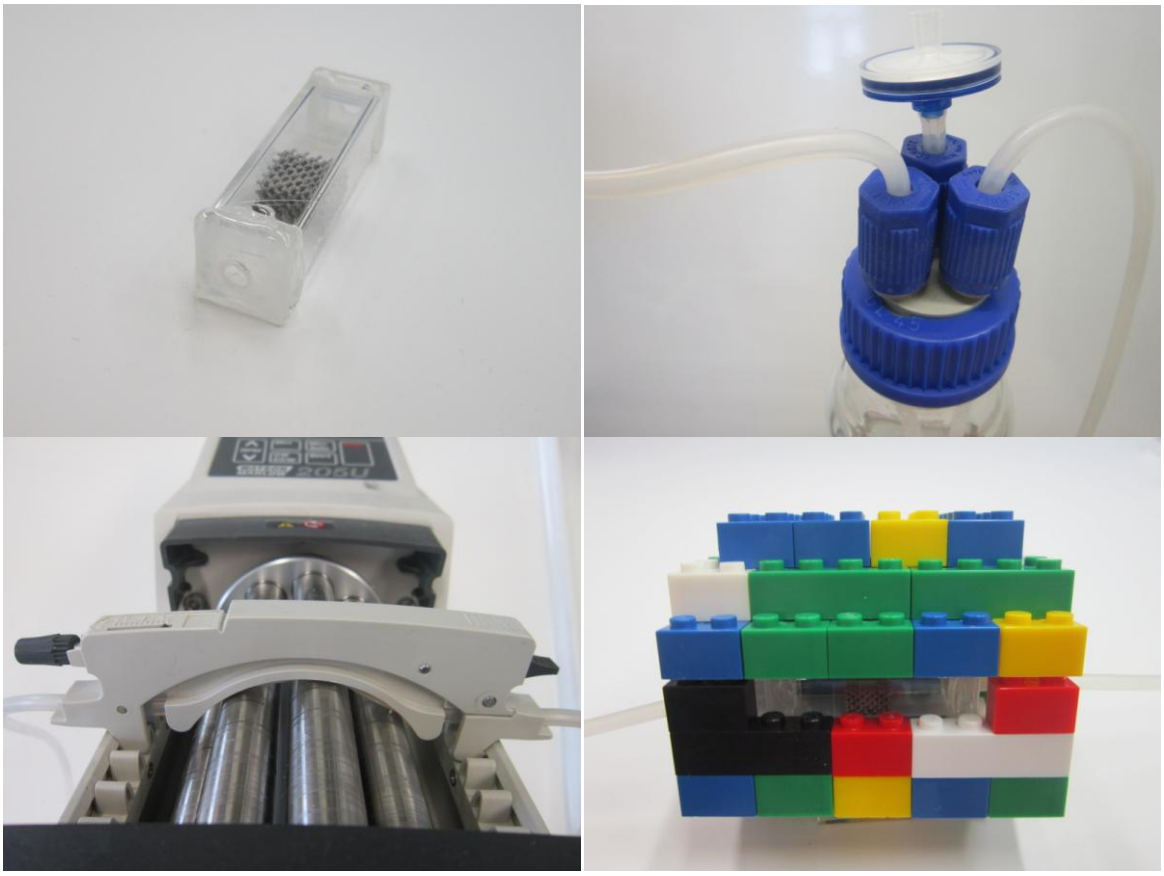

Figure 5.5: Components of the flow system. Top left: bioreactor with a titanium lattice, top right: lid of the medium reservoir with three openings for inflow of medium, outflow of medium and gas exchange, bottom left: peristaltic pump, bottom right: holder that was used to hold the bioreactor in position.

The fact that the bioreactor had to be sealed with resin before use meant that cells could not be seeded in exactly the same way as the static cultures in a well plate. Therefore, a slightly different approach was used to seed inside the bioreactor. The exact amount of cell-containing medium was first transferred to a 500 µL eppendorf tube. The connector that is attached to the short tube is then opened (see figure 5.6), so that the medium can be put on

the samples by a syringe with a 5 cm hypodermic needle. It allows the liquid to be added drop-by-drop with equal precision to the normal pipette-based seeding in a well plate.

The bioreactor was assembled as follows. A saw was used to cut off the bottom of the cuvette and a 4 mm gauge hand bore was used to create a hole in two cuvette lids. Tubes were cut (roughly) to the following lengths:

- Outlet of medium reservoir – 20 cm.
- Through the cassette – 30 cm
- Pump towards bioreactor – 50 cm
- Into the bioreactor – 2 cm
- Out of the bioreactor – 30 cm
- Inlet to medium reservoir – 20 cm

The lids for the bioreactor were soaked in 100% Industrial Methylated Spirits (IMS) overnight; cuvettes were cleaned with distilled water (dH_2O) and washed in 100% IMS (prolonged soaking in IMS causes the cuvettes to deform). The lid of the reservoir, the caps, and the plastic connectors were pre-sterilised using the standard autoclaving procedure and the samples were pre-sterilised by soaking in IMS followed by dH_2O and finally 0.1% peracetic acid in dH_2O.
For the assembly of the bioreactor the components of the resin were mixed in equal amounts (roughly 1 mL each) and stirred for 30-45 s with a disposable spatula. The resin was then applied to the outside of the bottom part of one of the lids, pushed firmly onto the cuvette for 2-3 minutes and the resin was allowed to set for around 3 hours. The samples were then placed inside the cuvette and the second lid was applied in the same way as the first lid. The resin was allowed to fully harden for at least 12 hours.

To set up the flow system the tubing and the connectors were used to connect the bioreactor to the cassettes of the pump and the medium reservoir. The entire system was cleaned with tissue and IMS and placed in a flow cabinet. Inside the flow cabinet the reservoir was opened and filled with 0.1% peracetic acid. The system was connected to the pump and switched on until the liquid had filled the entire system. The bioreactor was tapped and tilted to ensure that no air bubbles remained inside the chamber. The pump was then switched off so that the

inside of the flow system would soak in the peracetic acid solution for at least three hours. The bottle containing the peracetic acid was replaced with an empty bottle and the pump was switched on to replace the peracetic acid with air. Once all the liquid had been removed from the system the bottle was replaced with a full bottle of sterile PBS and the pump was switched on for another 10-15 minutes to remove traces of peracetic acid. Finally, the bottle of PBS was replaced with an empty bottle and the system was drained again.

For the cell seeding it is essential that there is no liquid remaining inside the pores of the samples, so once the system is drained any remaining PBS should be removed. The connector closest to the bioreactor was opened and a syringe with a 5 cm hypodermic needle was used to enter the bioreactor with the needle through the 2 cm tube so that the remaining PBS could be removed from the sample. After all remaining drops of liquid had been removed the system could be closed and is ready for use.

To seed the cells on the materials in the bioreactor a suspension of 1,000,000 cells per mL was prepared using standard techniques. 100 µL of cell suspension (containing 100,000 cells) was transferred to a 500 µL eppendorf tube and a 5 mL syringe with a 5 cm hypodermic needle was used to take up all the medium. The connector connected to the short tube coming out of the bioreactor was opened and the needle was inserted until the tip was located directly above the samples without touching it. The plunger of the syringe was then pushed with extreme care to ensure that the liquid comes out drop-by-drop. As soon as the medium started coming out the tip was moved slightly to ensure that the medium was equally spread across the sample. The needle was removed, the connector closed and the entire flow system was placed in the incubator.

After 2 hours the flow system was taken out of the incubator and the system was reconnected to the pump. The pump was set to a low speed and switched on until sufficient medium was pumped into the bioreactor to cover the sample. The flow system was then disconnected and incubated overnight.

Figure 5.6: Setup of the flow system with a vertical orientation of the bioreactor inside a biosafety level II cabinet.

5.5 Pump test

Before any flow experiments were carried out the flow velocity generated by the peristaltic pump was tested. The bioreactor system that was going to be used for the experiment was connected to the pump and a water reservoir and run for 1 minute at different speeds (the peristaltic pump indicates speed in rotations per minute, rpm). The amount of water that had passed through the system could then be weighed and converted to flow velocity (in mm/min) based on the number of bioreactors. Previous research has shown that a flow velocity of around 1 mm per minute can support matrix production by bone cells that is higher than static controls without cause a high percentage of cells to detach (Shaeri 2013). At speeds at which the flow velocity was close to this target the test was repeated in triplicate with steps of 1 rpm (figure 5.7).

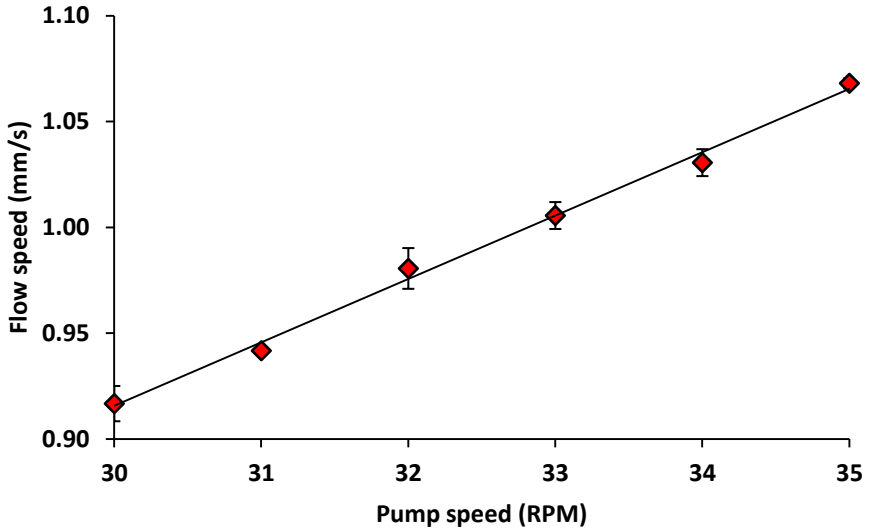

Figure 5.7: Measurement the flow velocity in the bioreactors at different pump speeds.

These values show a clear linear relation and very low standard deviations; based on this result a frequency of 33 rpm was used for the flow experiments.

5.6 Flow non-graded

In the first experiment which was performed before the graded lattices were available. The flow system was set up to compare uniform lattices with MG63 cells seeded on them in static and dynamic culture for three weeks. The bioreactor was used in an upright position with the medium flowing in an upward direction through the bioreactor. In order to fit inside the bioreactor the sample had to be slightly smaller than the inner dimensions of the bioreactor (between 9 and 10 mm). In order to avoid the structure slipping to the bottom of the bioreactor during culture a small piece of dental wire was used to keep the sample in position in the middle of the bioreactor.

The bioreactor was assembled and the cells were seeded onto the samples according to the protocol. 24 hours after seeding the flow system was removed from the incubator and connected to the pump for a flow session of 1 hour at 1 mm/min. As it was not always possible to carry out the flow sessions in the regular incubators flow sessions were done in so-called dry incubators which have no CO_2 injection and no water bath, but do maintain a temperature of 37.0 °C. The bioreactors and the medium reservoir form a closed system with very little gas exchange so it is expected that the CO_2 level in the bioreactor will not decrease

dramatically during these 1 hour flow sessions. Therefore, the static controls were not transferred to the dry incubators as the CO_2 level in a well plate would drop rapidly to atmospheric levels.

The flow sessions were repeated every day between day 1 and day 20. On day 21 the flow system was drained, the tubing was removed and the bioreactors were broken and the samples were transferred to a 6-well plate. A cell viability test was done of all samples followed by a washing step, fixation and a calcium and collagen assay (figure 5.8, 5.9 and 5.10).

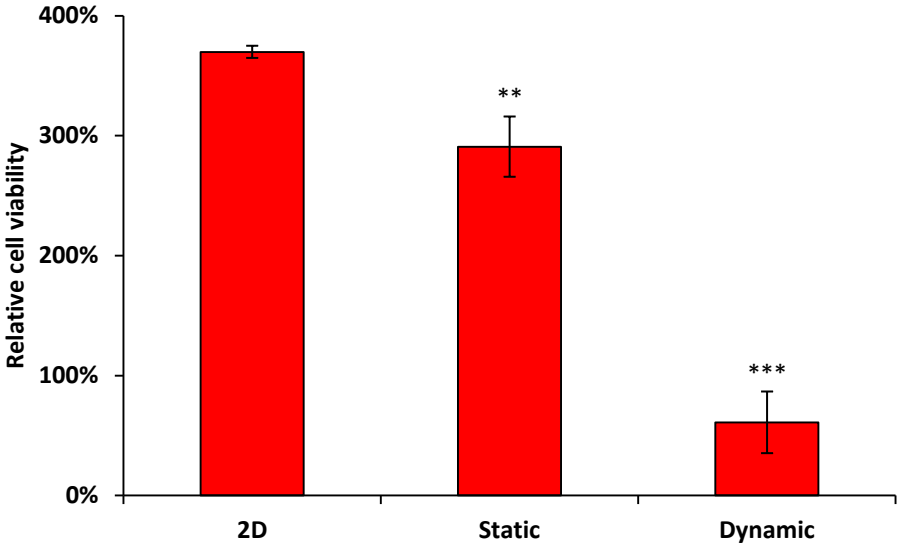

Figure 5.8: Cell viability data of MG63 cells seeded onto the uniform lattices after three weeks of culture under either static or dynamic conditions.

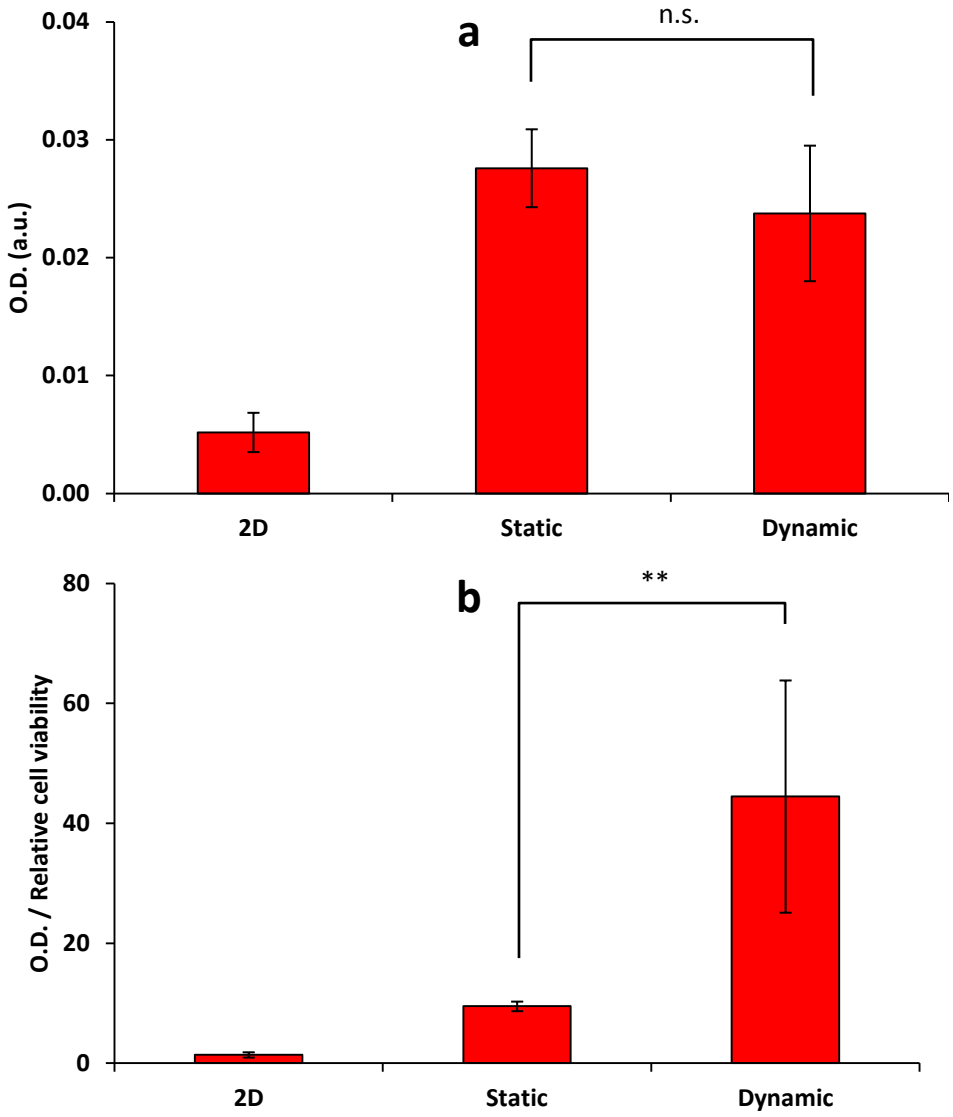

Figure 5.9: Results of the calcium assay of MG63 cells seeded onto the uniform lattices after three weeks of culture under either static or dynamic conditions, data are shown as total calcium content (a) and calcium content relative to cell number (b).

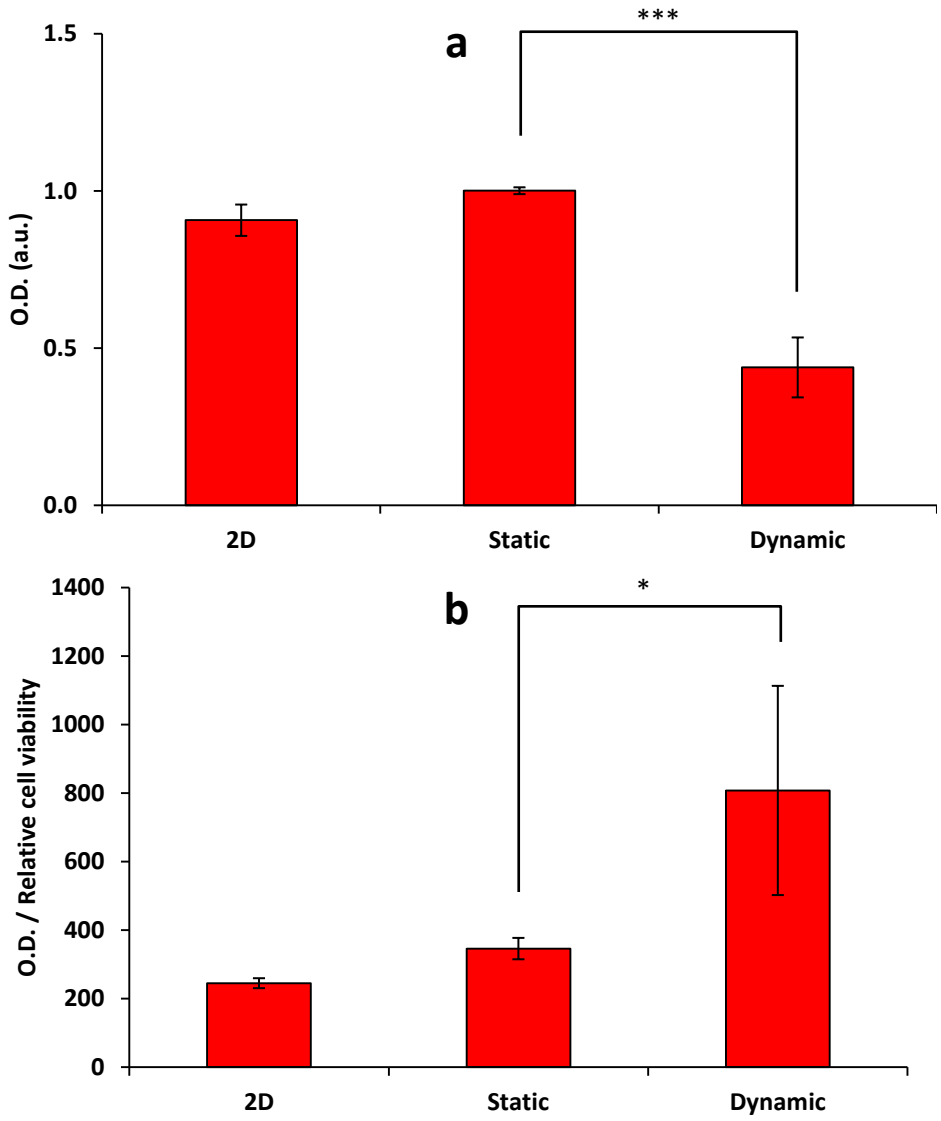

Figure 5.10: Results of the collagen assay of MG63 cells seeded onto the uniform lattices after three weeks of culture under either static or dynamic conditions, data are shown as total calcium content (a) and calcium content relative to cell number (b).

Cell viability of static samples was 78% of the 2D control after 3 weeks, which could be expected from earlier results. The flow samples in the bioreactor however had an average cell viability of 16% (or 21% compared to the static). These values were far lower than expected and made it difficult to interpret the data from the calcium assay and the collagen assay.

As the difference in cell viability between the static and the flow samples was very large the data from the extracellular matrix assays are presented in two ways. The top graphs represent averages of the total collagen content of the samples and the bottom graphs show these values

normalised to cell viability of the samples; this could be seen as an indicator of matrix production per cell.

The values for the calcium assay showed that virtually no calcium was produced in any of the samples including the static and 2D control. For completeness, the graphs are shown here in standard format (with the negative control subtracted and scaled based on the highest value), but based on values from similar mineralisation experiments it is assumed that mineralisation did not take place in any condition.

The collagen assay, however, did show a positive staining in all conditions and the values also showed a high degree of reproducibility in all conditions. The total collagen content in the flow samples was significantly lower than the other two conditions, but when the data from the collagen assay are normalised to cell viability the flow samples showed significantly higher values than the static and the 2D samples. This could indicate that cell attachment is lower, but that the cells that do attach produce more collagen as a response to the fluid flow. However due to the large difference in cell viability between the flow group and the other conditions, it would be desirable to verify these results in a situation where cell viabilities at the end of the experiment are the same or at least comparable.

Because of the low cell viability in the flow samples and the fact that there was virtually no mineralisation in any of the tested conditions it was decided to make several changes to the experiment. Firstly, because of the possibility that the MG63 cell line was not able to produce any mineral this cell line was compared to a different cell type, the Mouse Long-bone Osteocyte A5 (MLO-A5). Whereas the MG63 is an osteosarcoma cell line and is comparable to osteoprogenitor cells or pre-osteoblast cells in adult human bone the MLO-A5 cell line is defined as a post-osteoblast and is shown to be capable of mineralisation in vitro even in the absence of components usually added to the medium to induce mineralisation (Kato et al. 2001).

Cells of both cell lines were grown under static conditions in 2D and in 3D on the same titanium lattices. Each cell type was grown in its own mineralisation medium (with added AA BGP and Dex for the MG63 cell and AA BGP but not Dex for the MLO-A5). After 3 weeks of culture cell viability, mineral content and collagen content were measured (figure 5.11).

The cell viability data (figure 5.11 a) showed that the MG63 cells had proliferated significantly more than the MLO-A5. There could be several explanations for this difference, but it is likely that because the MG63 cell line is in an earlier developmental stage than the nearly terminally differentiated MLO-A5 it has more potential for proliferation.

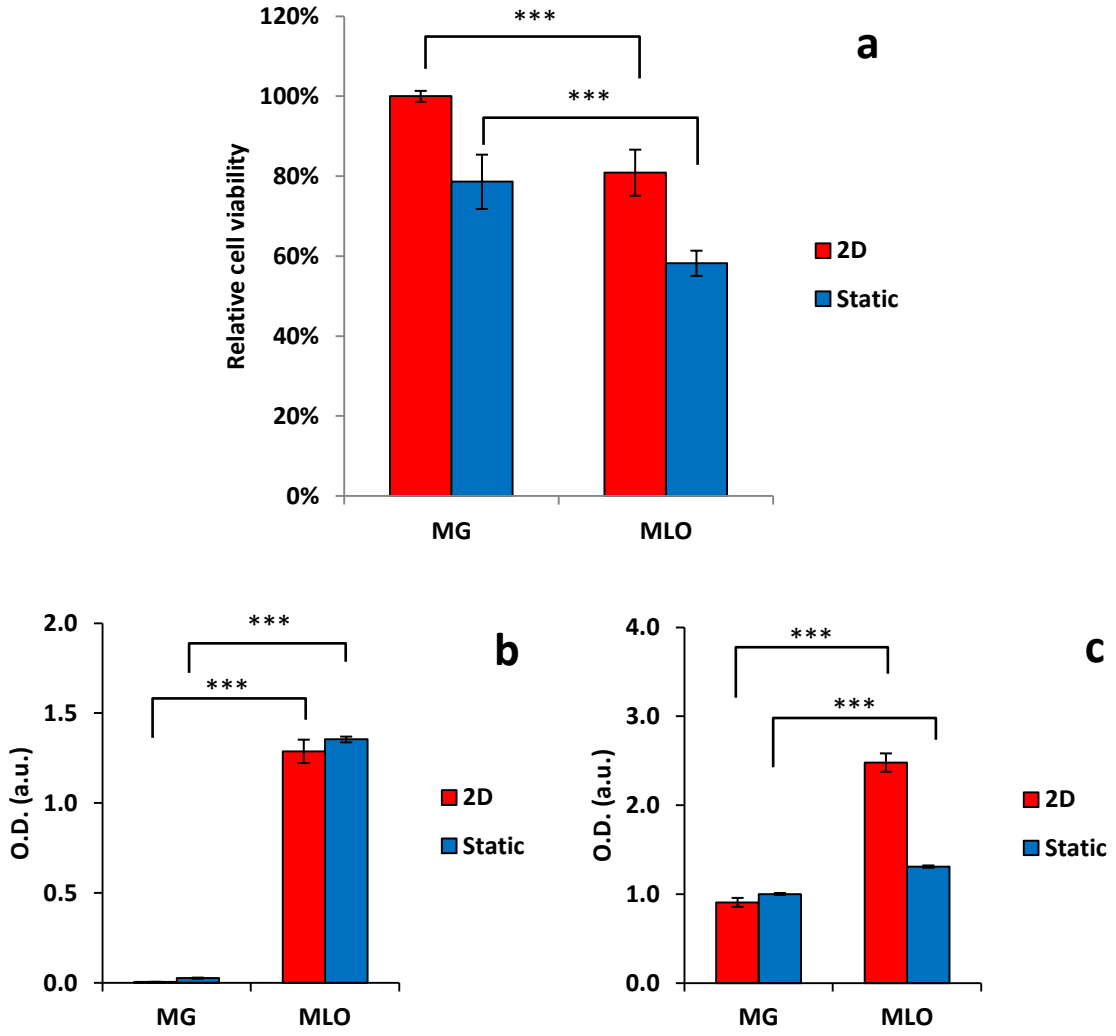

Figure 5.11: Cell viability (a), calcium content (b) and collagen content (c) of MG63 and MLO-A5 cells after three weeks of static culture on either tissue culture plastic or titanium lattices.

The results of the mineralisation assay showed again that mineralisation did not take place in the MG63 cultures. It is not known why mineralisation did not occur, especially as previous studies (Jeon et al. 2012; Tsai et al. 2012; Song et al. 2013) have shown mineralisation of MG63 in vitro. The MLO-A5 cultures, however, did show a clear positive staining for both calcium and collagen. Therefore, it was decided to use this cell line in all future bioreactor experiments, as the production of mineral is an essential element when investigating the response of bone cells to mechanical stimulation.

While these initial tests were carried out graded lattices were designed and produced on the EBM simultaneously. As soon as these structures were produced it was decided to do all future bioreactor testing on these materials. Also, the orientation of the bioreactor was changed from a vertical setup with the samples suspended in the middle to a horizontal setup with the samples placed horizontally in the bottom of the bioreactor. This was thought to be a better approximation of the situation in vivo where cells located on the outside of the implant will experience higher stresses than the more shielded cells in the inner pores. The final change to the original setup aimed at improving cell viability was to start the flow sessions on day 3 instead of day 1; this was done to give the cells more time to attach to the surface which might improve their bond to the surface of the titanium.

5.7 Flow graded

The first timepoints tested were 1 and 3 days. These timepoints were chosen to test whether the cell seeding efficiency is high enough and whether the first flow session (on day 3) causes a severe reduction in cell viability. Experiments were carried out in duplicate; the cell viability data are shown below (figure 5.12).

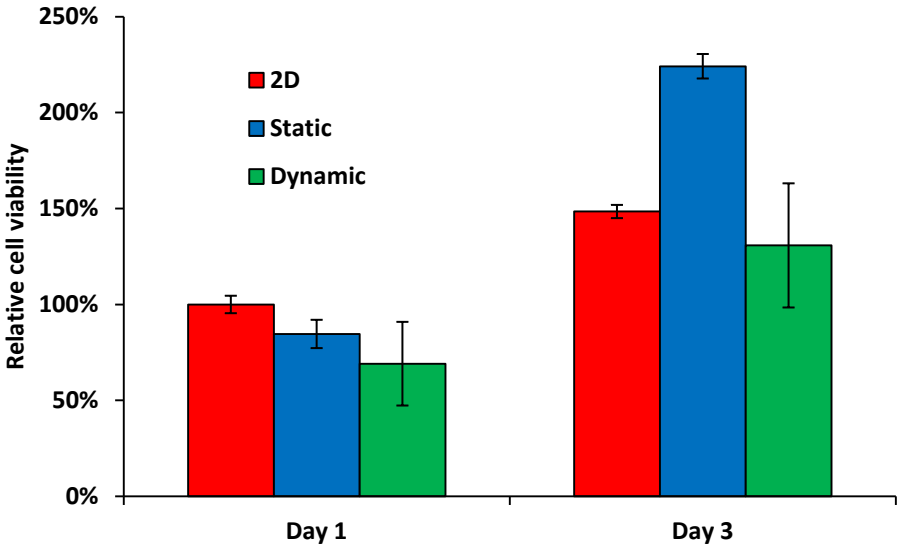

Figure 5.12: Cell viability of MLO-A5 cells after 1 and 3 days culture in the bioreactor compared to static culture in a well plate.

It can be seen that on both day 1 and 3 the cell viability was higher in the static samples. The values on day 1 (69% ± 23% and 85% ± 9%) were similar to cell seeding efficiencies in earlier experiments. The values on day 3 were measured directly after the first flow session,

so any adverse effect of this first hour of flow should be reflected in the data. The dynamic values on day 3 were lower than the static but the value is higher than the dynamic samples on day 1, which could indicate that the flow did not have the dramatic effect on cell viability which it had when the flow sessions were started 24 hour after seeding. The significance of the differences between the static and dynamic samples could not be determined because these values are only based on 2 samples of each condition.

As these results of two early timepoints did not show a dramatic reduction in cell viability seen in earlier experiments the same conditions were then used to investigate later timepoints. These conditions were used for measuring four samples of each condition on day 7, 14 and 21. Cell viability was measured as well as mineral and collagen content (figure 5.13 and 5.14) the cell viability graph also shows the two early timepoints (of N=2) for reference.

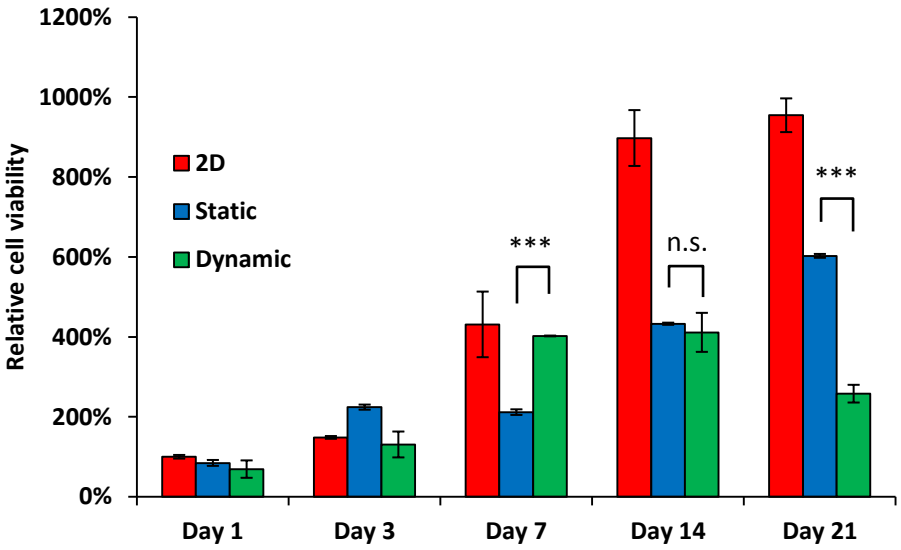

Figure 5.13: Cell viability of MLO-A5 cells cultured for 7, 14 and 21 days under static and dynamic conditions.

Both the 2D and the static samples showed a consistent growth over the five timepoints with especially the static samples showing low standard deviations. The result from the dynamic samples, however, was more difficult to interpret. Although the variations within each timepoint were small there was no clear trend in the cell viability over time. In particular, the low cell viability on day 21 compared with day 14 was unexpected. A possible reason for such a decrease could be that the cells that were initially only seeded on the structures may have spread to the inner surfaces of the bioreactor; this can cause a higher cell number inside

the bioreactor, but may have had an adverse effect on cell viability on the surface of the samples. Other explanations include variation between the cell stocks used for the different timepoints or variation of the conditions inside the bioreactor.

Calcium and collagen content were measured immediately after cell viability on day 7, 14 and 21 (figure 5.14). The results are represented as total calcium/collagen content and as calcium/collagen normalised to cell viability.

The data from the total mineral content show that mineral production of the dynamic samples is far lower than the static group. Even when the data are corrected for the higher cell viability in the static group the mineral produced per cell is still around 75% lower than the static group (cell viability values could not be matched with calcium/collagen values so SDs could not be determined). A similar effect can be observed in the results of the collagen assay (figure 14 c-d). However, in this case the effect is less obvious than in the mineralisation assay. Also, the total amounts of collagen on day 21 are significantly lower than on day 14 for both conditions; the reason behind these lower amounts of collagen is unknown.

In a separate experiment, but under the same conditions two static samples and two dynamic samples were cultured for three weeks to be used for histology (Figure 5.15).

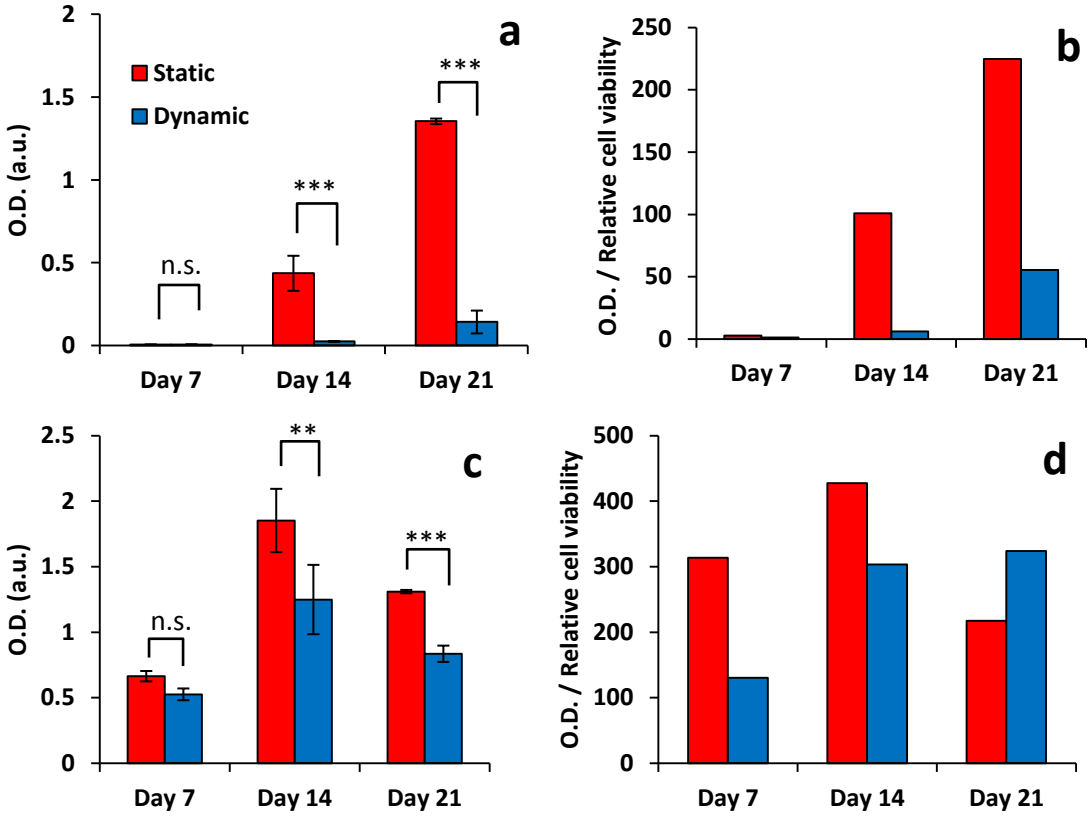

Figure 5.14: Results of the calcium (a-b) and collagen (c-d) assays of MLO-A5 cells cultured for 7, 14 and 21 days under static and dynamic conditions.

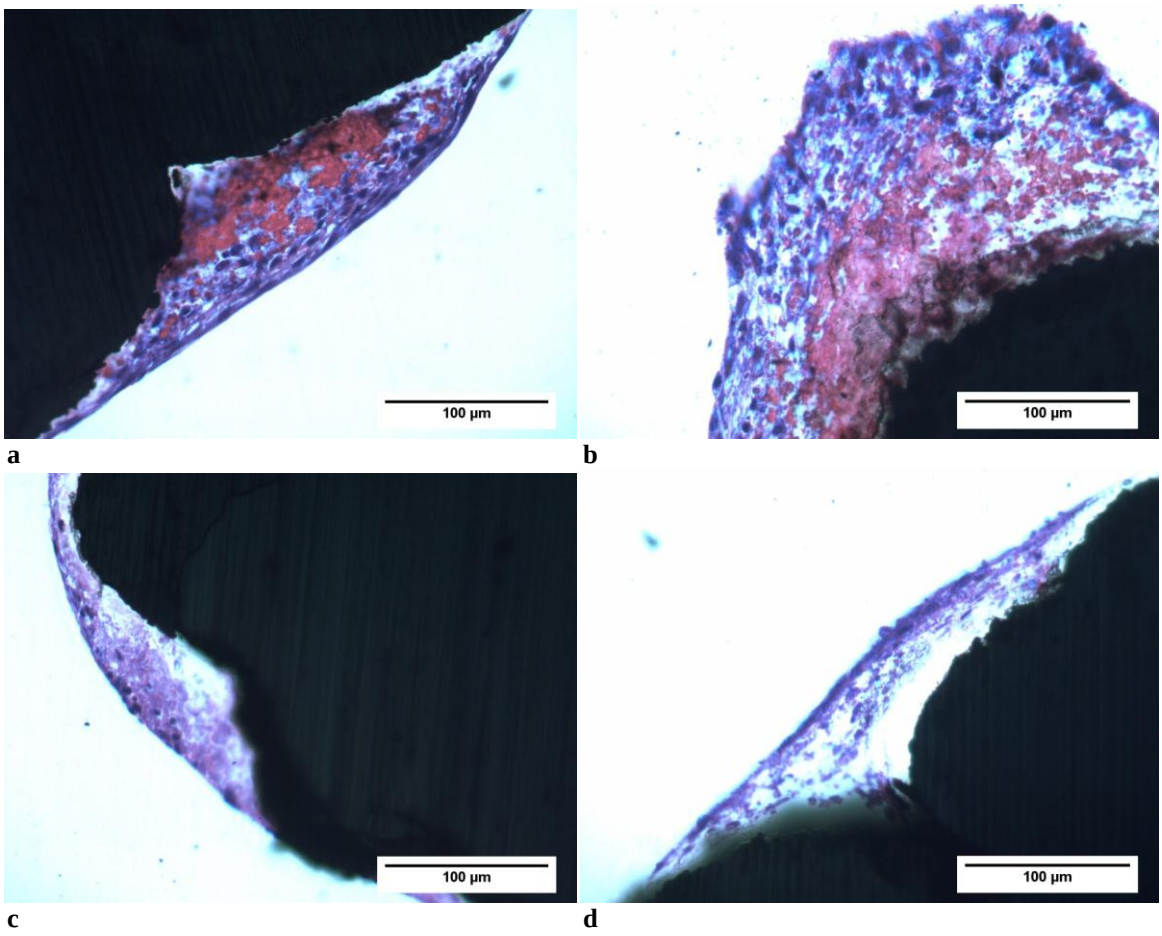

Figure 5.15: Light microscopy images of graded lattices after 3 weeks culture with MLO-A5 cells under static (a, b) or dynamic (c, d) conditions.

These images confirm the result for the calcium assay that culturing the MLO-A5 cells under dynamic conditions in the bioreactor has a strongly negative effect on the formation of mineral on the surface of the titanium samples. This can be seen by the pink staining which indicates the presence of mineral and which is absent in the flow samples; the purple colour indicates the presence of cells.

The low cell numbers of the samples cultured inside a bioreactor raised the question of whether the low cell number is mainly caused by the flow or that the conditions inside the bioreactor were generally worse than those for the static controls. To test this hypothesis the result from the samples that had been cultured under dynamic conditions in the bioreactor ('dynamic – bioreactor') for 3 weeks were compared to:

- Samples cultured statically in a 6-well plate (‘static – well’).
- Samples that were cultured in a bioreactor, but with minimal flow; with these samples the pump was only used to refresh the medium (‘static – bioreactor’).
- Samples cultured in a well plate, but under dynamic conditions (‘dynamic – well’).

To create dynamic conditions in a well plate these samples were placed on a rocking platform with a frequency on 45 oscillations per minute. This model has been described for cells cultured in monolayer by Delaine-Smith et al. (Delaine-Smith et al. 2012). Obviously, the effect of this type of flow on the cells seeded on the samples will not be the same as the flow conditions in the bioreactor, but it can still provide insight into the reasons behind the low cell viability after three weeks of flow inside the bioreactor. Similar to the bioreactor flow the rocking was also done for 1 hour every day starting on day 3 and ending on day 20. The results of these conditions as well as the samples grown in the bioreactor for 21 days are shown below (figure 5.16).

The cell viability data showed a clear difference between cells cultured in a well plate and cells cultured in the bioreactor but no significant differences between static and dynamic culture. Partially due to these low cell viabilities from the two bioreactor groups the values from the extracellular matrix assays were also lower than the samples cultured in a well plate. When these values were corrected for cell viability the values for the calcium assay were still significantly lower than the samples cultured in a well plate, but for the collagen assay the differences were not significant. In none of the assays was the rocking group significantly different to the static samples cultured in a well plate.

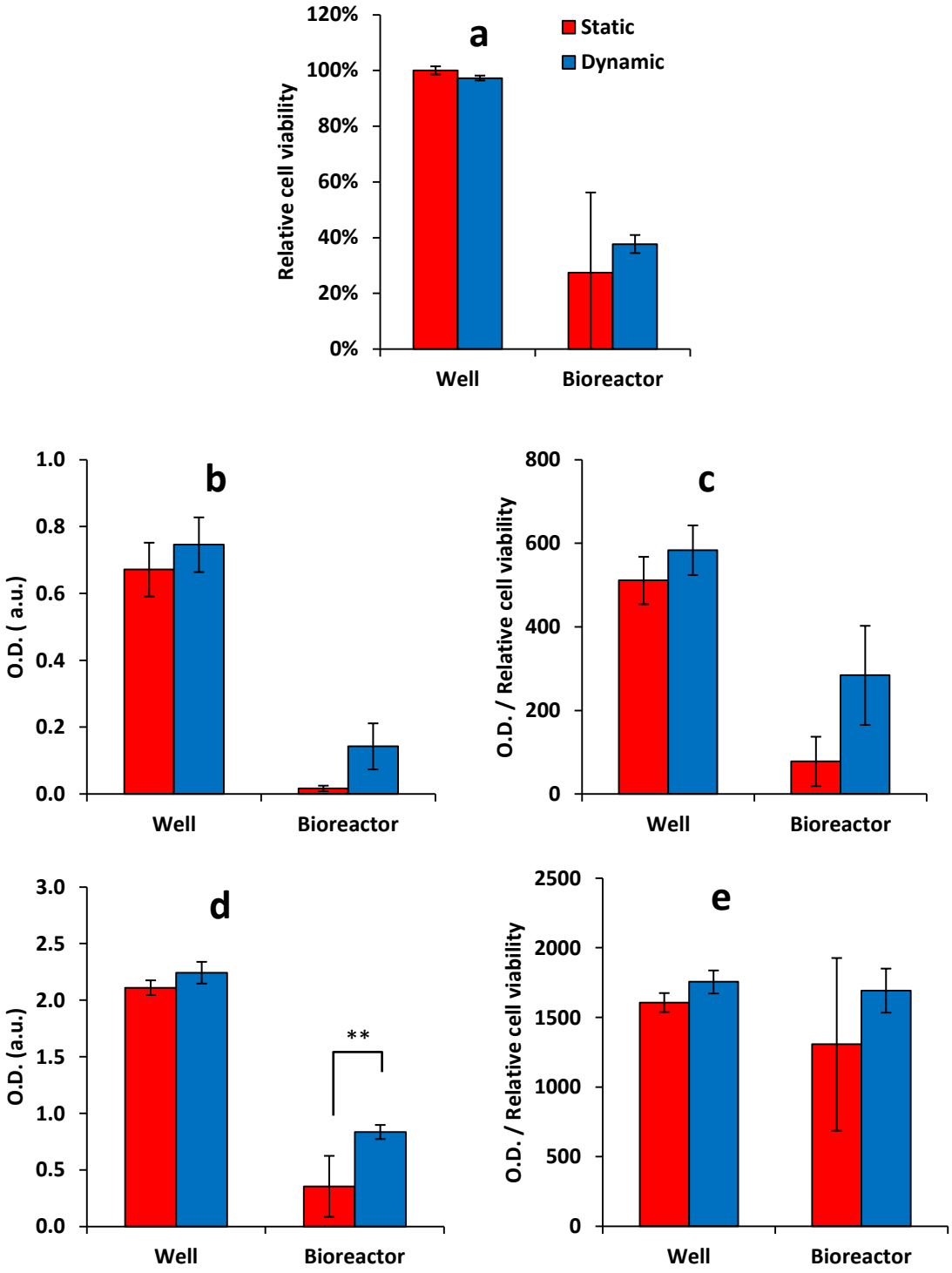

Figure 5.16: MLO-A5 cells cultured for 3 weeks under either static or dynamic conditions in either a well plate or in a bioreactor. a: Cell viability, b,c; mineral content, d,e: collagen content. Differences between static and dynamic are not significant unless indicated; bioreactor values are all significantly lower than corresponding well values in a, b, c and d, but not in e.

5.8 Comparison to other porous metals

In a separate experiment the newly developed graded porous lattices were compared to two other types of porous metal that were available. MG63 cells were cultured according to the standard protocol on the graded lattices, square lattices produced by selective laser sintering and a commercially available foam of CP-titanium (Gription). Both structures were cut to the same size as the graded lattices and were also comparable in terms of relative density (35-45%). The main structural difference between the three materials was the pore size, which was 500 – 800 µm and regular for the graded lattice, 500 µm and regular for the SLS materials and 300 µm and stochastic for the commercial metal foam. The total culture time was 3 weeks and cell viability was measured on day 1, 3, 7, 14 and 21 (figure 5.17).

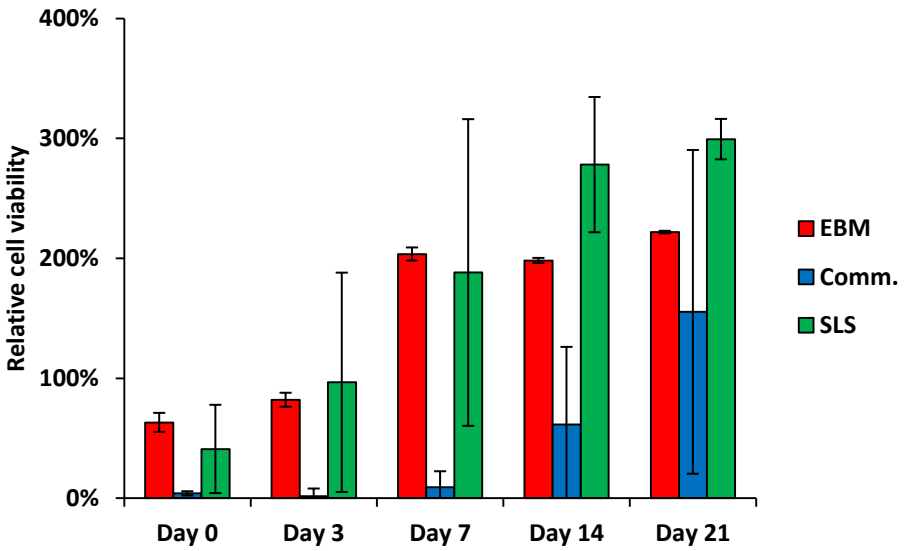

Figure 5.17: Cell viability data for MG-63 cells cultured for 3 weeks on 3 different porous metals.

Although all these materials were used for this experiment had the same dimensions there were many differences between the different structures, most notably the type of alloy, the relative density and the pore size. Therefore, it was not possible to determine the main reason for these large differences in cell viability. Nevertheless, it was considered to be important to know how this newly developed structure behaves in comparison with materials that are either already commercially available or that are being developed simultaneously.

The results showed that there are large differences between the structures made by EBM and the two other structures. Although all three structures show some degree of cell growth over time there were large differences in attachment and consistency. Cell attachment on the EBM

structures was over 50%, which was consistent with earlier results whereas the cell attachment on the samples made by SLS was highly variable; attachment on the commercial alloy were too low to measure (i.e. not significantly different from the negative control).
Cell growth over time was seen in all conditions, but the high variability as a result of the high variability in cell attachment remained. In the case of the samples produced by SLS the standard deviation decreased at day 21, this could be an indication that cell number in these samples has also reached a maximum and that the standard deviation dropped as a result of the samples with low initial cell attachment 'catching up'. The commercial porous structures also showed increases in cell number between day 7 and 21, but variability remained high and there was no evidence of the cell number reaching a plateau.

5.9 In vivo

In total, 25 metal foams and controls were implanted. However, due to severe problems during processing and transport of the samples some samples could not be sectioned and stained.
The specimens that were available for imaging contained many air bubbles which are the result of poor resin infiltration during the embedding step. These air bubbles resulted in black circles in the images and also resulted in high variability in the intensity of the stainings that were used. The reason for the variability in the staining intensity was that during staining the solutions penetrated the air bubbles but could not easily be washed out of the pores. This resulted in some areas and sections being stained for much longer than the times recommended in the protocols.
As a result of the low numbers of specimens available and the poor quality of the sections it was not possible to quantify any of the data obtained by histology. However, it does provide information on how this material behaves in a relevant bone defect model. Therefore, it was decided to include images of all samples that were sectioned and stained. These images contain many artefacts, caused by the poor infiltration of the resin, but nevertheless it is still possible to recognise different tissues in the images.

4 weeks:
From the 4 week timepoint 6 implants were available for histological analysis: 3 graded lattices (Gra, figure 5.18 a-f), 1 negative control (NC, figure 5.18 g-h) and 2 positive controls (PC, figure 5.18 i-l). Upon examination of all the available sections evidence of bone tissue

formation at the bone implant interface was not observed in the graded lattices (0/3) and the negative control (0/1) and in one of the positive controls (1/2). Bone-like tissue (which stains pink with dark cells) that is either in contact with the implant or appearing inside the pores of the implant is marked with arrowheads (figure 5.18 i-j); the new tissue was formed in one corner of the implant and penetrated around 1 mm into the implant. All other images show either no tissue-implant contact or show the presence of tissue that cannot be identified based on these stainings.

In two graded lattices (figure 5.18 a-d) there is a lot of other tissue formed inside the pores which is in direct contact with the metal. This would indicate that the implants have been sufficiently stabilised for fibrous tissue to grow in and attach to the struts. In the three remaining samples (one graded lattice, one negative control and one positive control) there is very little evidence of good tissue-implant contact which might indicate that the implant is insufficiently stabilised.

12 weeks:

From the 12-week timepoint there were also 6 implants available for histology, however none of the negative controls could be analysed. 4 graded lattices were analysed (figure 5.19 a-h) and 2 positive controls (figure 5.19 i-l). Most of these (Graded lattices 3/4, Positive controls 1/2) show some evidence of bone ingrowth or bone-implant contact. However, bone-like tissue is only present in the outermost region of the implant near the interface between the cortical bone and the cancellous bone and the depth of ingrowth does not exceed 1 mm for any of the implants.

The region with the most bone implant contact was the region on the outside of the bone where the implant touches the cortical bone. This effect was different to what was expected as it was thought that bone would grow more readily from the more cellular inner region of the bone that contains the bone marrow. A possible reason for this effect could be that there is more stability at the outside due to the higher stiffness of the cortical bone.

With regard to the effect of pore size on bone ingrowth, there is some evidence of the larger pores having bone formation in the centre of the pore as well as on the outside, but other images that clearly show osteoconduction along the metals struts without filling the centre of the pore. Overall, the amount of available data is not large enough to conclude whether the pores in the graded structures have a suitable size for bone ingrowth and implant stabilisation.

×40 ×100

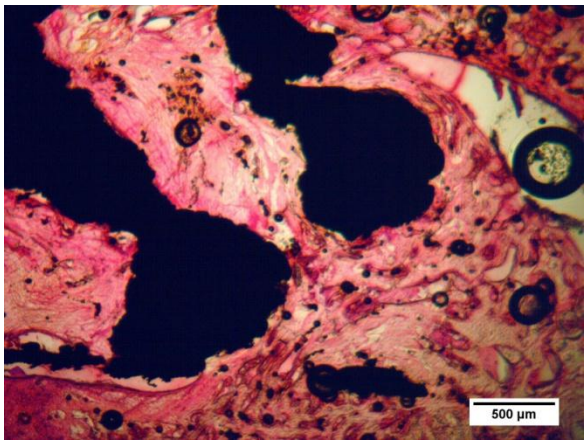

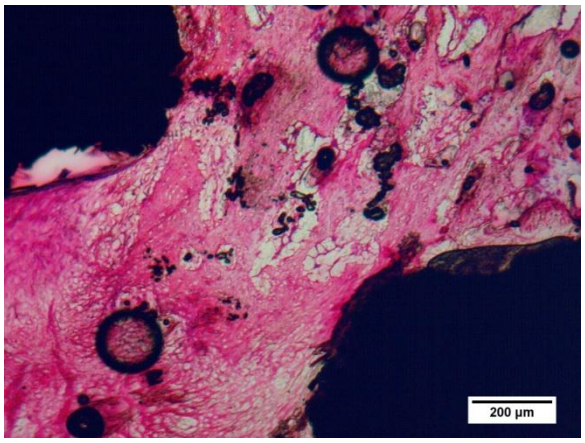

4 weeks Gra. 1 **a** **b**

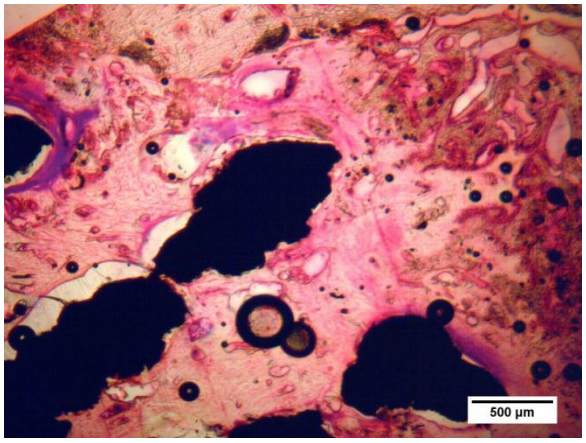

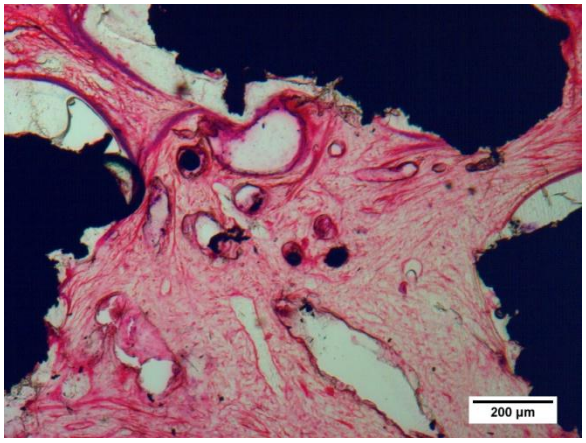

4 weeks Gra. 2 **c** **d**

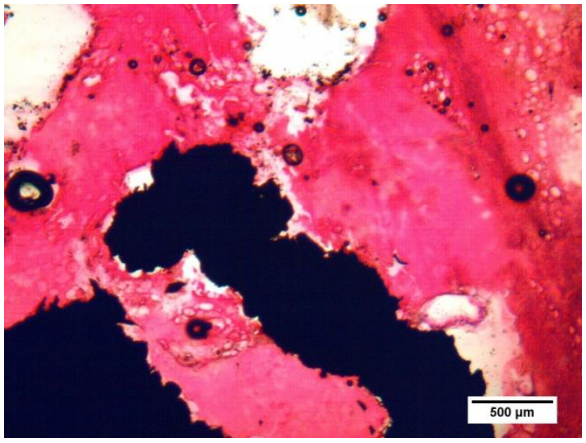

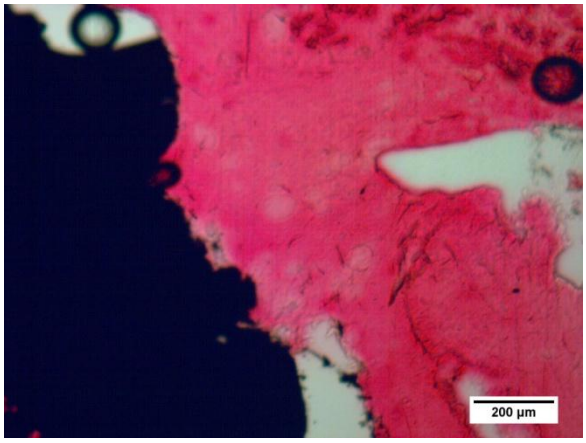

4 weeks Gra 3 **e** **f**

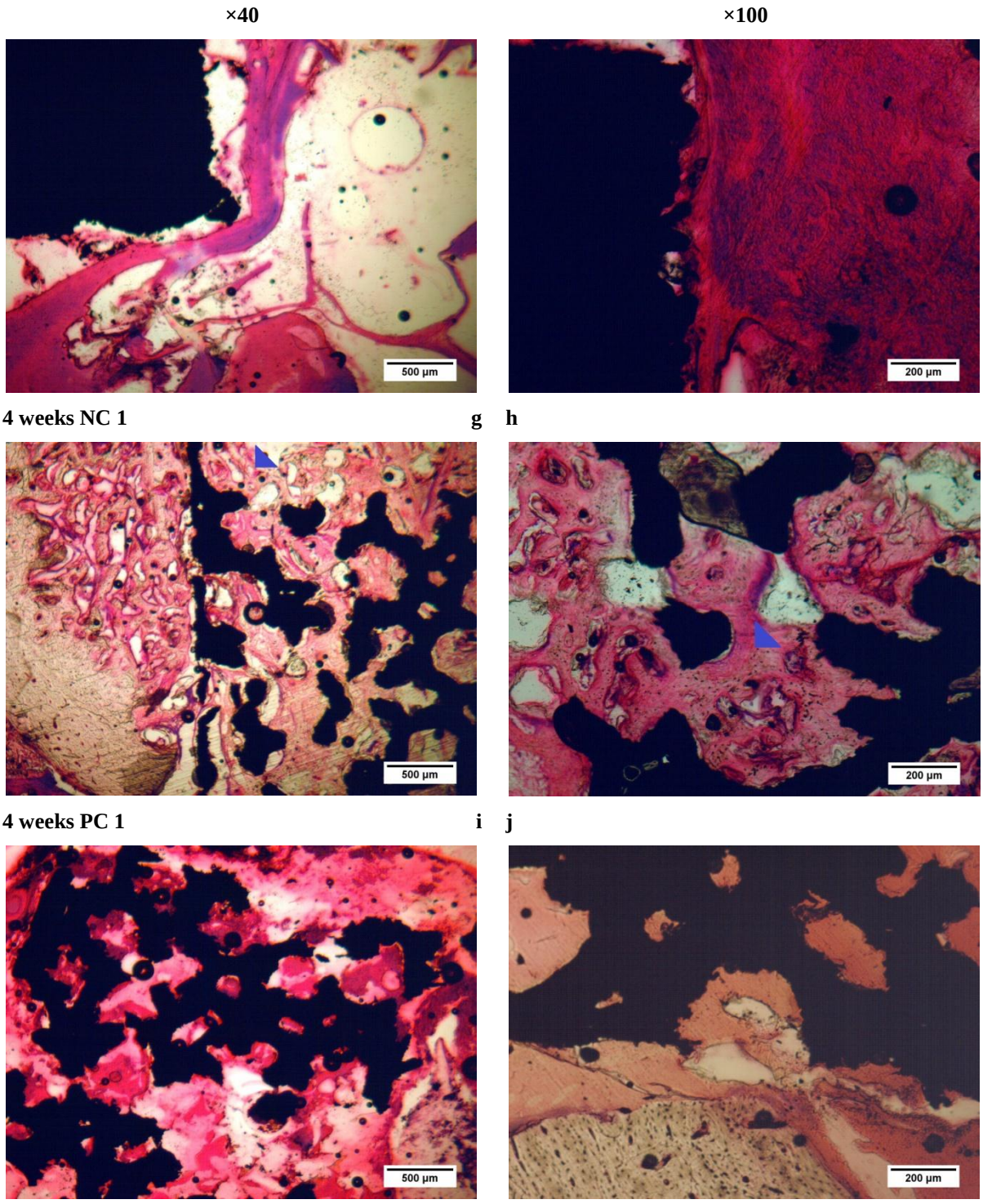

Figure 5.18: Images of the implants retrieved after 4 weeks at low magnification (left) and high magnification (right). a-f: graded lattice, g-h: negative control, i-l: positive control.

×40 **×100**

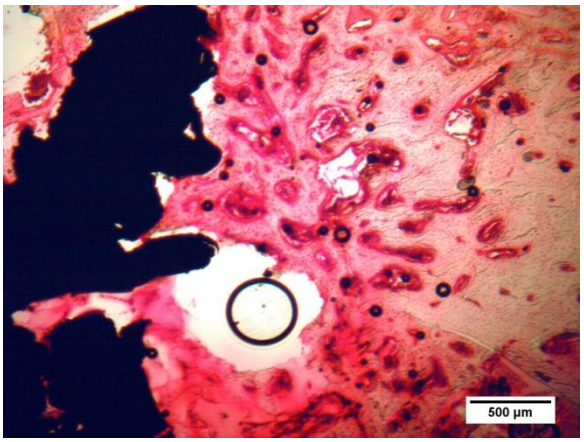

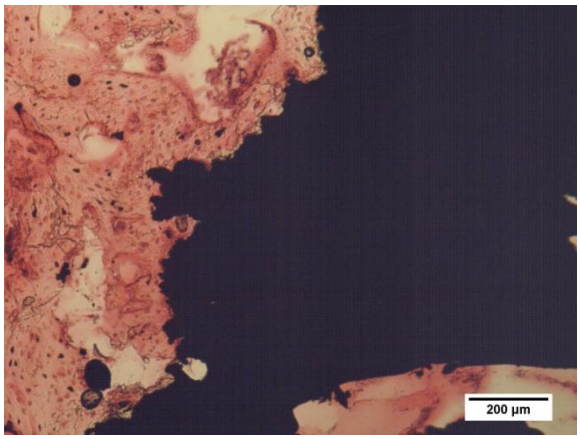

12 weeks Gra. 1 **a** **b**

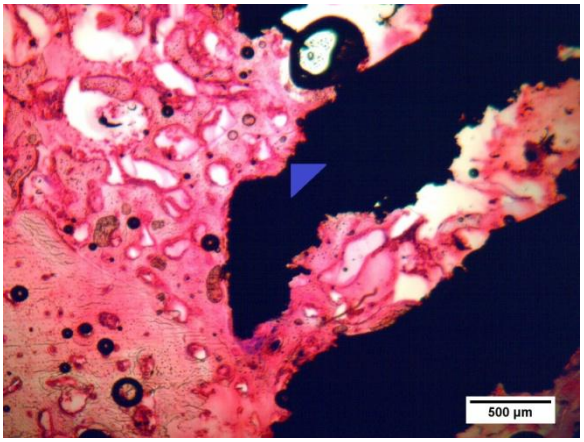

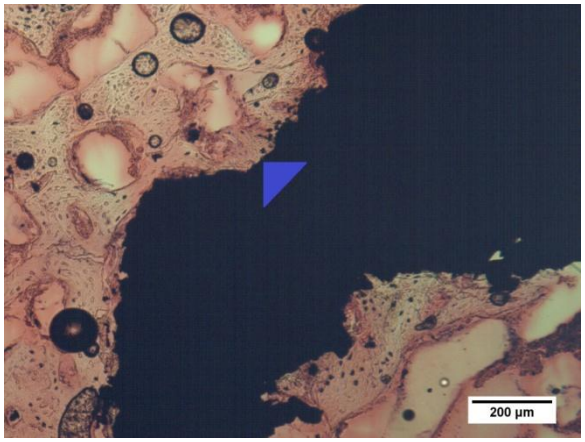

12 weeks Gra. 2 **c** **d**

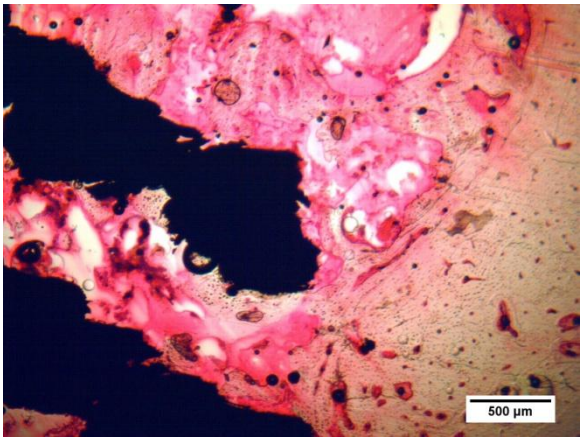

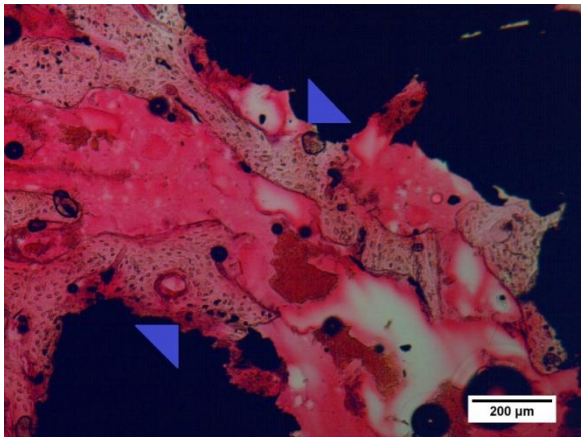

12 weeks Gra 3 **e** **f**

×40 ×100

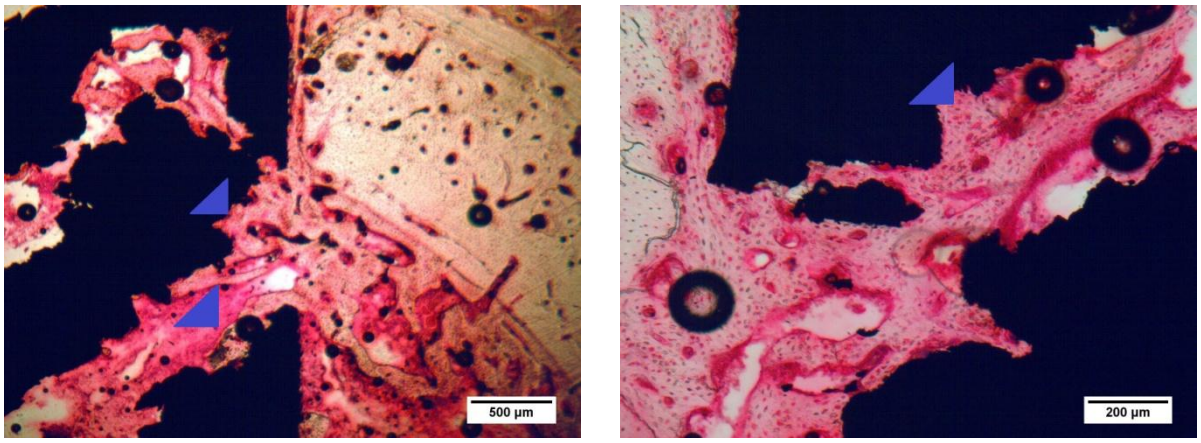

12 weeks Gra. 4 g h

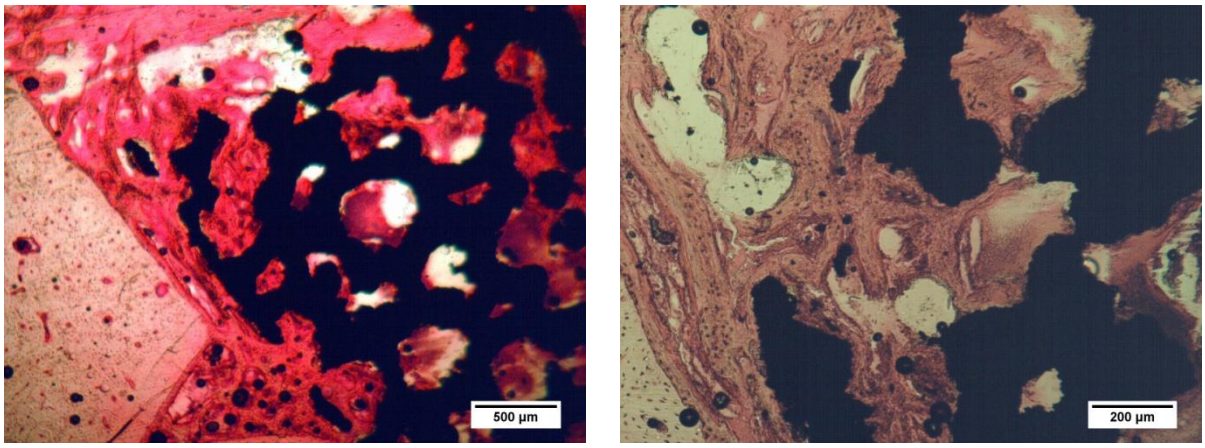

12 weeks PC 1 i j

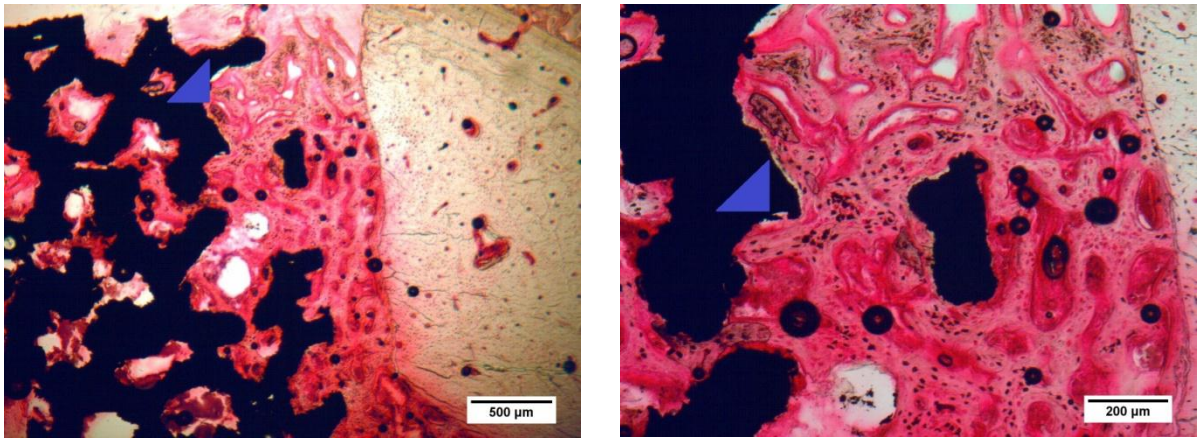

12 weeks PC 2 k l

Figure 5.19: Images of the implants retrieved after 12 weeks at low magnification (left) and high magnification (right). a-h: graded lattice, i-l: positive control.

To summarise, in this chapter the results of the biological testing of this project have been described. This involved tests on the most promising structures described in the previous chapters. The tests involved biocompatibility testing and following cell proliferation over time, quantification of bone-like ECM deposited on the materials, investigating the effect of fluid flow on cell behaviour and the in vivo tissue response after implantation. These results will be discussed in the following chapter.

6. Discussion

The aim of this study has been to investigate the fabrication and characterisation of porous metal structures for their use in orthopaedic implants to improve implant fixation and bone ingrowth. In order to achieve this aim, two different fabrication techniques were investigated: one space holder-based method and one method based on the principle of additive layer manufacturing. The results of the fabrication of these structures and the structural and mechanical characterisation of the resulting samples are described in chapters 3 and 4. The most promising structures were then biologically tested for cell and tissue ingrowth using a variety of techniques; these results are presented in chapter 5.

6.1 Space holder

A space holder-based fabrication method was chosen because of the many potential advantages, as outlined in 1.3.3, such as versatility, fast and easy production of structures and low cost. Porous metals produced using the space holder method can be used in applications such as filters, thermal insulators, shock absorbers and acoustic insulators. Ti6Al4V was chosen as a base material because it is an extremely well characterised alloy that has been used to produce orthopaedic implants for many decades and is known to have excellent biocompatibility.

Two powders were selected for the space holder method; a spherical powder was selected because of its uniform size and shape and because it would allow a better comparison to the EBM produced structures. However, when initial results (figure 3.9) showed unexpected mechanical properties it was decided to include an irregular shaped powder as well.

The choice of a space holder material is usually mainly determined by the desired architecture of the foam; the space holder material has to be able to take the shape of the desired porosity. Chemical and physical properties, such as the melting point, thermal decomposition and reactions with the metal phase, can also play a role Sodium chloride has been chosen because it can easily be obtained in large quantities and the required particle size. Sieving can be used to obtain a narrower particle size range. Also, the physical and chemical properties are suitable for use with titanium alloys.

For the first structures that were produced the sum of the volume of the powders was 6 cm^3 and the shape of the green body was a cylinder with a diameter of around 15 mm and a height

of around 20 mm. This shape was chosen because it produced a structure with suitable dimensions for subsequent mechanical testing, rather than a structure that was immediately intended to be used for biological testing. However, as previously described, due to the height of the samples and the low titanium content it was not possible to produce consistent uniform foams at these dimensions. An effect that was observed in all 6 cm^3 mixtures was that, even after prolonged mixing, it was not possible to obtain an equal distribution of titanium particles in the mixture. This can be explained by the fact that the titanium particles that were used were typically around 5 times smaller than the salt particles, and also have a very different density; when a low percentage of titanium is used, this difference causes separation because instead of taking up all the space in between the salt particles it will be easier for the titanium particles to fall between the salt particles and accumulate at the bottom of the mixture. It was expected that this effect could be significantly reduced by reducing the height of the sample and by mixing the samples again after the mixture is poured into the die for compression. After compression the mixture will form a solid green body and separation does not take place as long as the titanium content is high enough.

When the total volume of the mixtures was lowered to 2 cm^3 a clear difference was observed between the new green bodies and the 6 cm^3 green bodies. Firstly, the distribution of titanium particles appeared to be more uniform than in the larger samples, and secondly, probably as a result of the improved particle distribution, the green bodies were also stronger than the larger ones. This effect is due to the fact that a mixture of salt and titanium can form a strong, consistent green body with a percolating network of titanium particles loosely bonded by the compaction, whereas compressed salt alone cannot.

Although the 2 cm^3 green bodies are significantly stronger and more uniform than the larger green bodies, there was still some evidence of lower titanium content on the outside edges of the top of the green body. Therefore, one other mixing technique was investigated; in an attempt to improve distribution a few drops of hexane were added to the mixture. This had the effect of increasing the adhesion forces between the particles and preventing separation of the powders after mixing.

After the sintering step all samples were weighed, washed to remove the remaining salt and weighed again. The result (shown in figure 3.4) shows that although a large proportion of the salt has already been removed by the heat treatment it is still necessary to wash samples after

sintering as remaining salt may affect its properties. Although salt would have been expected to evaporate under the sintering conditions, the escape of vapour phase salt through the porous network may be slow, and it may redeposit on the metal during cooling.

The shrinkage test data (figure 3.5) shows that shrinkage of the samples is very variable but, contrary to what might be expected, not dependent on titanium content. In initial experiments in was observed that separation of the powders during the mixing stage, which inevitably leads to shrinkage, was most prominent in samples with a low titanium content. Therefore, it can be concluded that the two mixing methods are effective in reducing shrinkage by separation as it appears that foams with the lowest titanium content are keeping their dimensions during sintering as well as the foams with 40% titanium.

The only significant difference that was found in the shrinkage test was that the samples made with the spherical powder showed a higher percentage of shrinkage than the samples made with the non-spherical powder. The most likely reason for this difference is the fact that the spherical particles alone do not form a strong solid structure after compression (Fleck 1995; Goodall et al. 2014), and although the mixture of the spherical titanium and the salt forms a solid green body, the structure may become unstable as soon as the salt begins to melt or evaporate leading to shrinkage.

The relationship between the titanium content of the green body and the relative density after sintering can be determined from the cut surfaces of the foams (figure 3.6 – 3.8); the total area of the cut surfaces is of course indicative of the relative density of the foams. With regard to microporosity inside the struts there is a clear difference between the two titanium powders that were used. Whereas the foams made with the irregular powder show very little microporosity the spherical particles appear to be not as well sintered together as the irregular particles. For example, the left hand side of figure 3.7 b shows many small pores inside the struts, which are the result of incomplete sintering.

This difference between the two titanium powders is also evident on the walls of the pores; all images of foams made with the spherical powder show that although the particles have been partially melted together most particles on the pore walls have not fully fused with the surrounding particles. This is the reason that in figure 3.7 it is still possible to distinguish individual particles, whereas the images in figure 3.6 show smoother pore walls with better

fusion of particles. This effect should improve the structure of the foam (i.e. the cohesion between the metal) and therefore it is likely to have an effect on the mechanical properties of the foams.

The most likely reason for this difference in microporosity and the structure of the surface is again the fact that irregular-shaped particles are more likely to deform or rotate under compression allowing more efficient particle packing after compression. During the sintering step the tightly packed particles are more likely to fuse. The spherical particles on the other hand are likely to form a system where the particles are in direct contact with each other but, with a narrow size distribution, with more limited packing efficiency possible. Therefore, a higher temperature or more time would be required to ensure complete fusion.

The architecture of the pores in both the spherical and the irregular particles are largely in line with what was expected. For the foams made from the green bodies with the lowest titanium content (20% and 25%) the size and shape of the space holder particles is not recognisable from the SEM images, because the titanium content was too low to form complete struts between all space holder particles. This results in highly open foams with interconnected porosity and individual pores (if it is possible to identify them) that are much larger than the size of the space holder particles. In the samples with a higher relative density on the other hand it is much easier to identify individual pores that were formed by a single space holder particle (250 – 500 μm).

Finally, the addition of hexane during the mixing step (methods compared in figure 3.8) did not seem to have a large effect on the structure of the foam. All the foams that were compared showed no difference in the shape of the pores or the interconnections between the pores. Based on these observations the structures that are the most promising to be used for implant applications are the foams with the highest titanium content and the irregular-shaped powder.

Mechanical testing was performed by uniaxial compression; all 20 foams were tested once (as they were taken into the plastic deformation regime, repeat tests on the same sample were not possible) and based on these results tests on the 4 best performing foam types were repeated in triplicate. The objective was to see which foams would be able to combine a high yield strength combined with a suitable Young's Modulus (YM). However for many of the

foams tested, especially the foams that contained spherical particles and the foams with the lowest titanium content, it was not possible to determine a linear region in the stress-strain curve, indicating that these foams simply crumbled under compression, and showed no measurable elastic deformation stage. Therefore, the 3 foams that did show a linear region (irregular-wet-40%, irregular-wet-35% and irregular-dry-40%) and the irregular-wet-35% were repeated in triplicate.

The repeats of the most promising foams all showed a linear region in the first section of the stress strain curve; this means that the curves can be used to determine the average stiffness of the foams. The curves also showed are large variability in the stress strain curves, especially the strain at which the slope of the curve suddenly increases and the linear region begins. This phenomenon is an artefact of testing usually caused by the fact that the top surface of the sample is not entirely flat, which in turn could have been the result from unequal shrinkage during the sintering process. This offset varies between 0 and around 5 percent. From the averages of the YMs of the samples (figure 3.11) it can be seen that there is a very large variation between the samples with values varying between 0.25 and 3 GPa. As a result all differences between the different foams are not significant. There are many possible reasons for this high variability in the YMs of these space holder foams. There is the possibility of a connection with the fact that the surfaces were not entirely flat. These irregularities on the top surface of the samples have the effect of shifting the linear region of the stress-strain curve to a higher strain (in an ideally shaped specimen the linear region of course begins at 0% strain). Another reason could be inconsistent mixing of the powders or differences in the 'settling' of the powder between the mixing step and compression.

Several authors have, over the past decades, investigated the fabrication of metal foams using a variety of different alloys and space holders. In an early study, Wheeler et al. (cited by Dunand (Dunand 2004)) investigated Ti6Al4V foams produced with Mg wires as a space holder and found YMs between 3 and 9 GPa for foams with porosities between 25-82%. Assuming that the lowest stiffness corresponds to the highest porosity, these foams appeared to have a higher YM than the foams in the present study. More recent studies, such and Wen et al. (Wen et al. 2001) and Esen et al. (Esen et al. 2007), also produced Ti6Al4V foams that either had a similar YM at higher porosity or a higher YM at a similar porosity, indicating that the current processing route may not be optimal for producing highly porous foams with good and reproducible YMs. It must be said that these studies do not mention the n-number or SD of their tests, but it is expected that these results are more reproducible than the present samples.

Imwinkelried (Imwinkelried 2007) produced a large series of space holder foams using cpTi (which has a bulk YM that is only marginally higher than Ti6Al4V, 116 vs. 110 GPa). These data were used prove that the linear relationship between the YM and the relative density to the power 2 (as described by Gibson and Ashby (Gibson et al. 1997)), is valid for this type of foam. Based on these values the YM of the salt based samples is expected to be between 5 and 7 GPa for relative densities between 35% and 40 %.

From these results it can be concluded that it is possible to use these combinations of titanium powders and salt to produce highly porous foams using the space holder method. The porosity of the foams was shown to be highly interconnected and at lower porosities the individual pores closely resemble the size and shape of the space holder particles. Mechanical testing, however, revealed a high variability between samples of the same composition and fabrication technique and YMs that were considerably lower than what might be expected based on previous research on space holder-produced titanium foams. For biomedical applications of titanium foams it was considered to be essential that the production of these foams is consistent and highly reproducible. Based on these results it was thought that to produce consistent foams investigating a different fabrication method is more likely to achieve the desired properties that to continue optimising the current process. Therefore, it was decided not to investigate this process further.

6.2 Electron Beam Melting

Electron beam melting was chosen as a fabrication technique because of its potential to be used for the production of highly regular foams based on a model of a unit cell that is replicated in three dimensions, commonly known as lattices. Ti6Al4V is a frequently used alloy for EBM and the parameters and building conditions are well established. The optimal pore size required for bone ingrowth into bone implants is a subject of ongoing debate but most commercial porous bone implants have pore sizes from 200 µm up to 800 µm (Levine 2008; Wieding et al. 2014). It was expected that EBM can be used for building lattices in the largest part of this pore size range.

The first prototype that was produced mainly served to investigate many practical issues surrounding the EBM fabrication process; it was used to investigate how well the features

correspond to the CAD model, how long it takes to build these small structures and how fast and effective powder could be removed from the pores.
The diamond unit cell was chosen because it is a relatively simple structure which has a relatively low stiffness relative to its density (Ahmadi et al. 2014). As mentioned before, it is considered beneficial to an implant's success if the YM of the implant matches the surrounding tissue (Bugbee et al. 1997). Estimates of the YM of cancellous bone vary from lower than 1 GPa to close to 20 GPa (see table 1.1), which means that a porous Ti6Al4V lattice should have a YM that is 81-99% lower than its bulk stiffness. For a typical highly porous lattice with a relative density of 25% this would mean that the lattice should have a YM that is between 27% and 96% lower than the maximum YM based of the rule of mixtures; the Gibson and Ashby model predicts a YM of 7 GPa.

Heinl et al. tested two types of Ti6Al4V lattices: a hatched structure and a diamond structure. They found that the diamond lattices (ρ/ρ_0 = 19%) had an average YM that was 64% lower than the G&A model whereas the hatched lattice (ρ/ρ_0 = 40%) was only 27% lower than the G&A model when tested parallel to the building direction. Additionally, the diamond lattice has a more complex structure in which the YM is less dependent on the orientation of the lattice. Therefore, the diamond lattice can be seen as a suitable unit cell when aiming for a low stiffness lattice (Heinl et al. 2008).

Removal of the powder from the prototype was fast and efficient, mainly because of the regular orientation of the pores and the fact that no pores in the lattice are 'shielded' from the particles of the PRS. However, it was noted that powder removal from the outer pores was very rapid compared to the inner pores so it is possible that larger structures are more difficult to clean.
SEM was used to assess the structure of the prototype and to measure how the strut thickness compares to the CAD model. The strut size of the CAD model was set to 100 µm, a value that was known to be below the resolution of the electron beam, so that the minimal strut thickness could be determined. The average strut thickness of the prototype was found to be between 550 µm and 650 µm (see figure 4.6). For future EBM builds, however, the build parameters were optimised so that smaller strut thicknesses would be possible.

The aim of the next phase of the project was to determine whether it was possible to build smaller feature sizes without losing the interconnectivity or the ability to easily remove the

powder from the inner pores. To investigate this, structures with an overall size of 20 × 20 × 20 mm and unit cell sizes of 2.0, 1.5 and 1.0 mm were built (figure 4.4).
The structure with 2.0 mm unit cell was cleaned relatively quickly (5 minutes), which indicates that the powder from the PRS could easily travel though 700 µm pores for a distance of around 14 mm (to clean the inner pores the powder travels diagonally rather than perpendicular to the surface due to the orientation of the lattice). The penetration depths for the smaller unit cells were approximately 8 mm for the 1.5 mm unit cell and less than 1 mm for the 1.0 mm unit cell (figure 4.4).

These results confirm that fabrication of lattices with a unit cell size of 1.0 mm is not a viable option for this processing method; 1.5 mm unit cells are a possibility, but for a medical product efficient and complete removal of the powder is essential as remaining particles could potentially be released and initiate an inflammation reaction after implantation (Case et al. 1994; Cohen 2012). Nevertheless, the mechanical properties of the 2.0 and the 1.5 mm unit cell lattices were investigated. In order to get a good comparison between the two unit cells, smaller lattices were produced which had an overall size small enough to remove the powder from the entire structure.

Mechanical testing showed a highly reproducible initial stage of the stress strain curve for both samples. Some samples, especially the samples represented by the red line in the 1.5 mm graph, also show a large drop in stress followed by a second and a third (near) linear region (figure 4.7 a). This indicates that after the collapse of the first layer the rest of the lattice is still intact and behaves elastically before another failure event.
The YM of the structures was calculated (figure 4.8) and the results confirm that the diamond unit cells form lattices that have a far lower YM that what would be expected based on the G&A model. The lattice with 2.0 mm unit cells had a YM of 1.1 GPa (ρ/ρ_0 = 15%) which is 56% lower than the G&A model and the 1.5 lattice (ρ/ρ_0 = 37%) is 83% lower with a YM of 2.5 GPa. These values both lie within the range of the YMs measured for cancellous bone (see table 1.1), so from a mechanical point of view the materials created with these unit cell sizes could both be suitable for use in orthopaedic applications. However, for future experiments it was considered to be useful to produce lattices with different strut diameters in the same lattice. As removing the powder from the current lattice with the 1.5 mm unit cell was already problematic it is unlikely that it is possible to fine-tune the YM by changing the thickness of the struts. For the 2.0 mm unit cell it was expected that the relative density could

potentially be doubled without the pores being blocked by the remaining powder. This would create a large density range of potential structures between the point where the struts become too thin to be built by EBM and the point where the strut spacing becomes too narrow for the PRS to remove the powder. Therefore, a unit cell size of 2.0 mm would be a suitable option when building graded structures where different densities are required. However, for uniform lattices 1.5 mm might be preferable as these lattices will have more pores per surface area and a smaller pore diameter.

For the biological part of this project the aim was to test the behaviour of a graded lattice that had a highly porous outer layer and a core that was more dense and stiff while retaining full interconnectivity. To ensure that all the struts of adjacent cells were firmly connected to each other it was decided to use the same unit cell size in the entire structure with only the strut thickness as a variable.

In biocompatibility testing, the shape of a test sample is usually round or square with a length of around 10 mm and a height of a few millimetres. For the graded lattices, the height of the lattice should be large enough to have an effective graded porosity; it should also be thin enough to allow cells in the middle of the structure to have sufficient access to nutrients under static conditions (i.e. by diffusion alone). Therefore a height of 6 mm was chosen as it would be possible to have three unit cells in the z-direction that could be designed with different strut sizes.

To obtain the highest gradient in the lattice the strut thicknesses had to be as close as possible to the limits defined above. It was thought that the maximum strut thickness at which the powder could still be removed was around 1 mm, but as it was unknown whether at this strut thickness there would be a discrepancy between the model and the actual strut size. Therefore, a strut size of 800 µm was chosen for the bottom (most dense) layer. The middle layer and the top layer had modelled strut sizes of 500 µm and 200 µm, respectively.

After building the structure, SEM images were used to determine the actual strut sizes; these were found to be significantly higher for the top and the middle layer, but not for the bottom layer. The discrepancy is higher for the top layer than for the middle layer indicating that there is not one critical size below which the actual size suddenly starts to deviate from the model. It is expected that at a strut diameter of around 800 µm (but possibly higher) the actual size gradually starts to deviate from the model.

Despite this effect, the diameters of the struts and the relative density of the three layers were all significantly different from each other. The top layer has a relative density that is around

50% of the bottom layer. This means that the produced lattice achieved our core aim of a graded porous metal structure and therefore it was decided that this design will be used for all future mechanical and biological tests.

The stress-strain curves from the compression tests of the graded lattices showed a similar shape to the uniform lattices tested before. All graded lattices showed a clear linear region starting at 0% strain followed a large drop in stress corresponding to the initial failure of the lattice. The lattices also showed subsequent (near-) linear regions associated with the denser layers which failed at a higher stress.

These lattices were compared to specially designed lattices that had the unit cell properties of the layers of the graded lattice. Although these lattices were slightly smaller than the graded lattices because of potential problems in removing the powders from the pores, the relative density and the strut size were the same. The lattices were used for compression testing to investigate whether the properties can be predicted from the properties of the uniform lattices alone. As the mechanical behaviour of the lattices is so consistent, there is the possibility of predicting the behaviour of a graded lattice from the properties of its constituents using a simple procedure to estimate the location of cardinal points on the stress-strain curve.

The Young's modulus of the graded lattice can be predicted by assuming it is composite of three materials, arranged in layers. With the assumption that these three components have the same mechanical properties as the uniform lattices, the aforementioned rule of mixtures may be used. If the YM of the individual layers is known, the YM (E_{graded}) of the composite is given by the following formula.

Equation 6.1 $$\frac{1}{E_{Graded}} = \frac{1}{3E_1} + \frac{1}{3E_2} + \frac{1}{3E_3}$$

In this equation the subscripts 1-3 denote the different layers. Based on the average values for the three uniform lattices, the YM of the graded lattice was calculated to be 2.28 GPa; the measured average of the graded lattice was 2.08 GPa. This model can only be used to calculate the YM of the intact lattice as after crushing of the first layer the remaining composite will be different. However, due to the difficulty in estimating the YM of a partially crushed lattice, this value has also been used for the other stages of (near-) linear behaviour.

The other values that are important in making a prediction of the stress strain curve for a graded lattice are the yield strength and the subsequent peaks in stress. Observations confirmed that the top layer of the lattice (i.e. the layer with the lowest strut thickness) always fails first. From the way the lattice is orientated one could hypothesise that the yield strength of one layer is not affected by the other layers. This hypothesis would imply that the stress peaks in the graded lattice would correspond to the yield strengths of the uniform lattices, which were 37, 89 and 160 MPa (Table 4.1). In the graded lattice stress peaks are associated with the collapse of sequential layers. As densification is observed to occur in the uniform lattices at 43% strain, this would also be the level expected within each layer. As there are 3 layers, the offset between peaks should therefore be a strain of 14%. The predicted behaviour based on these points is indicated by the black line in figure 6.1.

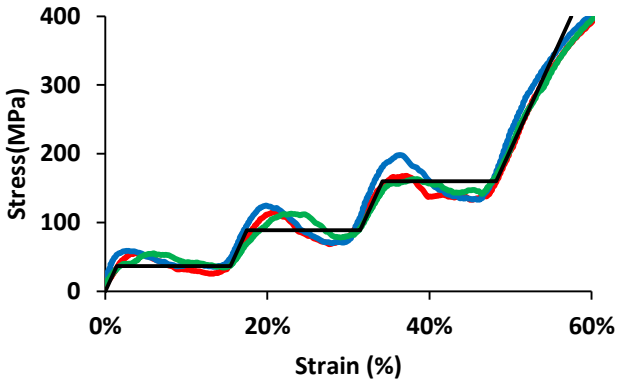

Figure 6.1: Stress-strain curve of 3 graded lattices and a black line indicating the predicted behaviour of the graded lattice based on the properties of the uniform lattices.

This comparison shows that the expected behaviour based on the model corresponds very well with the actual behaviour of the graded lattices, indicating that for a highly controlled fabrication process such as EBM the different layers of a lattice could be considered to behave independently of each other, making it easy to predict the stiffness and yield strength of other graded lattices based on the characteristics of the individual layers.

In summary, the variation of properties of structures of this type that can be built using the EBM process remains large. However, with the findings discussed above it is possible to give certain limits of the technique for a very specific type of lattice that has been shown to have great potential for implant applications, namely a thin diamond lattice.

- The lower limit in terms of unit cell size lies between 1.5 and 2.0 mm. At a unit cell size of 1.5 mm it is possible to remove to remove all powder up to a depth of 8 mm, but there is limited flexibility in the density of the structures that can be produced. The reason for this is that the density at minimum strut thickness and the density at which powder removal becomes problematic are close together. Using a unit cell size of 2.0 mm has shown much greater flexibility.
- At a unit cell size of 2.0 mm the minimum strut thickness that can be built is around 400 µm. Using this strut diameter results in a relative density of around 20% and a YM of just over 1 GPa. The strut diameter can be almost doubled in the case of this unit cell size (769±42 µm was the highest thickness measured), without losing the ability to easily remove the powder. These structures had a relative density of 43% and YM of 5.38 GPa on average.
- Multiple layers of unit cells of the same size form a structure of which the YM lies very close to the YM predicted by the rule of mixtures when the layers are orientated normal to the loading direction. This is useful when designing lattices for bone ingrowth as not only the mechanical properties are important but also the pore sizes in the different layers.

6.3 Biological assessment

Predicting the quality of the interface between bone tissue and an implant is extremely complex and the only method of truly assessing their long-term stability is by analysing large sets of data from patients who underwent arthroplasty and who were available for follow-up in the years after surgery. The current benchmark that is given by the National Institute of Health and Care Excellence (NICE) is called the 10A benchmark, which means that the implant has been studied clinically for at least 10 years (NICE). In 2012, the percentage of implants that has passed the 10A benchmark varied from 88% for cemented stems to only 3% for non-cemented acetabular cups (National Joint Registry 2013).

Before an implant can be marketed as a medical product, it goes through a long process of in vitro, in vivo and clinical testing all of which aim to predict the long term performance of the implant. In this study it was aimed to test porous metal structures produced by EBM primarily in vitro, although an opportunity for preliminary in vivo testing was also made use of. In an attempt to make an in vitro model that was closer to the in vivo environment

samples were also tested in a dynamic situation where cell-seeded constructs were exposed to forces caused by fluid flow.

In vitro cell culture on titanium structures has been performed many times and in several different ways during the course of this study, either as separate experiments or as controls for other experiments. The aims were to study cell attachment on the surfaces, the rate of proliferation of different cell types and formation of bone-like extracellular matrix.

In the first experiment the resazurin-based assay was tested and calibrated as this was a critical assay for further experimental work. There are many other assays available to measure the number of cells in a biological sample, such as MTT, MTS and several protein and DNA-based assays, but all these techniques involve analysis of either fixed cells or cell lysates whereas the resazurin-based assay is based on cell metabolism and is therefore performed on living cells. This allows different timepoints to be measured on the same samples which can be very important if few samples of a specific design are available.

Measurement of cell viability at different seeding densities showed a very clear linear relation; however, as mentioned in section 5.1, the subtraction of the background fluorescence is a critical step in comparing data between different timepoints and different experiments and is common practice (Mallick et al. 2012).

Using the resazurin assay the effect of encapsulating cells in a fibrin clot on their viability was measured. The conversion of the soluble protein fibrinogen to the polymerised non-soluble fibrin is a natural process which is a key feature of blood clotting and is frequently used both in vitro and in vivo for the encapsulation and targeted delivery of cells, growth factors or other substances (Trentin et al. 2005; Zhu et al. 2010; Cornelissen et al. 2012; Navaei-Nigjeh et al. 2013).

Cell viability of cultures seeded with and without a fibrin clot was first measured 4 hours after seeding. An incubation period of 4 hours is sufficient for cells to attach but not long enough for the fibrin clot to dissolve. 20 hours after seeding the fibrin clot will have been completely dissolved and the cells that attached to the TCPS should have recovered fully from the seeding.

At the 20 hour timepoint the values for the viability assay were 5 to 10 times higher than the values after 4 hours. In the first day after seeding there is usually no or very little proliferation of cells (Helfrich et al. 2012). Therefore, it is expected that this large difference between these timepoints in both conditions is due to a lowered metabolism as a result of insufficient recovery time after seeding. There is no significant difference between the cell viability of the

two conditions, but due to the low values this does not necessarily mean that there is no difference in the number of attached cells.
At the 20 hour timepoint, the cell viability values have returned to values that would be expected based on the number of cells seeded and statistical analysis showed that the cultures where cells were seeded in a fibrin clot had significantly lower cell viability than the cultures without fibrin. Therefore, it was decided that seeding in fibrin was not a necessary step for seeding bone cells and that seeding cells onto porous materials where the pores are sufficiently small to contain small amounts of liquid (typically 100 µL), a method without fibrin, such as the method described in 2.6, is preferable.

Using this seeding method cells were seeded on the prototypes and cultured for three weeks in osteogenic medium (figure 5.3). Seeding efficiency was 63% compared to the 2D control on day 1 which could be due to a lower affinity for the titanium surface and cells leaking out of the structure, although no leakage of liquid was visible. Comparing this result with work on similar structures was difficult as other studies that tested biocompatibility (Heinl et al. 2008) or cell attachment (Ponader et al. 2008; Haslauer et al. 2010; De Peppo et al. 2012; Hrabe et al. 2013) only compare their structures to other metal foams or flat metal surfaces but not to TCPS.
Over time the cells seeded on the structures increased in number to around 200% (of the number originally seeded) by day 7 and maintained that level up to day 21. These results were in line with what was expected and also with some results of other in vitro studies on EBM Ti6Al4V. However, the literature on in vitro studies on EBM Ti6Al4V covers a wide range of fully porous structures, surfaces, and coated structures and as a result reported cell viabilities can be as high as 600% and as low as 125% (De Peppo et al. 2012; Hrabe et al. 2013).
Both the cells cultured on the prototypes and the 2D controls show no significant increase in cell viability between 1 and 3 weeks of culture. This is likely to be caused by the change of medium at the start of the experiment; from day 0 the cells are cultured in the presence of AA, dex, and β-GP; this change in the culture medium causes cells to change phenotype from fast growing pre-osteoblasts to a mature ECM-producing osteoblast. A similar effect can be seen in e.g. Hrabe et al. where cells seeded on titanium show high proliferation and low matrix production in the early stages of culture followed by a phase of lower proliferation and an increase in collagen production in the later stages of culture (Hrabe et al. 2013). From these results it can be concluded that MG63 osteoblasts adhere well to these newly produced

structures, show a rapid increase in viability in the first 7 days after seeding and maintain this level of viability in subsequent weeks.

Following these successful initial results, work continued on the design of a simple perfusion system in which fully porous titanium lattices could be placed to investigate the proliferation of cells under dynamic conditions. After design and initial testing on the chamber and the pump (see figure 5.5-5.6), fully porous lattices were placed in the bioreactor, seeded with MG63 cells and cultured for three weeks under dynamic conditions as described in section 5.6.

Cell viability results showed that after three weeks of culture cells in the 2D and the static 3D group had proliferated more with increasing culture time, whereas the cells that were cultured under dynamic conditions showed a relative cell viability of below 100% which would indicate (based on the results in the previous experiment) that either no proliferation has taken place or that the flow through the lattices removes cells from the surfaces during the culture period. This value was far lower than what would be expected based on the control conditions and literature on other types of porous 3D scaffolds subjected to flow (McCoy et al. 2010; Shaeri 2013).

Measurement of collagen and calcium content on the same samples (figure 5.9-5.10) showed a significantly lower collagen content in the dynamic samples compared to the static conditions and no calcium content in any of the conditions, but when collagen content was corrected for cell number the values show that the amount of collagen produced per viable cell is significantly higher in dynamic culture.

The increase in collagen content per cell under dynamic conditions is in line with numerous studies, both on titanium and on other materials (Freed et al. 1998; Delaine-Smith 2013). However, due to the large difference in cell viability between the flow group and the other conditions, there could also be other reasons for this relative increase, such as incomplete removal of the staining solution, which become more pronounced when compensating for low cell numbers.

It is not known why mineralisation did not occur, especially as previous studies, such as Tsai et al. have shown mineralisation of MG63 in vitro (Jeon et al. 2012; Tsai et al. 2012; Song et al. 2013). However, other studies such as Czekanska et al. (Czekanska et al. 2013) also reported discrepancies in response of MG63 to osteogenic media compared to other bone cell lines and primary cells. Therefore, it was decided to compare these results to a different bone-like cell line, the MLO-A5 cell line.

The result of this comparison (figure 5.11) shows very clear differences between the two cell lines. The MLO-A5 cells show significantly lower proliferation after three weeks of culture, but far more mineral produced, indicating a difference in phenotype between the two cell lines. The MG63 cells proliferate extensively, especially in the first week of culture, but do not become mineralising mature osteoblasts despite being cultured in differentiation medium. The MLO-A5 cells, however, show a slightly lower cell viability (indicating a lower cell number) but produce considerably more ECM, especially mineralised matrix. This is in agreement with the reported phenotype of MLO-A5 which has been described as a late stage osteoblast or a pre-osteocyte by the group which developed it (Kato et al. 2001; Barragan-Adjemian et al. 2006).

From these data it can be concluded that the MLO-A5 cell line is much better suited to investigate the effect of mechanical stimuli on the formation of ECM. In order to investigate the problem of low cell number on the lattices cultured in the bioreactor for 3 weeks, two lattices were placed in the bioreactor and cultured for 1 and 3 days (figure 5.12). In this experiment the flow sessions were started on day 3, which is different from the earlier experiments where the first flow session took place 24 hours after seeding. This means that the samples taken on day 1 were removed before the first flow session and the samples taken on day 3 were removed directly after the first flow session.

The cell viability data from these early timepoints showed that cell viability is slightly, though not significantly, lower than the static control on day 1 and significantly lower after the first flow session on day 3. However, there is still an increase in cell viability between samples cultured in the bioreactor on day 1 and day 3, so if there is a negative effect of the flow sessions on cell viability it is expected to be less severe than in previous experiments where the flow was started the first day after cell seeding. Therefore, it was decided to use these parameters for three week cultures on the MLO-A5 cell line with intermediate timepoints at 7 and 14 days (figure 5.13).

The static group showed a steady increase in cell viability throughout the 3 weeks of culture. As discussed before, the MLO-A5, cell line does not grow as fast as the MG63 cell line and is therefore less likely to reach a plateau. The samples cultured in the bioreactor also show an increase in cell viability in the first two weeks of culture although there seems to be a lot of variation in the growth rate between different timepoints. For example, there is a more than 2-fold increase in the bioreactor group between day 3 and day 7 compared to virtually no difference in the static group between these timepoints. As the standard deviations within the

groups are not exceptionally high it is likely that the variation between experiments is high whereas the standard deviation within the groups is relatively low.

This problem could be solved if the cell viability could somehow be monitored during the experiment; many studies that use a bioreactor for mechanical stimulation of cells use a bioreactor from which the samples can be removed between flow sessions (Morris et al. 2010; Shaeri 2013). For the current design it was not possible to assemble the bioreactor in a way that the sample could be taken out during the experiment, but for future tests involving repeated fluid flow sessions this would be a useful improvement. As an alternative, it would be possible to do repeated measurements at each timepoint, but this would be a very time-consuming experiment and would also involve a large increase in the number of samples and cells required.

The low cell viability in the lattices that were cultured for 21 days (compared to the ones cultured for 14 days) was perhaps the most surprising. Again, this unexpected difference could be due to the high variability between experiments but may also be due to the conditions inside the bioreactor becoming less favourable to cells in the long term. A decrease in cell number over time in itself is not unique and has been reported to be accompanied with better distribution of cells inside a scaffold (McCoy et al. 2010; Partap et al. 2010); however, it does not explain the high cell viability on lattices cultured for 7 and 14 days.

A possible cause for this change in conditions is that cells, initially only seeded on the titanium lattice, migrate and proliferate on the inner surfaces of the bioreactor, leading to a lack of nutrients in the times between flow sessions. For the cell viability assay, only the lattice itself is measured so any cells growing on the inside of the bioreactor would not have an effect on the outcome. This possibility is supported by the observation that the culture medium in the bioreactor was changing colour from red to orange (indicating a lower pH, which is usually caused by cell waste) in the last week of culture.

Assessment of bone ingrowth into a porous metal is seen as an essential test to determine whether a porous structure is suitable for use in implant applications. Models that have been used in recent literature to investigate bone ingrowth into porous metal include rat (Wazen et al. 2010), rabbit (Thomsen et al. 2009; Pattanayak et al. 2011), goat (Biemond et al. 2011), pig (Ponader et al. 2010) and sheep (Assad et al. 2003; Assad et al. 2003; Assad et al. 2004; Bertollo et al. 2012). The quality of the bone-implant interface can be investigated by pull-out test as described earlier, but the majority of studies use histology as their main tool to assess

the extent of tissue ingrowth. Pull-out tests have the advantage of being quick and simple and that the results are easy to analyse. However, this form of testing often produces results with a high variability which means that a larger sample size may be required for statistical analysis. Histology on the other hand, allows more complex analysis and provides a far better insight of the mechanism behind implant integration (Svehla et al. 2000; Svehla et al. 2002; Svehla et al. 2005).

The aim of the present study was to carry out a preliminary assessment of bone ingrowth in a rabbit model and to analyse the results by histological analysis to investigate the difference in bone ingrowth into a graded porous metal structure and a commercially available non-graded structure. However, due to severe problems in the embedding and transport of the implants not all samples were available for histological analysis. In the samples that were analysed the intensity of the staining is highly inconsistent due to porosity in the PMMA. Nevertheless, a total of 12 implants were available for histology, all of which could be stained to produce images with sufficient detail to indentify some of the tissues. Therefore, it was decided to include the available data from this study in this thesis despite the fact that many of the samples were unavailable for analysis.

After 4 weeks in vivo all porous samples showed extensive tissue ingrowth but in the majority of samples no new bone was formed inside the pores. As this is a relatively early timepoint it is not surprising that bone formation inside the implant has not yet taken place in many of the implants. Many studies into bone ingrowth do not include a 4-week timepoint; however, one study (Ponader et al. 2010) found bone ingrowth up to 2 mm after 4 weeks implantation into pig skulls. However, it is difficult to compare these studies because this study involved a much larger animal model and the implants were placed in a flat bone, which is formed by intramembranous ossification, rather than a long bone which is formed by endochondral ossification.

The 12 week timepoint (or 3 months) is a commonly used timepoint in many bone ingrowth studies. In many cases it is also the final timepoint of the study indicating that if bone ingrowth has not taken place at this point it is unlikely to initiate after this timepoint. Occasionally, a 6 month timepoint is included to observe bone maturation and remodelling.

In the present study, 6 samples from the 12-week timepoint were analysed. In all cases the tissue that has formed inside the pores appears more organised when compared to the 4-week timepoint. Bone tissue inside the pores is difficult to assess in many of the sections due to the quality of the staining, but two of the specimens show bone tissue that is located inside the

pores, attached to the implant and attached to the old cancellous bone. In the remainder of the 12-week samples there is evidence of similar tissue formation at the bone implant interface, but it is unclear whether this is new bone formation and whether it is connected to the old cancellous bone.

Comparing the depth of bone ingrowth and the bone's ability to fill pores to similar bone ingrowth studies can be problematic as all relevant studies use different timepoints, animals, structures and coatings as well as presenting their findings in different ways. With regard to pore closure, Ponader et al. shows clear evidence of complete closure of the pores in their structure which are 450 μm on average after 60 days. In this time the bone has filled the entire porous structure which was 4 mm in diameter indicating an ingrowth depth of at least 2 mm (Ponader et al. 2010). Direct bone-implant contact of their porous samples, however, was low in this study reaching a maximum of around 6% after 60 days. There results (in pigs) show a sharp contrast with several other studies on non-porous and coated porous titanium in smaller animals; Pattanayak et al. (Pattanayak et al. 2011) (coated porous) presents histological images (though not quantified) that show a high bone-implant contact but do not fill the pores completely and Thomsen et al. (Thomsen et al. 2009) (non-porous) measured bone-implant contact percentages between 30 and 40% after 2 weeks in vivo.
Finally, Biemond et al. (Biemond et al. 2011) investigated porous surfaces with a much smaller pore diameter (no average given); their in vivo study is the only study that gives maximum ingrowth depth for all their samples. They found maximum ingrowth depths between 0.78 and 1.18 mm after 4 weeks and between 0.98 and 1.47 mm after 6 weeks. They also performed histomorphometric analysis to measure the percentage of bone-implant contact which was found to be approximately 25±10%.

Overall, there were many limitations to this study, and as a result of these limitations it has not been possible to conclude whether or not bone ingrowth or implant stability is as good as the positive control. For future studies, several recommendations could be given to improve the experiment and to increase the possibility of being able to conclude whether one implant shows better bone ingrowth than another. The most important recommendations are given below:

- Firstly, a rabbit model is a relatively small animal for a bone ingrowth study, especially when testing implants with large feature sizes. Bone ingrowth can be

studied more effectively when the implant is placed deeper into the cancellous bone. Therefore, it is recommended that a model is used where the implant can be inserted in length so that there is a high contact area between the cancellous bone and the implant. In the present study, the financial means and the technical expertise for a larger animal model were not available.

- After removal of the femur the tissue needs to be fixed, dehydrated and infiltrated with resin before it can be embedded. The rate of these processes depends on the ability of the fixative, the alcohols and the resin to penetrate the tissue. In many samples, it appeared that insufficient penetration of these chemicals had taken place resulting in insufficient hardening of the inner parts of the bone. As all samples had been treated for the amount of time recommended in the embedding protocols (48 hours per step), it is recommended that for future studies the bone samples are trimmed as much as possible, because smaller samples will have better penetration of liquids. In general, cancellous bone has a higher permeability than cortical bone so the removal of unnecessary cortical bone in particular would improve the embedding.
- Partially as a result of inadequate resin penetration many small air bubbles were formed inside the resin. These air bubbles do not only cause artefacts in the tissue sections but also cause problems in removing the staining solutions from the resin blocks leading to highly inconsistent staining of the sections. These issues could be prevented by increasing the time that the samples are left under vacuum before polymerising the resin or by leaving the samples under a higher vacuum.
- Finally, depending on the numbers of animals available, the addition of other porous samples could be considered. Bone ingrowth and implant integration depend on many different factors and although comparing a new material to a commercially available material might be the best option to assess its overall performance, to assess individual properties of the new material (such as pore size, pore gradient, Young's modulus etc.) different controls might be necessary. During the planning of this study several other options for different conditions were considered; however, due to limited availability of animals only three different materials were tested.

Using these recommendations, future experiments can be planned that produce higher quality results, mostly in terms of image quality, but also in terms of biological relevance. Especially the use of a larger animal model which would create the possibility of studying larger graded

lattices with shapes that better resemble a bone implant. Combining these techniques with the enormous versatility of the EBM process for producing high quality 3D printed titanium there is a near infinite number of possible structures that could be produced to improve the quality of the bone-implant interface.

7. Conclusions

In this thesis the fabrication and characterisation of several different types of porous metal have been described. The thesis also describes a range of biological tests, which were carried out in order to investigate how cells and tissues behave in and around such a metal structure. This chapter aims to give an overview of the most important findings of the work and to describe potential future directions for this research.

7.1 Space holder foams

Chapter 3 describes the production and testing of titanium foams produced by the space holder technique. As mentioned before, this is a highly versatile technique in which many parameters can be manipulated to alter the properties of the resulting foam. The effects of several of these parameters on the structure and properties of the foam produced have been investigated as part of this project, with the most important properties being the ratio between the quantity of space holder material and the metal, the shape of the metal powder and the mixing method.

The effect of the metal to space holder ratio was the most straightforward; as expected, a lower titanium content resulted in a higher porosity and more interconnections between the pores, but also resulted in more brittle foams. Compression tests confirmed this effect, as for the foams with the higher metal content it was possible to determine a value for the YM by conventional means, whereas the samples with the lower metal content appeared to crumble before showing measurable elastic behaviour.

More difficult to predict were the effects of the type of powder and the mixing method. Wet mixing appeared to produce more consistent foams, but these observations were not supported by the mechanical tests or the shrinkage tests, both finding no significant difference. The change from spherical to irregular shaped powder was clearly observed in SEM images where the microporosity (resulting from incomplete sintering and ubiquitous in the spherical powder samples) was mostly absent.

Apart from the parameters described above there are several other parameters of the process which have not been looked at in depth and which could potentially be optimised to produce more consistent foams. Two aspects of the fabrication process that will certainly have a large impact on the quality of the foams are the time and the temperature of sintering; an increase

in either the sintering time or the temperature of the green body will almost certainly result in better fusion of the metal particles, but could also cause unwanted side effects such as excessive shrinkage or loss of interconnections between the pores. In this study a sintering step at a temperature of 1100 °C for 1 hour was used whereas similar studies on the space holder for titanium and its alloys have used 800-1000 °C for 2 hours (Jha et al. 2013), 1200 °C for 1 hour (Esen et al. 2007) and 1300 °C for 3 hours (Imwinkelried 2007).

Another parameter that could be changed is the particle size of the titanium powder; irregular-shaped particles with a smaller average size could form a more tight packing around the space holder particles before and after compression which might lead to better fusion of the particles during the sintering step and to stronger struts. However, smaller particles have a larger surface area to volume ratio, which can increase the handling difficulties with metal powders (such as pyrophoric behaviour, particles becoming airborne, etc).

In general, the space holder technique is a relatively simple, versatile and inexpensive technique to produce porous metals. However, the work presented here shows that despite all the variations in the fabrication process, reproducibility remains a major issue. Because of the fact that consistency and reliability are two of the most important factors in fabrication of porous materials, especially in the medical field, any future work should be aimed primarily at addressing these issues.

7.2 Electron Beam Melting

Electron beam melting was used alongside the space holder technique as this technique is known for its ability to produce titanium components with great precision and reproducibility. One of the aims of this project was to explore the possibilities of this technique in producing porous structures relevant for medical applications.

During the course of this project many different structures were produced using the basic diamond lattice. It was found that a lattice with a unit cell size of 2 mm was the smallest feature size in which the powder could still be removed efficiently and reliably. The strut diameter in these lattices could be as low as 400 µm and as high as 750 µm, creating a range of possible densities and YMs. These lattices typically have a YM which is 95% to 99% lower than that of solid Ti6AL4V (1 – 6 GPa) bringing the YM within the range of human cancellous bone. The pore size (or strut spacing) of these lattices could be varied between 600 µm and 800 µm, which is in the range of pore sizes used in commercial porous implants.

One of the main challenges of designing porous implants for bone ingrowth is that the optimal YM for a porous implant is not known. It is generally assumed that the stiffness of the implant should be as close to the surrounding tissue as possible, but as mentioned before measurements on the mechanical properties of bone vary widely. The present work has shown that graded lattices with the diamond design presented here will have a YM corresponding to the lowest part of this range (1 – 6 GPa); in order to obtain lattices with a YM towards the high end of this range the relative density could be increased to 50% or higher, but this could cause problems in removing the powder and leaves a smaller volume for bone ingrowth. Alternatively, a different type of lattice such as the hatched-type lattice shown by Heinl et al. (Heinl et al. 2008) (ρ_{rel} = 40%, E = 13 GPa) could be used, although there is a limit to the YM that could be achieved without changing the density.

In terms of lattice design the EBM process is also a highly versatile technique, but unlike the space holder method the resulting lattices have highly consistent properties, shown, for example, by the large difference in standard deviation of the YM of the samples tested here (2-15% for EBM lattices vs. 50-90% for space holder samples). This combination makes EBM an extremely useful technique for high-value products such as implants. And again, the versatility of the technique leaves many possibilities unexplored.

Firstly, in this study only lattices based on the diamond unit cell have been produced; this was done because it is a relatively simple structure which not only has a low YM, but also has a YM that was shown to be less dependent on the loading direction. Nevertheless, there are many other unit cell designs that could be more suitable when aiming for a higher YM, higher yield strength or a different pore size; examples are the unit cells developed by Materialise (Leuven, Belgium) or Furth Innovative Technologien (Germany) and tested by Murr et al. (Murr et al. 2010).

Another relevant property of lattices produced by EBM, mainly from a biological perspective, are the features on the surface of the individual struts. Surface roughness, for example, can be altered by changing the parameters of the electron beam, but is usually done by adding an extra processing step after fabrication. More advanced methods can be used to produce surfaces with defined topographies. Surface properties of biomaterials are known to have a great effect on cell behaviour and could therefore also positively affect bone ingrowth (Dalby et al. 2007; Sjöström et al. 2009; McNamara et al. 2011).

Finally, the aspect of metal implants that has perhaps attracted the most interest and current research is the application of a coating on the surface of the porous structure after fabrication.

Thin ceramic coatings have been a feature of several highly successful porous and non-porous implants for decades and may be an essential element for the production of EBM produced implants that have sufficient osteoconductivity to achieve lasting implant stability.

7.3 Biological assessment

In vitro cell culture, matrix characterisation and in vivo implantation were carried out to predict the performance of the graded and uniform lattices when used as a bone implant. Viability assays and histology of the lattices has shown good cell attachment and proliferation (demonstrated by an increase in cell viability) that was comparable or better than the other porous metals that were investigated. Assays for the deposition of ECM showed mixed results, but when a mature bone cell line (MLO-A5) was used extensive formation of bone-like matrix was observed.

The experiments to investigate the effect of fluid flow on cell behaviour did not indicate a clear difference between cell number in static and in dynamic conditions, although the overall trend was somewhat unclear because there appeared to be a high variation between different experiments compared to the very low variation within one timepoint. Matrix deposition on the lattices was shown to be negatively affected by the dynamic conditions. This effect could be due to the fluid flow inside the bioreactor, but could also be caused by other adverse conditions related to the bioreactor. This hypothesis is supported by the finding that cells cultured on lattices under dynamic conditions in a well plate show higher values for cell number and mineral deposition (although it should be noted that that the properties of the flow are likely to be different).

The in vivo bone ingrowth study was set up to compare the tissue response and the bone ingrowth properties of the graded lattice compared to a commercially available porous metal. However, due to the low number of samples analysed (as discussed in 6.3) it can only be said that in the samples that were analysed bone ingrowth into both the graded lattices and the positive control was low and that from the data available it could not be determined whether bone ingrowth into the graded lattice was different to the positive control.

Based on the conclusions described here many recommendations can be given for experiments that can be carried out to improve the in vitro and in vivo models. With regard to the bioreactor, the main issue that has caused many difficulties in interpreting the data from the bioreactor experiments in the fact that cell viability of the samples could not be tracked

over time. Not only does this mean that a high number of samples is needed to show cell viability over time, it also means, if for practical reasons it is not possible to run two different experiments simultaneously, that measuring a trend over time is a lengthy process. Furthermore, when there is the possibility of high variation between experiments it is easier to estimate the extent of this effect if repeated measurements on the same samples can be performed.

As the shapes of both the lattice and the inside of the bioreactor are highly regular, another interesting addition to this project would be to calculate the forces that cells that are attached on the struts experience as a result of fluid flow. In collaboration with the INSIGNEO institute an initial study was undertaken to model the mechanical forces on the walls of a uniform lattice using the CAD model of the lattice and the measured strut thickness; the bioreactor was modelled as a cuboid with a 1 mm inlet and outlet. The expected forces based on these calculations are shown in figure 7.1. Extending this model to other lattices such as the graded lattice and to different orientations of the lattices inside the bioreactor would give a good opportunity to compare the in vitro model to an in vivo situation from a biomechanics perspective.

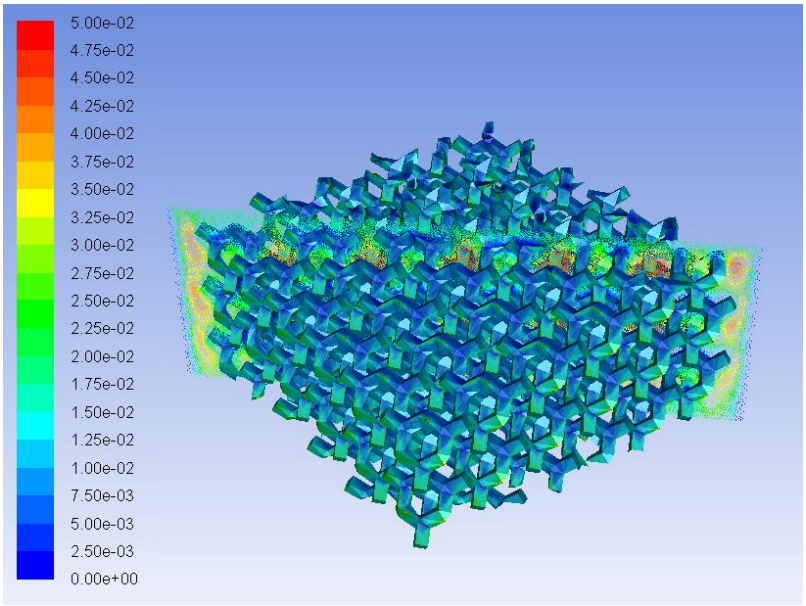

Figure 7.1: Model of the wall shear stresses (in Pa) on the uniform lattice in the bioreactor.

Recommendations regarding the testing of porous metals in a bone defect have been discussed in chapter 6, but nevertheless it is important to highlight the main issues regarding this study. Firstly, a rabbit model is a relatively small model to study bone ingrowth into

materials with relatively large features; doing a similar study in a larger animal would create the possibility of making a deeper defect and therefore a larger and more stable bone-implant interface. Furthermore, the controls that are used for comparison should be considered carefully as well as many of the technical aspects with regards to processing the specimens after extraction of the femurs (see chapter 6). With these modifications, a good comparison between EBM lattices with graded porosity and commercially available porous metals will be possible.

In summary, the work described in this thesis has produced a prototype design of a graded structure that shows much promise for fabrication of porous bone implants. The results include fabrication of metal structures, mechanical characterisation as well as biological evaluation of the prototype and show that electron beam melting should be considered as a highly promising technique for the fabrication of porous metal implants.

Appendices

Appendix A: List of abbreviations

AA	Ascorbic acid
ALP	Alkaline phosphatase
Alpha-MEM (α-MEM)	Minimal essential medium - alpha
ANOVA	Analysis of variance
a.u.	Arbitrary units
Beta-GP (β –GP)	Beta glycerophosphate
BMSC	Bone marrow stromal cell
BSP	Bone sialoprotein
CAD	Computer aided design
cAMP	Cyclic adenosine monophosphate
Col '#'	Type '#' collagen
cpTi	Commercially pure titanium
Dex	Dexamethasone
dH_2O	Distilled water
DJD	Degenerative joint disease
DMEM	Dulbecco's modified Eagle's medium
EBM	Electron beam melting
EDTA	Ethylenediaminetetraacetic acid
FCS	Foetal calf serum
G&A	Gibson and Ashby
Gra	Graded lattice
hESMP	Human embryonic stem cell-derived mesenchymal progenitor cell
IL '#'	Interleukin '#'
IMS	Industrial methylated spirits
Micro-CT (μCT)	Micro-computed tomography
MLO-A5	Mouse long-bone osteocyte A5
MMP	Matrix metalloproteinase
MSC	Mesenchymal stem cell
NC	Negative control
NICE	National institute for health and care excellence
NJR	National joint registry
NO	Nitrous oxide
NSAID	Non-steroidal anti inflammatory drug
OA	Osteoarthritis
O.D.	Optical density
OC	Osteocalcin
ON	Osteonectin
OP	Osteopontin
PBS	Phosphate buffered saline

PC	Positive control
PCR	Polymerase chain reaction
PGE2	Prostaglandin E2
PMMA	Polymethylmetacrylate
PRS	Powder recycling system
PTFE	Polytetrafluoroethylene
rpm	Rotations per minute
SD	Standard deviation
SEM	Scanning electron microscopy
SLS	Selective laser sintering
TCPS	Tissue culture-treated polystyrene
Ti6Al4V	Grade 5 titanium alloy (6% Al, 4% V)
TJA	Total joint arthroplasty
VEGF	Vascular endothelial growth factor
YM	Young's modulus
YS	Yield strength

Appendix B: Publications

Van Grunsven, W., Hernandez-Nava, E., Reilly, G.C. and Goodall, R., *Fabrication and mechanical characterisation of titanium lattices with graded porosity.* Metals, 2014. **4**: p. 401-409. DOI: 10.3390/met4030401. Invited feature paper.

Mallick, K.K., Winnett, J., Van Grunsven, W., Lapworth, J. and Reilly, G.C., *3-D porous bioscaffolds for bone tissue regeneration: fabrication via adaptive foam reticulation and freeze casting techniques, characterisation and cell study.* Journal of Biomedical Materials Research: Part A, 2012. **100A**(11): p. 2948-2959. DOI: 10.1002/jbm.a.34238.

Rouholamin, D., Smith, P.J., Ghassemieh, E., Van Grunsven, W. and Reilly, G.C., *The relationship between morphological and mechanical properties of porous $P_{DL}LA/HA$ scaffolds produced by supercritical CO_2 fluid technology.* Journal of Materials Science: Materials in Medicine, submitted.

Trinidad, J., Arruebarrena, G., Van Grunsven, W., Goodall, R., Sáenz de Argandoña, E. and Reilly, G., *Corrosion and cell viability characterization of Mg-Zn alloys for medical applications.* Proceedings of the Institution of Mechanical Engineers, Part H: Journal of Engineering in Medicine, submitted.

Appendix C: Conference contributions

2013 Van Grunsven, W., Goodall, R. and Reilly, G.C., *Graded porous titanium for improved osseointegration into bone implants*, 19th Congress of the European Society of Biomechanics, Patras (GR).

2012 Van Grunsven, W., Goodall, R. and Reilly, G.C., *Highly porous titanium alloy: fabrication and mechanical properties*, 18th Congress of the European Society of Biomechanics, Lisbon (PT). Published in: Journal of Biomechanics, vol. 45, suppl. 1, p. S339.

2012 Van Grunsven, W., Goodall, R. and Reilly, G.C., *Mechanical and biological properties of porous metal for bone implants*, 9th World Biomaterials Congress, Chengdu (CN).

2011 Van Grunsven, W., Goodall, R. and Reilly, G.C., *Porous metal implants for enhanced bone ingrowth and stability*, Tissue and Cell Engineering Society Annual Meeting, Leeds (UK). Published in: European Cells and Materials, vol. 22, suppl. 3, p. 1.

2011 Mallick, K.K., Winnett, J., Van Grunsven, W., Lapworth, J. and Reilly, G.C., *Fabrication approaches and characterization of porous 3D bioscaffolds for hard tissue augmentation*, Materials Science and Technology Conference ’11, Columbus (US).

2011 Van Grunsven, W., Reilly, G.C. and Goodall, R., *Porous metal implants for enhanced bone ingrowth and stability*, IMMPETUS Colloquium, Sheffield (UK).

References

Abdulkarim, A., Ellanti, P., Motterlini, N., Fahey, T. and O'Byrne, J. M. (2013). Cemented versus uncemented fixation in total hip replacement: a systematic review and meta-analysis of randomized controlled trials.

Ahmadi, S. M., Campoli, G., Amin Yavari, S., Sajadi, B., Wauthle, R., Schrooten, J., Weinans, H. and Zadpoor, A. A. (2014). "Mechanical behavior of regular open-cell porous biomaterials made of diamond lattice unit cells." Journal of the Mechanical Behavior of Biomedical Materials **34**: 106-115.

Al-Bermani, S. S. (2011). An investigation into microstructure and microstructural control of additive layer manufactured Ti-6Al-4V by electron beam melting. Department of Materials Science and Engineering. Sheffield, University of Sheffield. **PhD**.

Arthritis Care UK. "Website." from http://www.arthritiscare.org.uk.

Arthritis Foundation. "Website." from http://www.arthritis.org/.

Ashby, M. F., Evans, E. G., Fleck, N. A., Gibson, L. J., Hutchinson, J. W. and Wadley, H. N. G. (2000). Metal Foams: A Design Guide. Oxford, United Kingdom, Butterworth Heinemann.

Assad, M., Chernyshov, A. V., Jarzem, P., Leroux, M. A., Coillard, C., Charette, S. and Rivard, C. H. (2003). "Porous Titanium-Nickel for Intervertebral Fusion in a Sheep Model: Part 2. Surface Analysis and Nickel Release Assessment." Journal of Biomedical Materials Research - Part B Applied Biomaterials **64**(2): 121-129.

Assad, M., Jarzem, P., Leroux, M. A., Coillard, C., Chernyshov, A. V., Charette, S. and Rivard, C. H. (2003). "Porous Titanium-Nickel for Intervertebral Fusion in a Sheep Model: Part 1. Histomorphometric and Radiological Analysis." Journal of Biomedical Materials Research - Part B Applied Biomaterials **64**(2): 107-120.

Assad, M., Likibi, F., Jarzem, P., Leroux, M. A., Coillard, C. and Rivard, C. H. (2004). "Porous nitinol vs. titanium intervertebral fusion implants: Computer tomography, radiological and histological study of osseointegration capacity." Materialwissenschaft und Werkstofftechnik **35**(4): 219-223.

Aubin, J. E. and Bonnelye, E. (2000). "Osteoprotegerin and its ligand: A new paradigm for regulation of osteoclastogenesis and bone resorption." Osteoporosis International **11**(11): 905-913.

Bancroft, G. N., Sikavitsas, V. I., Van Den Dolder, J., Sheffield, T. L., Ambrose, C. G., Jansen, J. A. and Mikos, A. G. (2002). "Fluid flow increases mineralized matrix deposition in 3D perfusion culture of marrow stromal osteoblasts in a dose-dependent manner." Proceedings of the National Academy of Sciences of the United States of America **99**(20): 12600-12605.

Bansiddhi, A. and Dunand, D. C. (2008). "Shape-memory NiTi foams produced by replication of NaCl space-holders." Acta Biomaterialia **4**(6): 1996-2007.

Barragan-Adjemian, C., Nicolella, D., Dusevich, V., Dallas, M. R., Eick, J. D. and Bonewald, L. F. (2006). "Mechanism by which MLO-A5 late osteoblasts/early osteocytes mineralize in culture: Similarities with mineralization of lamellar bone." Calcified Tissue International **79**(5): 340-353.

Bassey, E. J. and Ramsdale, S. J. (1994). "Increase in femoral bone density in young women following high-impact exercise." Osteoporosis International **4**(2): 72-75.

Beck, M., Kalhor, M., Leunig, M. and Ganz, R. (2005). "Hip morphology influences the pattern of damage to the acetabular cartilage. Femoroacetabular impingement as a cause of early osteoarthritis of the hip." Journal of Bone and Joint Surgery - Series B **87**(7): 1012-1018.

Bertollo, N., Da Assuncao, R., Hancock, N. J., Lau, A. and Walsh, W. R. (2012). "Influence of Electron Beam Melting Manufactured Implants on Ingrowth and Shear Strength in an Ovine Model." Journal of Arthroplasty **27**(8): 1429-1436.

Biemond, J. E., Aquarius, R., Verdonschot, N. and Buma, P. (2011). "Frictional and bone ingrowth properties of engineered surface topographies produced by electron beam technology." Archives of Orthopaedic and Trauma Surgery **131**(5): 711-718.

Biemond, J. E., Eufrásio, T. S., Hannink, G., Verdonschot, N. and Buma, P. (2011). "Assessment of bone ingrowth potential of biomimetic hydroxyapatite and brushite coated porous E-beam structures." Journal of Materials Science: Materials in Medicine **22**(4): 917-925.

Biemond, J. E., Hannink, G., Jurrius, A. M. G., Verdonschot, N. and Buma, P. (2012). "In vivo assessment of bone ingrowth potential of three-dimensional E-beam produced implant surfaces and the effect of additional treatment by acid etching and hydroxyapatite coating." Journal of Biomaterials Applications **26**(7): 861-875.

Billiau, A., Edy, V. G., Heremans, H., Van Damme, J., Desmyter, J., Georgiades, J. A. and De Somer, P. (1977). "Human interferon: mass production in a newly established cell line, MG 63." Antimicrobial Agents and Chemotherapy **12**(1): 11-15.

Botchwey, E. A., Pollack, S. R., Levine, E. M. and Laurencin, C. T. (2001). "Bone tissue engineering in a rotating bioreactor using a microcarrier matrix system." Journal of Biomedical Materials Research **55**(2): 242-253.

Bram, M., Stiller, C., Buchkremer, H. P., Stöver, D. and Baur, H. (2000). "High-porosity titanium, stainless steel, and superalloy parts." Advanced Engineering Materials **2**(4): 196-199.

Bugbee, W. D., Culpepper, W. J., Engh Jr, C. A. and Engh Sr, C. A. (1997). "Long-term clinical consequences of stress-shielding after total hip arthroplasty without cement." Journal of Bone and Joint Surgery - Series A **79**(7): 1007-1013.

Canale, S. T. (1998). Campbell's operative orthopaedics. St. Louis, United States, Mosby-year book, Inc.

Case, C. P., Langkamer, V. G., James, C., Palmer, M. R., Kemp, A. J., Heap, P. F. and Solomon, L. (1994). "Widespread dissemination of metal debris from implants." Journal of Bone and Joint Surgery - Series B **76**(5): 701-712.

Chambers, T. J. (2000). "Regulation of the differentiation and function of osteoclasts." Journal of Pathology **192**(1): 4-13.

Charnley, J. (1960). "Anchorage of the femoral head prosthesis to the shaft of the femur." Journal of Bone and Joint Surgery - Series B **42 B**: 28-30.

Charnley, J. (1961). "Arthroplasty of the hip. A new operation." The Lancet **277**(7187): 1129-1132.

Charnley, J. (1965). "A biomechanical analysis of the use of cement to anchor the femoral head prosthesis." Journal of Bone and Joint Surgery - Series B **47**: 354-363.

Cohen, D. (2012). "How safe are metal-on-metal hip implants?" British Medical Journal **344**(7846).

Cormier, D., Harrysson, O. and West, H. (2004). "Characterization of H13 steel produced via electron beam melting." Rapid Prototyping Journal **10**(1): 35-41.

Cornelissen, C. G., Dietrich, M., Krüger, S., Spillner, J., Schmitz-Rode, T. and Jockenhoevel, S. (2012). "Fibrin gel as alternative scaffold for respiratory tissue engineering." Annals of Biomedical Engineering **40**(3): 679-687.

Cowin, S. C. (2004). "Tissue growth and remodeling." Annual Review of Biomedical Engineering **6**: 77-107.

Currey, J. D. (2002). Bones: Structure and Mechanics, Princeton University Press.

Czekanska, E. M., Stoddart, M. J., Ralphs, J. R., Richards, R. G. and Hayes, J. S. (2013). "A phenotypic comparison of osteoblast cell lines versus human primary osteoblasts for biomaterials testing." Journal of Biomedical Materials Research - Part A **102**(8): 2636-2643.

D'Antonio, J. A., Capello, W. N., Crothers, O. D., Jaffe, W. L. and Manley, M. T. (1992). "Early clinical experience with hydroxyapatite-coated femoral implants." Journal of Bone and Joint Surgery - Series A **74**(7): 995-1008.

D'Antonio, J. A., Capello, W. N. and Jaffe, W. L. (1992). "Hydroxylapatite-coated hip implants: Multicenter three-year clinical and roentgenographic results." Clinical Orthopaedics and Related Research **285**: 102-115.

D'Antonio, J. A., Capello, W. N., Manley, M. T. and Geesink, R. (2001). "Hydroxyapatite femoral stems for total hip arthroplasty 10- to 13-year followup." Clinical Orthopaedics and Related Research **393**: 101-111.

Dalby, M. J., Gadegaard, N., Tare, R., Andar, A., Riehle, M. O., Herzyk, P., Wilkinson, C. D. W. and Oreffo, R. O. C. (2007). "The control of human mesenchymal cell differentiation using nanoscale symmetry and disorder." Nature Materials **6**(12): 997-1003.

De Peppo, G. M., Palmquist, A., Borchardt, P., Lennerås, M., Hyllner, J., Snis, A., Lausmaa, J., Thomsen, P. and Karlsson, C. (2012). "Free-form-fabricated commercially pure Ti and Ti6Al4V porous scaffolds support the growth of human embryonic stem cell-derived mesodermal progenitors." The Scientific World Journal.

Delaine-Smith, R. M. (2013). Mechanical and physical guidance of osteogenic differentiation and matrix production. Department of Materials Science and Engineering. Sheffield, University of Sheffield. **PhD**.

Delaine-Smith, R. M., MacNeil, S. and Reilly, G. C. (2012). "Matrix production and collagen structure are enhanced in two types of osteogenic progenitor cells by a simple fluid shear stress stimulus." European Cells and Materials **24**: 162-174.

Dunand, D. C. (2004). "Processing of titanium foams." Advanced Engineering Materials **6**(6): 369-376.

Eftekhar, N. S. (1978). Principles of total hip arthroplasty. St. Louis, United States, The C.V. Mosby company.

El Haj, A. J. and Cartmell, S. H. (2010). "Bioreactors for bone tissue engineering." Proceedings of the Institution of Mechanical Engineers, Part H: Journal of Engineering in Medicine **224**(12): 1523-1532.

Engh, C. A., Bobyn, J. D. and Glassman, A. H. (1987). "Porous-coated hip replacement. The factors governing bone ingrowth, stress shielding, and clinical results." Journal of Bone and Joint Surgery - Series B **69**(1): 45-55.

Epinette, J. A. and Manley, M. T. (2007). "Hydroxyapatite-coated total knee replacement." Journal of Bone and Joint Surgery - Series B **89**(1): 34-38.

Esen, Z. and Bor, S. (2007). "Processing of titanium foams using magnesium spacer particles." Scripta Materialia **56**(5): 341-344.
Fleck, N. A. (1995). "On the cold compaction of powders." Journal of the Mechanics and Physics of Solids **43**(9): 1409-1431.
Freed, L. E., Hollander, A. P., Martin, I., Barry, J. R., Langer, R. and Vunjak-Novakovic, G. (1998). "Chondrogenesis in a cell-polymer-bioreactor system." Experimental Cell Research **240**(1): 58-65.
Furlong, R. J. and Osborn, J. F. (1991). "Fixation of hip prostheses by hydroxyapatite ceramic coatings." Journal of Bone and Joint Surgery - Series B **73**(5): 741-745.
Garvin, K. L. and Hanssen, A. D. (1995). "Infection after total hip arthroplasty: Past, present, and future." Journal of Bone and Joint Surgery - Series A **77**(10): 1576-1588.
Geesink, R. G. T., De Groot, K. and Klein, C. P. A. T. (1988). "Bonding of bone to apatite-coated implants." Journal of Bone and Joint Surgery - Series B **70**(1): 17-22.
Geesink, R. G. T. and Hoefnagels, N. H. M. (1995). "Six-year results of hydroxyapatite-coated total hip replacement." Journal of Bone and Joint Surgery - Series B **77**(4): 534-547.
Gibson, L. J. and Ashby, M. F. (1997). Cellular solids: Structure and properties. Cambridge, Cambridge University Press.
Goldring, S. R., Schiller, A. L. and Roelke, M. (1983). "The synovial-like membrane at the bone-cement interference in loose total hip replacements and its proposed role in bone lysis." Journal of Bone and Joint Surgery - Series A **65**(5): 575-584.
Goodall, R. and Mortensen, A. (2014). Porous metals. Physical Metallurgy. D. Laughlin and K. Kono, Elsevier.
Gruen, T. A., McNeice, G. M. and Amstutz, H. C. (1979). "'Modes of failure' of cemented stem-type femoral components. A radiographic analysis of loosening." Clinical Orthopaedics and Related Research **141**: 17-27.
Guh, D. P., Zhang, W., Bansback, N., Amarsi, Z., Birmingham, C. L. and Anis, A. H. (2009). "The incidence of co-morbidities related to obesity and overweight: A systematic review and meta-analysis." BMC Public Health **9**.
Haase, K. and Rouhi, G. (2010). "A discussion on plating factors that affect stress shielding using finite element analysis." Journal of Biomechanical Science and Engineering **5**(2): 129-141.
Haddad, S. L., Coetzee, J. C., Estok, R., Fahrbach, K., Banel, D. and Nalysnyk, L. (2007). "Intermediate and long-term outcomes of total ankle arthroplasty and ankle arthrodesis: A systematic review of the literature." Journal of Bone and Joint Surgery - Series A **89**(9): 1899-1905.
Halgrin, J., Chaari, F. and Markiewicz, É. (2012). "On the effect of marrow in the mechanical behavior and crush response of trabecular bone." Journal of the Mechanical Behavior of Biomedical Materials **5**(1): 231-237.
Haslauer, C. M., Springer, J. C., Harrysson, O. L. A., Loboa, E. G., Monteiro-Riviere, N. A. and Marcellin-Little, D. J. (2010). "In vitro biocompatibility of titanium alloy discs made using direct metal fabrication." Medical Engineering and Physics **32**(6): 645-652.
Heinl, P., Körner, C. and Singer, R. F. (2008). "Selective electron beam melting of cellular titanium: Mechanical properties." Advanced Engineering Materials **10**(9): 882-888.
Heinl, P., Müller, L., Körner, C., Singer, R. F. and Müller, F. A. (2008). "Cellular Ti-6Al-4V structures with interconnected macro porosity for bone implants fabricated by selective electron beam melting." Acta Biomaterialia **4**(5): 1536-1544.
Heinl, P., Rottmair, A., Körner, C. and Singer, R. F. (2007). "Cellular titanium by selective electron beam melting." Advanced Engineering Materials **9**(5): 360-364.
Helfrich, M. H. and Ralston, S. H. (2012). Bone Research Protocols, Humana Press.
Hennessy, D. W., Callaghan, J. J. and Liu, S. S. (2009). "Second-generation extensively porous-coated THA stems at minimum 10-year followup." Clinical Orthopaedics and Related Research **467**(9): 2290-2296.
Hettfleisch, J. and Wissenbach, R. (1994). "Forty-year survival of a Judet hip porsthesis: a case report." Journal of Bone and Joint Surgery - Series B **76-B**: 671-672.
Hrabe, N. W., Heinl, P., Bordia, R. K., Körner, C. and Fernandes, R. J. (2013). "Maintenance of a bone collagen phenotype by osteoblast-like cells in 3D periodic porous titanium (Ti-6Al-4 V) structures fabricated by selective electron beam melting." Connective Tissue Research **54**(6): 351-360.
Huey, D. J., Hu, J. C. and Athanasiou, K. A. (2012). "Unlike bone, cartilage regeneration remains elusive." Science **338**(6109): 917-921.
Hungerford, D. S. and Kenna, R. V. (1983). "Preliminary experience with a total knee prosthesis with porous coating used without cement." Clinical Orthopaedics and Related Research **176**: 95-107.
Hungerford, D. S., Kenna, R. V. and Krackow, K. A. (1982). "The porous-coated anatomic total knee." Orthopedic Clinics of North America **13**(1): 103-122.
Hunziker, E. B. (2001). "Growth-factor-induced healing of partial-thickness defects in adult articular cartilage." Osteoarthritis and Cartilage **9**(1): 22-32.

Hwang, S. C., Kong, J. Y., Nam, D. C., Kim, D. H., Park, H. B., Jeong, S. T. and Cho, S. H. (2010). "Revision total knee arthroplasty with a cemented posterior stabilized, condylar constrained or fully constrained prosthesis: A minimum 2-year follow-up analysis." Clinics in Orthopedic Surgery **2**(2): 112-120.

Imwinkelried, T. (2007). "Mechanical properties of open-pore titanium foam." Journal of Biomedical Materials Research - Part A **81**(4): 964-970.

Janmey, P. A. and McCulloch, C. A. (2007). "Cell mechanics: Integrating cell responses to mechanical stimuli." Annual Review of Biomedical Engineering **9**: 1-34.

Jeon, H. and Kim, G. (2012). "Effects of a cell-imprinted poly(dimethylsiloxane) surface on the cellular activities of MG63 osteoblast-like cells: Preparation of a patterned surface, surface characterization, and bone mineralization." Langmuir **28**(37): 13423-13430.

Jha, N., Mondal, D. P., Dutta Majumdar, J., Badkul, A., Jha, A. K. and Khare, A. K. (2013). "Highly porous open cell Ti-foam using NaCl as temporary space holder through powder metallurgy route." Materials and Design **47**: 810-819.

Johnson, D. L., McAllister, T. N. and Frangos, J. A. (1996). "Fluid flow stimulates rapid and continuous release of nitric oxide in osteoblasts." American Journal of Physiology - Endocrinology and Metabolism **271**(134-1): E205-E208.

Kato, Y., Boskey, A., Spevak, L., Dallas, M., Hori, M. and Bonewald, L. F. (2001). "Establishment of an osteoid preosteocyte-like cell MLO-A5 that spontaneously mineralizes in culture." Journal of Bone and Mineral Research **16**(9): 1622-1633.

Kienapfel, H., Sprey, C., Wilke, A. and Griss, P. (1999). "Implant fixation by bone ingrowth." Journal of Arthroplasty **14**(3): 355-368.

Kokubo, T. and Takadama, H. (2006). "How useful is SBF in predicting in vivo bone bioactivity?" Biomaterials **27**(15): 2907-2915.

Komori, T. (2002). "Runx2, a multifunctional transcription factor in skeletal development." Journal of Cellular Biochemistry **87**(1): 1-8.

Koopman, W. J. and Moreland, L. W. (2005). Arthritis and allied conditions. Philadelphia, United States, Lippincott Williams & Wilkins.

Kronenberg, H. M. (2003). "Developmental regulation of the growth plate." Nature **423**(6937): 332-336.

Learmonth, I. D., Young, C. and Rorabeck, C. (2007). "The operation of the century: total hip replacement." Lancet **370**(9597): 1508-1519.

Levine, B. (2008). "A new era in porous metals: Applications in orthopaedics." Advanced Engineering Materials **10**(9): 788-792.

Lewis, G. (2008). "Alternative acrylic bone cement formulations for cemented arthroplasties: Present status, key issues, and future prospects." Journal of Biomedical Materials Research - Part B Applied Biomaterials **84**(2): 301-319.

Long, M. and Rack, H. J. (1998). "Titanium alloys in total joint replacement - A materials science perspective." Biomaterials **19**(18): 1621-1639.

Lübbeke, A., Duc, S., Garavaglia, G., Finckh, A. and Hoffmeyer, P. (2009). "BMI and severity of clinical and radiographic signs of hip osteoarthritis." Obesity **17**(7): 1414-1419.

Lützner, J., Kasten, P., Günther, K. P. and Kirschner, S. (2009). "Surgical options for patients with osteoarthritis of the knee." Nature reviews. Rheumatology **5**(6): 309-316.

MacDonald, S. J., Rosenzweig, S., Guerin, J. S., McCalden, R. W., Bohm, E. R., Bourne, R. B., Rorabeck, C. H. and Barrack, R. L. (2010). "Proximally versus fully porous-coated femoral stems: A multicenter randomized trial." Clinical Orthopaedics and Related Research **468**(2): 424-432.

Mackie, E. J., Ahmed, Y. A., Tatarczuch, L., Chen, K. S. and Mirams, M. (2008). "Endochondral ossification: How cartilage is converted into bone in the developing skeleton." International Journal of Biochemistry and Cell Biology **40**(1): 46-62.

Mahmoudifar, N. and Doran, P. M. (2012). "Chondrogenesis and cartilage tissue engineering: The longer road to technology development." Trends in Biotechnology **30**(3): 166-176.

Mallick, K. K., Winnett, J., Van Grunsven, W., Lapworth, J. and Reilly, G. C. (2012). "Three-dimensional porous bioscaffolds for bone tissue regeneration: Fabrication via adaptive foam reticulation and freeze casting techniques, characterization, and cell study." Journal of Biomedical Materials Research - Part A **100 A**(11): 2948-2959.

Malone, A. M. D., Anderson, C. T., Tummala, P., Kwon, R. Y., Johnston, T. R., Stearns, T. and Jacobs, C. R. (2007). "Primary cilia mediate mechanosensing in bone cells by a calcium-independent mechanism." Proceedings of the National Academy of Sciences of the United States of America **104**(33): 13325-13330.

Manley, M. T., Capello, W. N., D'Antonio, J. A., Edidin, A. A. and Geesink, R. G. T. (1998). "Fixation of acetabular cups without cement in total hip arthroplasty: A comparison of three different implant surfaces at a minimum duration of follow-up of five years." Journal of Bone and Joint Surgery - Series A **80**(8): 1175-1185.

Marieb, E. N. (2004). Human Anatomy & Physiology, Pearson Education inc.

McCoy, R. J. and O'Brien, F. J. (2010). "Influence of shear stress in perfusion bioreactor cultures for the development of three-dimensional bone tissue constructs: A review." Tissue Engineering - Part B: Reviews **16**(6): 587-601.

McNamara, L. E., Sjöström, T., et al. (2011). "Skeletal stem cell physiology on functionally distinct titania nanotopographies." Biomaterials **32**(30): 7403-7410.

Messier, S. P., Loeser, R. F., Miller, G. D., Morgan, T. M., Rejeski, W. J., Sevick, M. A., Ettinger Jr, W. H., Pahor, M. and Williamson, J. D. (2004). "Exercise and Dietary Weight Loss in Overweight and Obese Older Adults with Knee Osteoarthritis: The Arthritis, Diet, and Activity Promotion Trial." Arthritis and Rheumatism **50**(5): 1501-1510.

Morris, H. L., Reed, C. I., Haycock, J. W. and Reilly, G. C. (2010). "Mechanisms of fluid-flow-induced matrix production in bone tissue engineering." Proceedings of the Institution of Mechanical Engineers, Part H: Journal of Engineering in Medicine **224**(12): 1509-1521.

Mortensen, A., Conde, Y., Rossoll, A. and San Marchi, C. (2013). "Scaling of conductivity and Young's modulus in replicated microcellular materials." Journal of Materials Science **48**(23): 8140-8146.

Moskowitz, R. W., Altman, R. D., Hochberg, M. C., Buckwalter, J. A. and Goldberg, V. M. (2007). Osteoarthritis. Philadelphia, United States, Lippincott Williams & Wilkins.

Mullender, M., El Haj, A. J., Yang, Y., van Duin, M. A., Burger, E. H. and Klein-Nulend, J. (2004). "Mechanotransduction of bone cells in vitro: Mechanobiology of bone tissue." Medical and Biological Engineering and Computing **42**(1): 14-21.

Murr, L. E., Gaytan, S. M., et al. (2010). "Next-generation biomedical implants using additive manufacturing of complex cellular and functional mesh arrays." Philosophical Transactions of the Royal Society A: Mathematical, Physical and Engineering Sciences **368**(1917): 1999-2032.

National Joint Registry. (2013). "10th Annual Report." from http://www.njrcentre.org.uk.

Navaei-Nigjeh, M., Amoabedini, G., Noroozi, A., Azami, M., Asmani, M. N., Ebrahimi-Barough, S., Saberi, H., Ai, A. and Ai, J. (2013). "Enhancing neuronal growth from human endometrial stem cells derived neuron-like cells in three-dimensional fibrin gel for nerve tissue engineering." Journal of Biomedical Materials Research - Part A **102**(8): 2533-2543.

Neer, C. S., Watson, K. C. and Stanton, P. J. (1982). "Recent experience in total shoulder replacement." Journal of Bone and Joint Surgery - Series A **64**(3): 319-337.

NHS. "Website." from http://www.nhs.uk.

NICE. "Website." from www.nice.org.uk.

Nilsson, K. G., Kärrholm, J., Carlsson, L. and Dalén, T. (1999). "Hydroxyapatite coating versus cemented fixation of the tibial component in total knee arthroplasty: Prospective randomized comparison of hydroxyapatite-coated and cemented tibial components with 5-year follow-up using radiostereometry." Journal of Arthroplasty **14**(1): 9-20.

Niu, J., Zhang, Y. Q., et al. (2009). "Is obesity a risk factor for progressive radiographic knee osteoarthritis?" Arthritis Care and Research **61**(3): 329-335.

O'Brien, J., Wilson, I., Orton, T. and Pognan, F. (2000). "Investigation of the Alamar Blue (resazurin) fluorescent dye for the assessment of mammalian cell cytotoxicity." European Journal of Biochemistry **267**(17): 5421-5426.

O'Neil, C. K., Hanlon, J. T. and Marcum, Z. A. (2012). "Adverse effects of analgesics commonly used by older adults with osteoarthritis: Focus on non-opioid and opioid analgesics." American Journal of Geriatric Pharmacotherapy **10**(6): 331-342.

Panesar, S. S., Cleary, K., Bhandari, M. and Sheikh, A. (2009). "To cement or not in hip fracture surgery?" The Lancet **374**(9695): 1047-1049.

Parker, M. J., Gurusamy, K. S. and Azegami, S. (2010). "Arthroplasties (with and without bone cement) for proximal femoral fractures in adults." Cochrane database of systematic reviews **6**.

Partap, S., Plunkett, N. A., Kelly, D. J. and O'Brien, F. J. (2010). "Stimulation of osteoblasts using rest periods during bioreactor culture on collagen-glycosaminoglycan scaffolds." Journal of materials science. Materials in medicine **21**(8): 2325-2330.

Pattanayak, D. K., Fukuda, A., Matsushita, T., Takemoto, M., Fujibayashi, S., Sasaki, K., Nishida, N., Nakamura, T. and Kokubo, T. (2011). "Bioactive Ti metal analogous to human cancellous bone: Fabrication by selective laser melting and chemical treatments." Acta Biomaterialia **7**(3): 1398-1405.

Ponader, S., Vairaktaris, E., et al. (2008). "Effects of topographical surface modifications of electron beam melted Ti-6Al-4V titanium on human fetal osteoblasts." Journal of Biomedical Materials Research - Part A **84**(4): 1111-1119.
Ponader, S., Von Wilmowsky, C., et al. (2010). "In vivo performance of selective electron beam-melted Ti-6Al-4V structures." Journal of Biomedical Materials Research - Part A **92**(1): 56-62.
Qiu, Q., Ducheyne, P., Gao, H. and Ayyaswamy, P. (1998). "Formation and differentiation of three-dimensional rat marrow stromal cell culture on microcarriers in a rotating-wall vessel." Tissue Engineering **4**(1): 19-34.
Rho, J. Y., Kuhn-Spearing, L. and Zioupos, P. (1998). "Mechanical properties and the hierarchical structure of bone." Medical Engineering and Physics **20**(2): 92-102.
Ruff, C., Holt, B. and Trinkaus, E. (2006). "Who's afraid of the big bad Wolff?: "Wolff's law" and bone functional adaptation." American Journal of Physical Anthropology **129**(4): 484-498.
Sellam, J. and Berenbaum, F. (2010). "The role of synovitis in pathophysiology and clinical symptoms of osteoarthritis." Nature Reviews Rheumatology **6**(11): 625-635.
Shaeri, M. (2013). Dynamic culture of osteogenic mesenchymal progenitor cells in a 3D porous scaffold. Department of Materials Science and Engineering. Sheffield, University of Sheffield. **PhD**.
Shapiro, F. (2008). "Bone development and its relation to fracture repair. The role of mesenchymal osteoblasts and surface osteoblasts." European Cells and Materials **15**: 53-76.
Shiers, L. G. (1954). "Arthroplasty of the knee; preliminary report of new method." Journal of Bone and Joint Surgery - Series B **36 B**(4): 553-560.
Shimizu, T., Matsuzaki, K., Nagai, H. and Kanetake, N. (2012). "Production of high porosity metal foams using EPS beads as space holders." Materials Science and Engineering A **558**: 343-348.
Singer, S., Klejman, S., Pinsker, E., Houck, J. and Daniels, T. (2013). "Ankle arthroplasty and ankle arthrodesis: Gait analysis compared with normal controls." Journal of Bone and Joint Surgery - Series A **95**(24): e1911-e19110.
Singh, R., Lee, P. D., Lindley, T. C., Dashwood, R. J., Ferrie, E. and Imwinkelried, T. (2009). "Characterization of the structure and permeability of titanium foams for spinal fusion devices." Acta Biomaterialia **5**(1): 477-487.
Sittichokechaiwut, A. (2009). Dynamic Mechanical Stimulation for Bone Tissue Engineering. Materials Science and Engineering. Sheffield, University of Sheffield. **PhD**.
Sjöström, T., Dalby, M. J., Hart, A., Tare, R., Oreffo, R. O. C. and Su, B. (2009). "Fabrication of pillar-like titania nanostructures on titanium and their interactions with human skeletal stem cells." Acta Biomaterialia **5**(5): 1433-1441.
Smith-Petersen, M. N. (1948). "Evolution of mould arthroplasty of the hip joint." Journal of Bone and Joint Surgery - Series A **30 B**(1): 59-75.
Song, Y., Ju, Y., Morita, Y. and Song, G. (2013). "Effect of the nanostructure of porous alumina on growth behavior of MG63 osteoblast-like cells." Journal of Bioscience and Bioengineering **116**(4): 509-515.
Svehla, M., Morberg, P., Bruce, W. and Walsh, W. R. (2005). "No effect of a type I collagen gel coating in uncemented implant fixation." Journal of Biomedical Materials Research - Part B Applied Biomaterials **74**(1): 423-428.
Svehla, M., Morberg, P., Bruce, W., Zicat, B. and Walsh, W. R. (2002). "The effect of substrate roughness and hydroxyapatite coating thickness on implant shear strength." Journal of Arthroplasty **17**(3): 304-311.
Svehla, M., Morberg, P., Zicat, B., Bruce, W., Sonnabend, D. and Walsh, W. R. (2000). "Morphometric and mechanical evaluation of titanium implant integration: Comparison of five surface structures." Journal of Biomedical Materials Research **51**(1): 15-22.
Tarala, M., Waanders, D., Biemond, J. E., Hannink, G., Janssen, D., Buma, P. and Verdonschot, N. (2011). "The effect of bone ingrowth depth on the tensile and shear strength of the implant-bone e-beam produced interface." Journal of Materials Science: Materials in Medicine **22**(10): 2339-2346.
Thomsen, P., Malmström, J., Emanuelsson, L., René, M. and Snis, A. (2009). "Electron beam-melted, free-form-fabricated titanium alloy implants: Material surface characterization and early bone response in rabbits." Journal of Biomedical Materials Research - Part B Applied Biomaterials **90**(1): 35-44.
Trentin, D., Hubbell, J. and Hall, H. (2005). "Non-viral gene delivery for local and controlled DNA release." Journal of Controlled Release **102**(1): 263-275.
Tsai, S. W., Liou, H. M., Lin, C. J., Kuo, K. L., Hung, Y. S., Weng, R. C. and Hsu, F. Y. (2012). "MG63 osteoblast-like cells exhibit different behavior when grown on electrospun collagen matrix versus electrospun gelatin matrix." PLoS ONE **7**(2).
Van Blitterswijk, C. A. (2008). Tissue Engineering, Academic Press.
Van Grunsven, W. (2010). Devitalised cartilage matrix as a template for bone formation. Department of Tissue Regeneration. Enschede, University of Twente. **MSc**.

Van Grunsven, W., Hernandez-Nava, E., Reilly, G. C. and Goodall, R. (2014). "Fabrication and Mechanical Characterisation of Titanium Lattices with Graded Porosity." Metals **4**: 401-409.

Vunjak-Novakovic, G., Martin, I., Obradovic, B., Treppo, S., Grodzinsky, A. J., Langer, R. and Freed, L. E. (1999). "Bioreactor cultivation conditions modulate the composition and mechanical properties of tissue-engineered cartilage." Journal of Orthopaedic Research **17**(1): 130-138.

Vunjak-Novakovic, G., Obradovic, B., Martin, I., Bursac, P. M., Langer, R. and Freed, L. E. (1998). "Dynamic cell seeding of polymer scaffolds for cartilage tissue engineering." Biotechnology Progress **14**(2): 193-202.

Wazen, R. M., Lefebvre, L. P., Baril, E. and Nanci, A. (2010). "Initial evaluation of bone ingrowth into a novel porous titanium coating." Journal of Biomedical Materials Research - Part B Applied Biomaterials **94**(1): 64-71.

Welsh, R. P., Pilliar, R. M. and Macnab, I. (1971). "Surgical implants. The role of surface porosity in fixation to bone and acrylic." Journal of Bone and Joint Surgery - Series A **53**(5): 963-977.

Wen, C. E., Mabuchi, M., Yamada, Y., Shimojima, K., Chino, Y. and Asahina, T. (2001). "Processing of biocompatible porous Ti and Mg." Scripta Materialia **45**(10): 1147-1153.

Wieding, J., Wolf, A. and Bader, R. (2014). "Numerical optimization of open-porous bone scaffold structures to match the elastic properties of human cortical bone." Journal of the Mechanical Behavior of Biomedical Materials **37**: 56-68.

Wilkinson, M. (2001). Pathogenisis and prevention of aseptic loosening after total hip arthroplasty. Division of Clinical Sciences. Sheffield, University of Sheffield. **PhD**.

Woolson, S. T. and Comstock, C. P. (1996). "Porous pad separation and loosening of Harris-Galante femoral hip components." Journal of Arthroplasty **11**(4): 474-477.

Zhu, H., Schulz, J. and Schliephake, H. (2010). "Human bone marrow stroma stem cell distribution in calcium carbonate scaffolds using two different seeding methods." Clinical Oral Implants Research **21**(2): 182-188.